Evaluation of large-scale spatiotemporal changes in the tree-community composition of Bornean rain forests using remote sensing techniques

Shogoro Fujiki

2017

Contents

Acknowledgements

First of all, I would like to express my sincere gratefulness to my supervisor, Prof. K. Kitayama for providing me with the precious opportunity to study Bornean tropical rain forests. He always guided me with patience and gave me a number of encouragements. I learned many things, not only the academic advices but also philosophical things. I feel very fortune to have met him in Kyoto University.

I would like express my sincere gratitude to Prof. M. Kanzaki, Prof. K. Kitajima, Prof. Y. Kosugi and Prof. E. Nawata for reviewing my thesis. I am deeply grateful to Dr. R. Aoyagi, Dr. K. Okada, Dr. A. Tanaka, Dr. N. Imai, Dr. H. Samejima and Mr. S. Nishio for their valuable advices and supports in my study. I am thankful to Mr. M. Poster, Mr. J. B. Dawat and Mr. Sutrisno for helping tree species identification; Mr. I. Sarjuni and the staffs of the FMUs for assisting field survey; and, Mr. D.A. Riyono, Mr. A.D. Kusuma, Mr. Y. Kurniawan and Mr. M. Hashimoto for arranging my field survey.

I was very fortunate to have inspirations and various support from the present and former members at the Laboratory of Forest Ecology, Kyoto University. I would like to thank Dr. N. Osawa and Dr. Y. Onoda, for their providing various suggestions for my study. I am very grateful to Ms. T. Norimoto with many arrangements for my researches. She always gave me a lot of encouragements in my study life in the laboratory. I also thank Dr. A. Langner, Dr. A. Hidaka, Dr. M. Ushio, Dr. T. Mori, Mr. N. Endo, Mr. H. Iidzuka, Ms. L. Sun, Mr. M. Tatsuno, Mr. K. Mizoguchi, Ms. Y. Ichitsuka, Ms. C. Ikeda, Mr. H. Ito, Mr. K. Nakashima, Mr. Y. Tsujii, Mr. D. Yokoyama, Mr. N. Kagami, Ms. M. Mukai, Ms. X. Su, Mr. G. Amada, Mr. T. Genroku, Ms. M. Hozawa, Ms. H. Nagano, Ms. M. Okano, Ms. R. Bando, Mr. H.

Sonoda, Mr. T. Takumi, Ms. S. Yanou, Mr. T. Shindo, Mr. H. Taga and Mr. M. Yoshida.

This study was partly supported by Mitsui & Co., Ltd. (R11-G4-1014) and the Global Environment Research Fund 1-1403 of the Ministry of the Environment, Japan, to K. Kitayama, and by Grant-in-Aid for JSPS Fellows (15J02671) to S. Fujiki.

Finally, I would like to thank my parents, Mr. Tetsuo Fujiki and Ms. Keiko Fujiki, for understanding me and wholehearted supports.

Shogoro Fujiki

Abstract

Facing the recent rapid loss of biodiversity in tropical forest ecosystems, there is an increasing need for developing a practical means for monitoring biodiversity, which is spatiotemporally sensitive and robust. However, there is so far no consensus about global, harmonized observation system for delivering regular, timely data on biodiversity change. Recently, it has been proposed that tree-community composition based on count-plot surveys could serve as a robust, sensitive, and cost-effective biodiversity indicator for forest disturbances. In the present thesis, I aimed to examine whether tree (plant)-community composition can be mapped at a landscape level, and to develop practical methods for monitoring biodiversity based on plant-community composition (Chapter 2 & 3) and canopy-tree community composition (Chapter 4). I targeted the two major types of tropical forests, secondary vegetation after shifting cultivation and selectively-logged lowland forests in Borneo.

In Chapter 2, I developed a new algorithm to estimate stand age of secondary vegetation after shifting cultivation. I combined a single-time, high-resolution WorldView-2 imagery with time-series Landsat images to derive models for estimating stand age, and subsequently applied the models to the entire landscape on the WorldView-2 imagery. The overall accuracy of identifying vegetation types reflecting stand ages was high (84.28%). Subsequently in Chapter 3, I evaluated the spatiotemporal patterns of ecosystem services (i.e. plant community composition and carbon stock) by extrapolating the explicit temporal patterns of species composition and biomass derived from an earlier study into the stand-age algorithm developed in Chapter 2. The stand age map combined with the field-based AGB accumulation model was effective to estimate AGB of secondary vegetation after shifting cultivation at a landscape level (RMSE: 24.4 Mg ha^{-1}). I, then, simulated the patterns of the

above-ground biomass and plant community distributions using three land-use scenarios: 1) reducing the area of shifting cultivation, 2) shortening the minimum fallow period, and 3) elongating the minimum fallow period. Results indicated that the land use based on the scenario 1) and 2) can increase the total carbon stock while maintaining cultivation. My methods were effective in mapping structure and composition of highly dynamic forests at a landscape level, and in predicting the future patterns of important ecosystem services based on land-use scenarios.

In Chapter 4, I developed an algorithm to map tree-community composition across the entire landscape based on Landsat imagery in selectively-logged lowland forests. I targeted six forest management units (FMUs), each of which ranged from 50,000 to 100,000 ha in area, covering a broad geographic range spanning the most area of Borneo. Approximately fifty 20 m-radius circular plots were established in each FMU, and the differences in tree-community composition among plots were examined using an ordination with non-metric multidimensional scaling (nMDS). Subsequently, I developed a linear regression model based on Landsat metrics (e.g., reflectance value, vegetation indices and textures) to explain the nMDS axis-1 scores of the plots, and extrapolated the model to the landscape to establish a tree-community composition map in each FMU. The tree-community composition could be estimated with a high accuracy (R^2: 0.51–0.74). My study indicates that tree-community composition, which was reported as a robust biodiversity indicator, can be mapped at a landscape level to quantitatively assess the spatiotemporal patterns of biodiversity in Bornean rain forests.

Demonstrating the new potentials of Landsat series is my original and novel contribution to the remote sensing science. With large pixel sizes of Landsat imagery (i.e., 30 m), pixel-level mixing of multiple species with different functional traits has been considered to prevent from comprehensive mapping of individual tree species or

assemblages. In the present thesis, I tried to overcome such a limitation and demonstrated the potentials of Landsat imagery to elucidate tree (plant)-community composition. The present thesis provides cost-effective means for repeatedly mapping tree (plant)-community composition in two major types of tropical vegetation. I propose two practical methods for large-scale forest biodiversity/ecosystem assessments and monitoring.

Chapter 1: General introduction

1.1. Deforestation and forest degradation in the tropics

Tropical rain forests are the most biologically diverse ecosystems on Earth (Myers *et al*., 2000; Gardner *et al*., 2009). However, recent deforestation and forest degradation are becoming a serious threat to biodiversity in tropical forest ecosystems (Peres & Laurance, 2006; Gardner *et al*., 2010; Wilcove *et al*., 2013). Deforestation is a long-term reduction of tree canopy cover to 10–30% or lower. Forest degradation, on the other hand, is typically considered partial deforestation, with more than 10–30% of forest cover remaining (van der Werf *et al*., 2009). The tropical domain experienced the greatest total deforestation of the four climate domains (i.e., tropical, subtropical, temperate, and boreal) and was the only climate domain to exhibit a significant trend of increasing forest loss from 2000 to 2012 (Hansen *et al*., 2013). Deforestation in Insular Southeast Asia was remarkably high among all humid tropical regions of the world. Insular Southeast Asia experienced a deforestation rate of 1.7% yr^{-1} for the entire decade of 1990-2000 (FAO, 2006) and 1.0% yr^{-1} for 2000-2010 (Miettinen *et al*., 2011). In addition, a detailed analysis of Borneo revealed an annual deforestation rate of 1.7% between 2002 and 2005 (Langner *et al*., 2007). Consequently, the tropical deforestation is responsible for the total global carbon emission of 887 (range 646-1238) MtC yr^{-1} for 1990–2000 (Achard *et al*., 2014) and 880 (range 602-1237) MtC yr^{-1} for 2000–2010 (Baccini *et al*., 2012; Achard *et al*., 2014) with an associated catastrophic biodiversity loss (Novacek and Cleland, 2001; Brook *et al*., 2003; Pandit *et al*., 2007; Allnutt *et al*., 2008).

Forest degradation also causes a considerable biodiversity loss (Wilcove *et al*., 2013; Edwards *et al*., 2014) and carbon emissions into the atmosphere (Achard *et al*., 2002; Asner *et al*., 2005, 2010; Langner *et al*., 2012). Forest degradation was

responsible for the greater net carbon emissions than deforestation alone was (Asner *et al*., 2005). For example, forest degradation in Amazonian forests increased annual carbon emissions by 47% compared with the emission by deforestation alone (Asner *et al*., 2010). Furthermore, there is a positive feedback between forest degradation and fire (Cochrane, 2003). Degraded forests show significantly greater vulnerability to fire than undisturbed forests do (Asner *et al*., 2005; Langner *et al*., 2007). Deforestation and forest degradation in the tropics together are responsible for approximately 20% of anthropogenic carbon emissions, being the second largest anthropogenic emission source (van der Werf *et al*., 2009).

There are many drivers of deforestation and forest degradation in Southeast Asia such as commercial agriculture, mining, infrastructure building, selective logging, shifting cultivation, small-holder forest encroachments, fuel wood collection, wood extraction for charcoal production, overgrazing and fires (Hosonuma *et al*., 2012; Miettinen *et al*., 2014). Of these drivers, commercial and subsistence agriculture are the most important driver of deforestation in tropical Asian countries, accounting for around 70% of deforestation. On the other hand, timber extraction and logging are the most important driver of forest degradation, accounting for more than 80% of degradation (Hosonuma *et al*., 2012). Four main types of disturbances (i.e., forest clearing for commercial agriculture, shifting cultivation, fire and selective logging) account for the majority of deforestation and forest degradation in the tropical forests of Southeast Asia (Stibig *et al*., 2007; Hosonuma *et al*., 2012; Miettinen *et al*., 2014). Reducing the rate of deforestation and forest degradation in the tropics is urgently needed to preserve biodiversity. One practical way to reduce the rate of deforestation and forest degradation is to reconcile the conservation of tropical forests with land uses through sustainable mechanisms.

1.2. International conventions to reduce deforestation and forest degradation

To date, coordinated international efforts have resulted in two international conventions that attempt to reduce the rate of tropical deforestation and forest degradation, and the associated biodiversity losses: the United Nations Framework Convention on Climate Change (UNFCCC) and the Convention on Biological Diversity (CBD). The UNFCCC is a convention primarily targeting the mitigation of and adaptation to climate change. Reducing Emissions from Deforestation and Forest Degradation Plus (REDD+), a post-Kyoto Protocol mechanism developed under UNFCCC is an incentive based policy mechanism often described as a payment-for-performance system. Participating developing countries receive financial incentives for their verified performance in reducing carbon emissions from deforestation and/or forest degradation. REDD+ is expected to have positive effects not only on reducing carbon emissions but also on biodiversity conservation because its main targets are natural tropical forests (Imai *et al*., 2014). When considering the impact of REDD+, it is important to consider REDD+ activities with biodiversity trade-offs. For example, if low-carbon, high-biodiversity tropical forests are converted into high-carbon, low-biodiversity forests, REDD+ may have an overall negative effect on biodiversity conservation (Miles and Kapos, 2008; Paoli *et al*., 2010). Measures to safeguard biodiversity have been extensively discussed in this context under UNFCCC (CCBA, 2008; Gardner *et al*., 2012; GCS, 2011). The premise of these safeguards is a compliance system where each REDD+ project is required to comply with standards and indicators to qualify for REDD+ credits. Such a compliance system must involve third party auditing and verification based on standards and indicators.

The CBD has set a strategic plan for biodiversity for 2011–2020 with the Aichi Biodiversity Targets, which include several targets for forest conservation and their sustainable use (CBD, 2014). The 5th Aichi Target is set forth to reduce the rates

of loss, degradation, and fragmentation of all high biodiversity habitats, including forests (CBD, 2011). It is necessary to quantitatively assess the progress of the Aichi Biodiversity Targets, and there has been intensive discussion on which indicators should be used for monitoring them (GEO BON, 2011; Pereira *et al*., 2013). The development of essential biodiversity variables as a measurement for studying, reporting, and managing changes in biodiversity is a prerequisite for achieving the targets (Pereira *et al*., 2013). Therefore, there is an urgent need to develop robust indicators to both accurately assess the progress of the Aichi Biodiversity Targets and avoid overall negative effects on biodiversity caused by the implementation of REDD+. However, along with inadequate human and financial resources (Martin *et al*., 2012), a key obstacle is the lack of consensus about what to monitor (Pereira *et al*., 2013).

1.3. Indicators for biodiversity

As mentioned above, robust indicators of biodiversity are needed for achieving the goals. Indicators for compliance systems can be generic or specific. Generic indicators (sensu FSC, 2012) are a set of indicators applicable to all forest types and regions; they may be largely based on readily available statistical data or actual prescribed management plans such as the presence/area of forests with high conservation value, presence/type of conservation measures, and presence/magnitude of mitigation measures. Specific indicators are a set of indicators that involve direct measurements in the field such as changes in the distribution/number of endangered species, changes in the area of intact ecosystems, and changes in species richness. For indicators to be reliable and practical, they must be cost-effective, be easily identified, be proxies for ecosystem integrity, and have cross-taxon congruency (Su *et al*., 2004). They must be also robust and sensitive to consistently respond to spatiotemporally changes of tropical forests (Imai *et al*., 2014). Generic indicators are superior in cost effectiveness,

while specific indicators are superior as proxies of biodiversity and sensitivity. Many possible biodiversity indicators have been proposed and discussed so far (Pereira *et al*., 2013).

Recently, Imai *et al*. (2014) proposed that the community composition of canopy trees as a specific indicator for biodiversity in spatiotemporally dynamic tropical forests, which satisfies the above-listed requirements for indicators. They quantified the community composition using axis-1 scores of an ordination of vegetation plots across a spectrum from primary forests to severely disturbed forests in Bornean production forests. They found that the index of community composition is a sensitive and robust indicator, which could be used to evaluate the impacts of disturbance on forest ecosystems, compared with species richness. However, there still is an unresolved issue related to the tree compositional indicator, which is the extraporation to landscapes; the indicator derived from field inventory plots needs to be extrapolated to the landscape, because field-based surveys to acquire such information at regional or national scales are not practical due to the large spatial extent involved, inaccessibility of some areas, and laborious work.

1.4. Remote sensing of tree-community composition

In order to apply the indicator to landscape level, integration of the tree compositional indicator with remote sensing is necessary. Remote sensing enables the acquisition of information about an object or phenomenon through a device that is not in a physical contact (Jones and Vaughan, 2010). Remote sensing has considerable potential as a source of information on biodiversity at landscape, regional, continental, and global spatial scales (Nagendra, 2001; Willis & Whittaker, 2002; Turner *et al*., 2003, Gillespie *et al*., 2008; Hansen and Loveland, 2012; Townshend *et al*., 2012; Zhu *et al*., 2012). In the remote sensing science, there are several types of sensors historically used. Over

the past 30 years, moderate-resolution optical sensors onboard such satellites such as the NASA Landsat series have been used for mapping the state of vegetation at landscape, regional, continental and global spatial scales (Roughgarden *et al*., 1991; Turner *et al*., 2003; Duro *et al*., 2007; Gillespie *et al*., 2008; Horning *et al*., 2010). High spatial resolution optical sensors (pixel size <10 m^2) on commercial satellites such as World View-2 have provided a new opportunity for habitat mapping at a finer spatial scale than moderate-resolution optical sensors (Clark *et al*., 2004; Nagendra *et al*., 2013). Imaging spectroscopy (also known as hyperspectral imagery) has improved accuracy for plant species identification, soil properties monitoring and habitat mapping, as well as plant physiological assessment (Ustin *et al*., 2004; Asner and Vitousek, 2005; Clark *et al*., 2005; Pu, 2009; Dahlin *et al*., 2013; Asner *et al*., 2014, 2015). Instruments such as a synthetic aperture radar (SAR) and light detection and ranging (LiDAR) are increasingly being used in ecology and natural resource management, providing significant opportunities for estimating aboveground biomass and 3D structures of forests (Vierling *et al*., 2008; Goetz *et al*., 2009).

Many remote sensing methods using imaging spectroscopy and airborne LiDAR have been developed to map ordination scores of community composition (Schmidtlein & Sassin, 2004; Schmidtlein *et al*., 2007; Feilhauer & Schmidtlein, 2009; Feilhauer *et al*., 2011; Gu *et al*., 2015; Higgins at al., 2015; Ioki *et al*., 2016). Althogh these sensors have a potential to detect small-scale disturbances that would not have been detectable by satellite remote sensing, the sensors are inferior in terms of scalability, continuity, affordability, and accessibility. In practical terms, the only realistic way to acquire repeated information at a broad spatial scale is still through satellite remote sensing (Foody *et al*., 2003; Turner *et al*., 2015). The NASA Landsat series are the most widely used sensor due to the ease in which the data can be obtained with ensured long time series and a low cost (Gillespie *et al*., 2008). The

series have significant importance on the utility of remote sensing for monitoring biodiversity change because they have its continuity, affordability, and accessibility (Turner *et al*., 2015). However, with relatively large pixel sizes of Landsat imagery (i.e., 30 m), pixel-level mixing of multiple species with different functional traits prevents comprehensive mapping of individual tree species or assemblages from progressing (Rocchini, 2007).

Using a gradient of community composition based on such ordination techniques as Imai *et al*. (2014) is one of the solutions to this problem. Ordination techniques facilitate comprehensive mapping by focusing on assemblages of taxa (species or genera) exhibiting profiles of ecological traits that can be estimated using remote sensing (Gu *et al*., 2015). However, the methods to estimate the ordination scores using Landsat imagery are very rare. Ohman & Gregory (2002), Thessler *et al*. (2005) and Higgins *et al*. (2012) estimated the variations of community composition according to environmental gradients based on Landsat imagery. Foody & Cutler (2003) classified Landsat imagery into nine forest classes defined on the basis of similarity in tree species composition using ordination scores. These studies showed a potential of Landsat imagery to characterize variations of tree-community composition based on ordination techniques. However, the studies using satellite remote sensing to quantitatively estimate tree-community composition based on ordination techniques are completely lacking for dynamic secondary tropical forests after clear cutting or selectively logging. If an indicator based on tree-community composition can be extrapolated to a landscape using Landsat imagery, repeated monitoring will be possible to monitor large-scale spatiotemporal changes of tropical forests, which will provide reliable assessments of the progress of the Aichi Biodiversity Targets and effectiveness of REDD+ safeguards.

1.5. Bridging gaps between ecology and remote sensing and research objectives

In order to develop a practical indicator that is spatiotemporally sensitive and robust, the synergy between remote sensing science and ecological understandings is a key (Pettorelli *et al*., 2016). There are two general approaches to integrate ecological understandings of biodiversity into remote sensing (Turner *et al*., 2003; Duro *et al*., 2007). One is the direct remote sensing of individual organisms, species assemblages or ecological communities. This approach can be used to directly quantify elements of biodiversity (e.g., individual or composition of species to derive maps of the pattern of species richness), assuming the direct link between the spectral, radar and light detection patterns and elements of biodiversity (Duro *et al*., 2007). The other approach is the indirect remote sensing, which uses remotely sensed data to measure variables that are known to correlate with biodiversity. Such variables include climatic and geophysical variables, which are then used for mapping vegetation types and habitats (Turner *et al*., 2003). In both approaches, there needs to be a sufficient theoretical basis to link the remotely sensed variables and aspects of biodiversity based on the understandings of ecological processes. Therefore, field data need to be collected and interpreted under a set of well-controlled observing conditions.

In order to collect sound field data in my thesis, I used two types of tropical forests as model system: secondary forests after shifting cultivation and production forests where timber is produced by selective logging. This is because these are the two anthropogenic disturbances accounting for the majority of deforestation and forest degradation in the tropical forests of Southeast Asia (Langner *et al*., 2007; Stibig *et al*., 2007; Hosonuma *et al*., 2012; Miettinen *et al*., 2014). Anthropogenic disturbances, such as clearing for agriculture or selective logging, cause wide-ranging impacts on canopy-tree species and structure, which depend on the duration, intensity, and frequency of the disturbances (Chazdon, 2003; Dent &Wright, 2009; Sodhi *et al*.,

2010).

Shifting cultivation is a direct cause of deforestation in tropical regions, and the area of associated secondary forests is expanding particularly in Borneo (Riswan & Hartanti, 1995; Langner *et al*., 2007). However, shifting cultivations consisting of temporarily cultivated land and associated fallows often do not appear on land use maps or in statistical records. This is partly due to the fact that shifting cultivation is a diverse and dynamic land use system, which is difficult to map (Scmidt-Vogt *et al*., 2009). In fact, the structure and composition of secondary forests after shifting cultivation are constantly changing (Spies, 1998) at a range of scales in space and time (He *et al*., 2011), but few researchers clarified the spatio-temporal dynamics of shifting cultivation. One of the reasons for this is a technological limitation. Remote sensing techniques with Geographic Information System (GIS) are specialized in a spatial analysis but not suitable for analyzing temporal information. In order to evaluate them legitimately in an ecological context, it is necessary to identify vegetation patches after shifting cultivation with distinct boundaries, spatial extent, and temporal information (particularly ages of the vegetation patches). Remote sensing techniques to date have emphasized to detect boundaries and spatial extents but temporal analyses remain immature. Therefore, I address the 1st research question how remote sensing technique can analyze temporal information of vegetation patches on such a spatiotemporally dynamic landscape (*Question 1*). If an algorithm using remote sensing could estimate stand age (i.e. the time elapsed after slash and burn) of a forest, the tree (plant)-community composition of a forest would be estimated indirectly because stand age is significantly related with the structure and composition of secondary vegetation (Fujiki *et al*., 2017). Therefore, I address the 2nd research question whether such an algorithm can evaluate the spatio-temporal dynamics of tree (plant)-community composition in secondary vegetation after shifting cultivation (*Question 2*).

Production forests where timber is produced by selective logging occupy a large chunk of the landscapes in Southeast Asian tropical rain forests (ITTO, 2006). Although selective logging has considerably high impacts on carbon emissions (Achard *et al*., 2002; Asner *et al*., 2005, 2010; Langner *et al*., 2012), earlier studies suggest that selective logging does not much reduce total species richness across a range of taxonomic groups (Gibson *et al*., 2011; Putz *et al*., 2012). Tree-community composition, however, is strongly affected by selective logging, as the number of pioneer species declines (Laurance & Laurance, 1996; Sekercioglu, 2002; Edwards *et al*., 2011) and the number of climax species increases (Hamer *et al*., 2003; Kitayama 2013; Imai *et al*., 2014). The mixing ratio of these two functional guilds apparently changes as logging intensity increases (Davis, 2000; Edwards *et al*., 2011, 2012). Therefore, I address the 3rd research question pertinent to production forests how remote sensing using moderate-resolution satellite imagery can characterize the interaction of linearly increasing pioneer guild and linearly decreasing climax guild with increasing logging intensity (*Question 3*). Because logging intensity varies greatly depending on different forest management practices (Langner *et al*., 2012; Putz *et al*., 2012), tree-community composition can express logging intensity and effects of management practices in tropical production forests (Imai *et al*., 2014). Therefore, I also examined the 4th research question whether the developed method can capture the effects of forest management practices using tree-community composition indicator in tropical production forests in a landscape context (*Question 4*).

The central aim of the present thesis is to examine the spatial representativeness of tree (plant)-community composition by developing algorithms to examine spatiotemporal changes of composition in tropical rain forests at a landscape level, and to examine the patterns of vegetation in relation to forest management schemes. I examine mosaics of secondary vegetation with various ages after shifting

cultivation and selectively-logged lowland forests in Borneo in the following chapters. Borneo is one of the most species-rich forests in the world (Myers *et al*., 2000) but at the same time cultivated land and logged-over lowland forests cover approximately 75 % of the total forest area (Langner *et al*., 2007). Evaluating the spatio-temporal effects of human disturbances on biodiversity is critical for effective conservation of tropical biodiversity. In such tropical forests, I address the following research questions:

Question 1 (Chapter 2): How can remote sensing technique analyze temporal information of vegetation patches on such a spatiotemporally dynamic landscape?
Question 2 (Chapter 3): Can algorithm in Chapter 2 evaluate the spatio-temporal dynamics of tree (plant)-community composition in secondary vegetation after shifting cultivation?
Question 3 (Chapter 4): How can remote sensing using moderate-resolution satellite imagery characterize the interaction of linearly increasing pioneer guilds and linearly decreasing climax guilds with increased logging intensity?
Question 4 (Chapter 4): Can the developed method capture the effects of forest management practices using tree-community composition indicator in tropical production forests in a landscape context?

I addressed Question 1 and 2 in secondary vegetation after shifting cultivation, and Question 3 and 4 in production forests where timber is produced by selective logging.

Chapter 2: Approach to estimate the ages of tropical secondary forests after shifting cultivation combining a high-resolution satellite image and time-series LANDSAT images

2.1. Abstract

I developed a new method to estimate stand ages of secondary vegetation in the Bornean montane zone, where local people conduct traditional shifting cultivation and protected areas are surrounded by patches of recovering secondary vegetation of various ages. Identifying stand ages at the landscape level is critical to improve conservation policies. I combined a high-resolution satellite image (WorldView-2) with time-series Landsat images. I extracted stand ages (the time elapsed since the most recent slash and burn) from a change-detection analysis with Landsat time-series images and superimposed the derived stand ages on the segments classified by object-based image analysis using WorldView-2. I regarded stand ages as a response variable, and object-based metrics as independent variables, to develop regression models that explain stand ages. Subsequently, I classified the vegetation of the target area into six age units and one rubber plantation unit (1–3 yr, 3–5 yr, 5–7 yr, 7–30 yr, 30–50 yr, > 50 yr and 'rubber plantation') using regression models and linear discriminant analyses. Validation demonstrated an accuracy of 84.3%. My approach is particularly effective in classifying highly dynamic pioneer vegetation younger than 7 years into 2-yr intervals, suggesting that rapid changes in vegetation canopies can be detected with high accuracy. The combination of a spectral time-series analysis and object-based metrics based on high-resolution imagery enabled the classification of dynamic vegetation under intensive shifting cultivation and yielded an informative land cover map based on stand ages.

2.2. Introduction

Only about 12% of Earth's land is allocated as protected areas (Hoekstra *et al*., 2005; UNEP-WCMC, 2008). Although strictly protected areas are essential for any credible conservation strategy (Margules and Pressey, 2000), it has become clear that reserves alone will not protect biodiversity because they are too isolated, too few, and too static (Liu *et al*., 2001; Bengtsson *et al*., 2003; Rodrigues *et al*., 2004). For these reasons, management outside of protected areas has become a crucial concern (Gaveau *et al*., 2013). Secondary forests surrounding patches of native vegetation are often termed a "matrix" (Forman, 1995). Matrices (i.e., protected areas with patches of surrounding secondary forest) are a dominant landscape element, and play an important role in ecosystem function (Fischer *et al*., 2006). For example, matrices provide a habitat for native species (Lindenmayer and Franklin 2002; Benton *et al*., 2003; Mayfield and Daily 2005; Fischer *et al*., 2005), enhance landscape connectivity by providing stepping stones or corridors (Baum *et al*., 2004), and reduce edge effects (Ries *et al*., 2004; Harper, 2005). To fully understand the function of a matrix and to design effective conservation strategies, information about related spatiotemporal patterns is crucial (Trejo and Dirzo, 2000; Sánchez-Azofeifa *et al*., 2005; Miles *et al*., 2006).

Many researchers have investigated vegetation patches in matrices based on spatial information such as shape, size, inter-patch distance, and edge width (Ranta *et al*., 1998). These pieces of information are key indicators of ecosystem function. However, "space-oriented" analyses often regard vegetation patches as spatially static. The structure and composition of matrices are constantly changing (Spies, 1998) on a range of spatial and temporal scales (He *et al*., 2011). In these dynamic systems, it has been shown that stand age is one of the most important predictors of ecosystem function (Hernández-Stefanoni *et al*., 2011; Becknell and Powers, 2014). For example, stand age is related to net primary productivity (He *et al*., 2012) and to the magnitude

and seasonality of carbon fluxes (Coursolle *et al*., 2012). However, stand ages in patches of secondary forest have rarely been studied at the landscape level. This is due in part to the lack of a standard procedure for documenting stand ages at the landscape level (Groeneveld *et al*., 2009). Thus, establishing a robust procedure for estimating stand ages at the landscape level is essential to understand the function of matrices and build effective strategies for conservation (Dash *et al*., 2015).

Moderate-resolution satellite images such as Landsat have been shown to be capable of obtaining local- or regional-scale forest variables (Wulder *et al*., 2004; Gaveau *et al*., 2014; Miettinen *et al*., 2014; Stibig *et al*., 2014; Chen *et al*., 2015; Dube and Mutanga, 2015a). However, they are inferior to higher-resolution satellite images for analyzing small and complex vegetation patches. A comparative study found that, in most cases, the accuracy of the retrieval of stand variables increased with higher spatial resolution (Hyyppä *et al*., 2000). However, a disadvantage of high-resolution satellite images (e.g., ground sample distance [GSD] < 4 m) is that solar canopy illumination and topographic effects cause high reflectance variability within a target domain (e.g., forest stand) in a pixel-based approach. Therefore, pixel-based approaches based solely on spectral information may not work successfully for high-resolution images, and can result in salt-and-pepper noise in the classification output (Ke *et al*., 2010). As an alternative approach, an object-based image analysis has been developed to solve the problems associated with the high-resolution domain (Blaschke *et al*., 2014). An object-based image analysis can use spatial information such as texture, size, shape, boundary conditions and contextual relationships in addition to spectral information. These spatial variables are often related to properties of vegetation cover, thus allowing for improved vegetation classification (Ke *et al*., 2010). In particular, image texture measures are related to complex forest canopy structures and can enhance the detection of biophysical properties even on closed

canopies (Dube and Mutanga, 2015b). For these reasons, object-based image analysis using high-resolution satellite images seems to be a feasible approach for analyzing small and complex vegetation patches (e.g., Burnett and Blaschke, 2003; Devereux *et al*., 2004; Laliberte *et al*., 2004; Langanke *et al*., 2007; Arvor *et al*., 2013).

Time-series satellite images can be used to investigate stand ages within vegetation patches, because past images can be used to reconstruct the time/place when/where forest disturbances occurred. However, the application of high-resolution satellite images to multi-temporal analysis is difficult because archived images may not be available and the associated monetary cost is high. On the other hand, Landsat images are useful for time-series analysis (Kennedy *et al*., 2007; Masek *et al*., 2008; Helmer *et al*., 2009; Huang *et al*., 2010; Hansen *et al*., 2013; Achard *et al*., 2014), and are also cost-effective, but are not readily applicable to tropical areas because available archived images are often compromised by clouds/haze (Hoekman, 1997; Asner, 2001; Hansen *et al*., 2008, 2009; Broich *et al*., 2011). The analysis of a single-date satellite image to derive information on forest disturbance and succession dynamics has been proposed to overcome this problem when a cloud-free image is available. Some studies have successfully classified tropical secondary forests into a certain range of stand age units using Landsat images (e.g., 1–5 yr, 6–10 yr, and 10–15 yr, Moran *et al*., 1994; 2–3 yr, 3–6 yr, 6–14 yr, and > 14 yr, Foody *et al*., 1996; 1–5 yr and 5–8 yr, Rignot *et al*., 1997; 3–6 yr, 10–20 yr, and 40–70 yr, Vieira *et al*., 2003; and 0–5 yr, 6–18 yr, Kuplich, 2006). These results indicate that secondary forests can be classified into age units at 5-year spans or greater with a high accuracy (approximately over 80%) using Landsat images. However, classifying forest into smaller age spans using single-date Landsat Thematic Mapper (TM) images may not be reliable (Nelson *et al*., 2000).

In this study, I propose a procedure for distinguishing boundaries and identifying stand ages within vegetation patches at shorter time intervals using remote

sensing techniques. The vegetation patches in the present study formed a component of a vegetation matrix consisting of protected areas and slash-and-burn fields in north Borneo. Specifically, I aimed to develop an approach that combines object-based analysis using a high-resolution satellite image with time-series analysis using moderate-resolution Landsat images. I used this approach to analyze spatiotemporal patterns among small and complex vegetation patches in a shifting cultivation area in Borneo, and aimed to classify stand ages into intervals shorter than 5 years. I assess the accuracy of this approach-based classification and discuss the ecological implications of the results.

2.3. Methodology

2.3.1. Study area and field survey

Kinabalu Park and Crocker Range Park, Sabah, Malaysia, include some of the most species-rich forests in the world (Beaman, 2005). My study area was located between these parks (Figure 2.1). The total size of the area is about 21,000 ha, and the altitude ranges from 300 m to 1,700 m. The center point of the study site is at 5°58′ N and 116°29′ E (Path 118 / Row 56). The total annual rainfall and mean annual temperature are approximately 2,000–2,500 mm and 15–24 °C, respectively. There is no significant seasonal variation in vegetation within this region. The geology of this area consists of tertiary sedimentary rock of the West Crocker Formation (ERE Consulting Group Sdn Bhd, 2011). The original vegetation is lower montane tropical rainforest, dominated by the families Fagaceae, Myrtaceae and Lauraceae (Kitayama, 1992; Aiba and Kitayama, 1999). In between the two parks, there is another local forest reserve with pristine vegetation, which is strictly protected from any subsistence uses by local regulations. Local people, therefore, conduct traditional shifting cultivation outside of the parks and the reserve. Within the local forest reserve, there are a variety of plant communities,

from primary forests to young secondary forests to herbaceous communities. Owing to a long history of shifting cultivation, very small patches of fragmented forest (smallest patch: < $90m^2$) are scattered throughout this area. The major crop of shifting cultivation in this area is hill paddy. Local people harvest it once or twice in the first year after slash and burn, and then abandon the farmland for fallow. The average fallow period of this area is 6.5 years, according to interviews with local people (n = 7).

I conducted a reconnaissance survey by driving and walking through the entire area. I visually identified vegetation patches and interviewed local people to identify the age of each patch (i.e., the time elapsed since the most recent slash and burn). I then selected representative vegetation patches with different ages to place inventory plots. The stand age and dominant species within each plot are shown in Appendix 2.1. The biomass and species composition in relation to stand ages are shown in Chapter 3. Field surveys were conducted in August 2012 and August 2013.

2.3.2. Outline of the approach

Landsat time-series images were used for change-detection analysis to detect past vegetation clearances (presumably slash and burn for shifting cultivation) that occurred just prior to the images being taken. The extents and ages of cleared areas were determined. I used a WorldView-2 image to classify the vegetation within the entire project area using object-based image analysis. Object-based classification generally consists of three steps: 1) creation of image segments, 2) extraction of object-based metrics, and 3) classification using the object-based metrics. As the first step of the object-based classification, I created the image segments and calculated object-based metrics. At this point, I overlaid the ages of cleared areas (as elucidated from the Landsat change-detection) on the segments created by the object-based image analysis,

and extracted the segments where vegetation clearance (slash and burn) occurred. The extracted segments contain both object-based metrics and stand age information. Outlier segments that do not represent true ages were removed based on a discrimination function determined by the object-based metrics. I established regression models for explaining stand age as a response variable, with object-based metrics as independent variables among the extracted segments. Subsequently, I classified the high-resolution satellite image into stand age units based on the model. The overall workflow of the approach is shown in Figure 2.2. I used ERDAS Imagine (ver. 11.0; ERDAS Inc., Atlanta, GA, USA) for change-detection analysis, and eCognition Developer (ver. 8.7; (Definiens AG, Munich, Germany) for object-based analyses.

2.3.3. Estimation of stand ages

2.3.3.1. Satellite images and image pre-processing

Orthorectified WorldView-2 multi spectral images (June 22, 2010), Landsat-5 TM (March 1, 1988; June 14, 1991; August 22, 1993; February 1, 1995; June 14, 1997; September 8, 1999; June 17, 2004; June 7, 2006; April 28, 2009), and Landsat-7 ETM+ (March 19, 2002) images were used in this study. The time intervals of the Landsat images used were not identical, because only cloud-free images (cloud cover < approximately 30%) were used in this study. The WorldView-2 satellite sensors consist of band 1 (blue: 450 to 510 nm), band 2 (green: 510 to 580 nm), band 3 (red: 630 to 690 nm), and band 4 (near-infrared: 770 to 895 nm). During pre-processing, raw digital numbers of each image were first converted into top-of-atmosphere radiance, from which I conducted atmospheric correction using the 6S (Second Simulation of a Satellite Signal in the Solar Spectrum) model (Vermote *et al*., 1997). Subsequently, topographically induced local variations in angular viewing geometry were reduced

using the method described by Ekstrand (1996). All clouds and cloud-shadows in each image were removed by unsupervised classification with ISODATA and visual inspection. ERDAS Imagine (ver.11.0; ERDAS Inc.) and ArcGIS 9.3 (ESRI, Redlands, CA, USA) were used during the entire pre-processing process.

2.3.3.2. Change-detection analysis

To derive stand age information, I conducted change-detection analysis with time-series Landsat images. Several change-detection techniques have been developed to date (Vogelmann *et al*., 2009; Raši *et al*., 2011; Hansen *et al*., 2012; Hussain *et al*., 2013; Vollmar *et al*., 2013). In this study, I applied the vegetation index differencing technique. This technique consists of separately calculating vegetation indexes from satellite images taken on two different dates, then subtracting the later vegetation index from the earlier vegetation index and identifying a suitable threshold for deriving meaningful vegetation changes (e.g., Townshend, 1995). This procedure meets my primary objective of detecting vegetation clearance only. In my study, the normalized difference vegetation index (NDVI) was used as a vegetation index to detect vegetation clearance because of its known theoretical and empirical relationships with vegetation abundance and greenness (Goward *et al*., 1991; Pettorelli *et al*., 2005; Wang *et al*., 2005; Veraverbeke *et al*., 2012). A total of 10 Landsat time-series images were separately converted into NDVI images. Adjoining images were successively subtracted (earlier minus later image) and NDVI differences were produced as new images (hereafter termed “difference image”). Subsequently, I collected approximately 300 pixels in each cleared and non-cleared area from each difference image by visual inspection. I compared those pixels in cleared areas with the same number of pixels in non-cleared areas (Figure 2.3). Thresholds of vegetation clearance were defined by the mean value of the first and third quartiles of each sample. Thresholds were 0.101

(2009), 0.088 (2006), 0.158 (2004), 0.13 (2002), 0.082 (1999), 0.162 (1996), 0.175 (1993), 0.153 (1991), and -0.2 (1988) (parenthetical numbers indicate years when vegetation was cleared). I used these procedures to detect and map cleared areas in each year for which images were available (Figure 2.4).

The 1988 difference image was created by subtracting the 1988 NDVI image from the 1991 NDVI image (later minus earlier image), and identifying the areas where the NDVI increased. Because most of the NDVI increments were due to vegetation recovery after clearance, the detected areas must have been affected by the vegetation clearance in 1988. This was necessary because there was no image from earlier than 1988 in this area.

2.3.3.3. Creation of image segmentation

I used a WorldView-2 image to create image segments based on object-based image analysis. Image segmentation requires several user-specified parameters. The weight parameters associated with input image layers were all set at 1. The input layers are shown in Table 2.1. A color/shape parameter associated with the spectral/shape criterion of homogeneity was set at 0.2. A compactness/smoothness parameter associated with the optimization criteria for object shape was set at 0.5. A scale parameter associated with the average size of resultant objects was set at 90. Each parameter was derived and adjusted by reiterating the image segmentation procedure (i.e. trial-and-error procedure) so that the vegetation patches where vegetation count-plots were placed could be clearly distinguished. I evaluated the results using visual inspection.

2.3.3.4. Extraction of object-based metrics

Object-based metrics were calculated based on the image layers shown in Table 2.1. I

calculated the mean, max, minimum, standard deviation values, and textures of the grey level co-occurrence matrix (GLCM) (Haralick, 1986) of each layer, and the brightness and maximum difference of all layers. GLCM is a tabulation of how often different combinations of grey levels occur at a specified distance and orientation in an image object (Baatz *et al*., 2004). GLCM was calculated using all pixels within the object. Texture metrics of objects (homogeneity, contrast, ang. 2nd moment, entropy, dissimilarity, correlation, mean, and standard deviation) were used for calculations. A total of 106 metrics were generated, including 34 metrics derived from WorldView-2 multispectral band value and vegetation indices, and 72 metrics from texture value. I regard these object-based metrics as independent variables to create the model that explains stand age.

2.3.3.5. Segment sampling

I integrated stand age data into object-based metrics to establish regression models. I overlaid the layer of the results of the Landsat change-detection with the results of the segmentation (Figure 2.5a). Subsequently, I manually extracted the segments that were inside the area where vegetation clearance occurred in a certain year (Figure 2.5b). I extracted all available sample segments across the area. At this point, the extracted segments had some uncertainties that needed to be reduced.

First, there may have been errors in the change-detection process. Therefore, when segments were extracted, I checked whether each segment area was cleared in a certain year by visually inspecting past Landsat images. Secondly, segments could be inadvertently identified as an older stand age than the actual age, because the specific stands corresponding to the segments could have been burnt later. For example, Figure 2.6a shows the segments extracted from an area cleared in 1991 (i.e., stand age of 19 years as of 2010). However, the upper part of the segments was cleared again in 2004

(i.e., stand age of 6 years). Such discrepancies were occasionally encountered in this procedure. To remove the segments representing incorrect stand ages, I conducted a linear discriminant analysis (LDA) among sample segments. LDA is a common classifier that has been used in many previous studies, e.g., tree species classification (Pu, 2009) and individual tree crown classification (Gong *et al*., 1997; Fung *et al*., 1998; Van Aardt and Wynne, 2000; Clark *et al*., 2005). This technique, which is based upon a multivariate linear model, can be used when there is a grouping variable and a set of predictors that can distinguish members of two or more groups. The technique identifies a weight for each of the predictors such that their linear combination maximally separates groups from one another (Duda & Hart, 1973; Tabachnick & Fidell, 2001; Huberty & Olejnik, 2006; Finch, 2014). Predictor variables used in LDA were chosen by a step-wise selection ($P < 0.01$).

I randomly divided the sample segments into two groups: two thirds of the sample segments were used as training data for LDA, and one third was used for validation. From the training sample segments, I built discriminant functions to distinguish outlier segments from the segments that represented an accurate age. Segments that were classified by LDA as being younger than their own age were removed as follows: 1-year-old segments were removed from 4-year-old segments (Figure 2.6b), 1- and 4-year-old segments were removed from 6-year-old segments (Figure 2.6c,d), and 1 to 6-year-old segments were removed from 8 to 22-year-old segments (Figure 2.6e). It was difficult to distinguish outlier segments after 6 years of age (e.g. 8-year-old segments vs 11-year-old segments) using LDA. I tried this correction but the accuracy was low (< 70%). Considering the low accuracy and the present fallow period of this area (6.5 years on average), I decided not to add corrections after 6 years of age.

A third source of error was that the shapes of segments did not completely

match the shapes of cleared areas identified on Landsat images (Figure 2.7a). For example, some segments were mixed with surrounding (older) vegetation. To remove the segments erroneously regarded as extremely old, I conducted LDA between 1–22-year-old segments and segments of primary forest. Segments of primary forest were extracted at random from the area inside the local primary forest reserve. The results of LDA are shown in Figure 2.7b. 1–22-year-old segments that were erroneously classified as primary forest were removed from the following analyses.

In addition to the segments derived from the procedure above, I used several additional segments based on my field survey to build my models (including 6 segments 30–40 years old, 8 segments 50 years old, and 23 segments 100 years old). I also added segments from old-growth primary forest (presumably much more than 100 years old). Rubber plantations represented one of the types of land cover in my study area. I identified a total of 403 segments that corresponded to rubber plantations based on my field reconnaissance and visual inspection of the WorldView-2 image. Table 2.2 shows the entire set of segments used for establishing the following models.

2.3.3.6. Model establishment

I established regression models among selected segments using the ages of the segments extracted in the above procedure as response variables and metrics of the segments on the WorldView-2 image as independent variables. Before establishing the regression models, I divided the WorldView-2 segments into some broad vegetation types with a decision tree method, using an NDVI threshold and LDA. This was because it is difficult to establish a single regression model that can estimate the ages of all vegetation patches at the same time. Separately establishing regression models for each vegetation type provided superior accuracy. The Pearson correlation coefficient was used for analysis of correlation between stand ages and selected model

variables. The predictor variables of LDA and explanatory variables of regression models were chosen by step-wise selection ($P < 0.01$).

2.3.3.7. Decision tree

First, I identified non-vegetated segments and segments older than 50 years from the entire target area using an NDVI threshold and an LDA; these segments were eliminated using the following procedure. Bare ground and a sparse herbaceous community (occurring typically a few months after burning) were defined as "non-vegetated" segments, and only segments that were completely covered with vegetation (grasses or trees) were defined as "vegetated" segments. This was necessary because an aggrading phase of the herbaceous community represented a broad continuum from bare ground and yet was distinct from denser grassland at 1 year after burning. Subsequently, vegetation less than 50 years old was subdivided into vegetation younger than 7 years and vegetation older than 7 years by LDA, since the regression model using 1–50-yr-old vegetation became saturated after 7 years. Vegetation more than 7 years old was further subdivided into 'rubber plantations' and 'other vegetation' using LDA. Finally, I established a multivariate regression model for vegetation less than 7 years old and a single regression model for 7–50-year-old vegetation to classify them further into subdivisions.

2.3.4. Assessment of classification accuracy

The ages of 97 areas of secondary vegetation stands and 44 areas of rubber plantations were determined by interviewing local people. However, the ages derived from these interviews were not always accurate (based on Landsat images). This suggests that even land owners do not remember the year when they conducted the last slash and burn. Therefore, the ages derived from interviews could not be used for validation.

Instead, I divided all sample segments, except for rubber plantations, randomly into two categories: two thirds for building the model and one third for validation (Table 2.2). For rubber plantations, only samples obtained in the field survey were used for validation. The accuracy of classification was assessed and expressed as the percentage correct allocation and the kappa coefficient of agreement (Rosenfield and Fitzpatricklins, 1986), which are widely used in the assessment of image classifications.

2.3.5. Ecological implications of the selected model variables

To investigate the vegetation properties that the selected model variables could explain, I compared model variables with biomass and canopy heterogeneity patterns using the chronosequences of rubber plantations and secondary vegetation in slash-and-burn areas. Biomass increases with age in both chronosequences. However, canopy heterogeneity is consistently low in the rubber plantation chronosequence consisting of a single tree species throughout, whereas canopy heterogeneity is much greater and temporally variable in the secondary-vegetation chronosequence consisting of many canopy species. I investigated the response of the selected model variables to canopy properties by comparing these two vegetation types. Stepwise linear regression analysis was applied to the segments where stand ages were identified (either rubber plantations or secondary vegetation) with the logarithm of stand ages as the response variable and object-based metrics as independent variables. Pearson's correlation coefficient was used to assess correlations among the stand ages and the selected model variables.

2.4. Results

2.4.1. Decision tree and model establishment

An NDVI threshold of 0.715 was selected to divide non-vegetated segments from vegetated segments. The value of this threshold was determined based on visual inspection. Subsequently, LDA was conducted to classify vegetated segments (NDVI 0.715 or greater) into further subdivisions (i.e., vegetation more than 50 years old and vegetation less than 50 years old). The results of LDA are shown in Figure 2.8a. Subsequently, vegetation less than 50 years old was subdivided into vegetation less than 7 years old and vegetation more than 7 years old using LDA; the results are shown in Figure 2.8b. Vegetation more than 7 years old was further subdivided into 'rubber plantations' and 'other vegetation' using LDA (Figure 2.8c). The error rate of LDA in discriminating rubber plantations from other vegetation was very low (0.009).

I established a multivariate regression model for vegetation less than 7 years old. The model showed a good fit (R^2 = 0.841, and R^2adj = 0.837) (Figure 2.9a). Table 2.3 shows the variables selected by stepwise selection. Variables are arranged in order of decreasing correlation based on Pearson's correlation coefficient. This model (Model 1) was applied to the segments that were classified as vegetation less than 7 years old. Although the model's coefficient of correlation was high, the accuracy of age classification using 1-year increments was relatively low: 50%, 36% and 29% for the 1-year, 4-year and 6-year ages, respectively (Appendix 2.10). I judged that ages could not be reliably estimated using 1-year increments, and that estimating the ages of stands using 2-year intervals (i.e., 1- to 3-yr, 3- to 5-yr and 5- to 7-yr) is optimal. The segments that were classified as 'vegetation older than 7 years' using this model were all checked by visual inspection, and all of them were found to be non-vegetation (shadow-covered bare ground). Consequently, I removed them from the analysis.

For 7–50-year-old vegetation, I established a single regression model using the mean value of band 2 (Mean_Band2) with an R^2 value of 0.609 (Figure 2.9b, Table 2.3). This model (Model 2) was applied to segments that were classified by LDA as

7–50 years old, yielding two vegetation subgroups (7–30-yr-old vegetation and 30–50-yr-old vegetation). The results of decision tree analysis are shown in Figure 2.10.

2.4.2. Stand age map

The final results of the classification are shown in Figure 2.11. Strictly protected areas were classified as more than 50 years old (dark blue color), including the local forest reserve and the two parks: Kinabalu Park (upper-right side of the image) and Crocker Range Park (lower-left side of the image). Furthermore, dense rubber plantations (left side of the image) were clearly detected. The relative area of each classified unit within the entire target area was 7.5% for non-vegetated stands, 4.9% for 1- to 3-year-old vegetation, 9.2% for 3- to 5-year-old vegetation, 9.1% for 5- to 7-year-old vegetation, 27.9% for 7- to 30-year-old vegetation, 5.4% for 30- to 50-year-old vegetation, 32.5% for vegetation older than 50 years, and 3.4% for rubber plantations. Figure 2.12 shows a histogram of estimated ages among 1–50-year-old segments based on Model 1 and Model 2 (Figure 2.9a,b). The number of segments rapidly decreased in vegetation older than 6.5 years.

2.4.3. Classification accuracy and the selected model variables

I compared the results of the classification with the results determined through my validation procedure (Table 2.4). The overall accuracy of the classification was 84.28% and the overall kappa coefficient was 0.7677. The producer's accuracy of each classified unit was 88.98% (1- to 3-yr-old segments), 52.63% (3- to 5-yr-old segments), 53.85% (5- to 7-yr-old segments), 75.6% (7- to 30-yr-old segments), 100% (30- to 50-yr-old segments), 94.68% (> 50-yr-old segments), and 79.55% (rubber). Thus, classification showed a reasonable degree of accuracy. A large proportion of observed

errors arose from misallocations between neighboring units. There was great variability associated with the variation in sample size. For example, there were only two sample segments between 30 and 50 years old, an age interval that had a very low accuracy.

Only Mean_Band2 was chosen as an effective variable in the stepwise linear regression analysis of rubber plantations when I compared the selected variables with the chronosequences of rubber plantations and secondary vegetation. On the other hand, texture metrics (including standard deviation) in addition to Mean_Band2 were chosen as effective variables in the regression analysis of secondary vegetation (Appendix 2.11).

2.5. Discussion

My results show that stand ages of tropical secondary vegetation can be identified and vegetation types based on stand age can be mapped with a high accuracy (84.28%) based on the combination of WorldView-2 and time-series Landsat images. The high accuracy of the stand age map is attributed to the use of object-based metrics. In my models, metrics related to the mean value of the green wavelength (Mean_Band2; wavelength 510–580 nm) and to the texture (including standard deviation) were selected. These metrics likely represent variation in the uppermost layer of vegetation in terms of foliar properties and canopy heterogeneity. The high accuracy may in part be explained by the LDA procedure applied to remove outlier segments a priori (see 2.3.3.5: Segment sampling). Certainly, it is due to the use of my models with meaningful variables and object-based metrics. I elaborate below on the variables selected.

Mean_Band2 is related to the green wavelength of 510–580 nm. The green wavelength is known to be strongly related to chlorophyll-a concentration. Gitelson *et al.* (1996) showed that the maximum sensitivity of chlorophyll-a concentration occurs

in the green band from 520 to 630 nm, and that the inverse of the reflectance in the green band was proportional to chlorophyll-a concentration with $R^2 > 0.95$. Another study using Quickbird satellite data showed that relative green waveband digital number (DN) had a higher correlation than any of the other indices investigated with respect to foliar nitrogen concentration ($R^2 = 0.91$), relative grain yield ($R^2 = 0.81$) and relative total biomass in crops ($R^2 = 0.59$) (Bausch *et al*., 2008). The high accuracy of my classification based on segment metrics may be related to the inclusion of the green wavelength, which reflects changes in foliar properties (e.g. chlorophyll-a and nitrogen concentration) during forest succession.

As for texture metrics, they are known to capture heterogeneity of tree structural attributes. Previous studies have demonstrated the application of texture metrics derived from high-resolution sensors to estimate various tree structural attributes such as tree height, leaf area index, stand density, and biomass (Pandey *et al*., 2010; Nichol and Sarker, 2011; Ozdemir and Karnieli, 2011; Sarker and Nichol, 2011; Eckert, 2012; Shamsoddini *et al*., 2013). For example, Eckert (2012) showed that WorldView-2 texture metrics correlated better with tree structure (R^2adj = 0.84) than spectral reflectance or band ratios, owing to their sensitivity to the spatial aspects of canopy shadow. Shamsoddini *et al*. (2013) and Ozdemir and Karnieli (2011) also found a very strong relationship between WorldView-2 texture metrics and variables related to tree structure (stand volume, basal area, stand density, and tree height). Consistent with these studies, texture metrics enhanced above-ground biomass estimates by increasing a saturation level that occurs at a much lower biomass value in the analyses using only spectral indices (Kuplich *et al*., 2005; Sarker and Nichol, 2011; Xu *et al*., 2011; Eckert, 2012; Vashum and Jayakumar, 2012; Dube and Mutanga, 2015b).

My suggestions regarding the significance of model variables described above are corroborated by the results of the comparison between rubber plantation vs.

secondary vegetation chronosequences. The Mean_Band2 and texture metrics were chosen as effective variables in secondary vegetation, whereas only Mean_Band2 was chosen for use in rubber plantations. Secondary vegetation consists of multiple canopy species, with canopy species shifting continuously along the vegetation chronosequence and giving rise to a variety of foliar and structural attributes within and among vegetation types. Therefore, textural metrics were chosen only for secondary vegetation but not for rubber plantations. In contrast, Mean_Band2 was chosen for both secondary vegetation and rubber plantations because the mean value of band 2 is related to the foliar chlorophyll-a concentration, which changes with canopy development in both secondary vegetation and rubber plantations. The selected object-based metrics in my models appear to reflect variation in canopy heterogeneity and foliar properties in the uppermost layer of vegetation in successional sere. One reason for the high accuracy of my approach is, thus, related to the inclusion of object-based metrics.

The inclusion of object-based metrics probably also increased the model fitness per se. The coefficient of determination (R^2 = 0.841) of my model for 1–7-year-old vegetation was much higher than that of comparable previous studies (i.e., R^2 = 0.37 for 1–7-year-old vegetation, Nelson *et al*., 2000; R^2 = 0.75 for 1–9-year-old vegetation, Kims *et al*., 1999). In contrast, the coefficient of determination of the model for vegetation older than 7 years was lower. This is because the estimated age of a given segment becomes saturated after trees form a closed upper canopy (i.e. 7 years). Previous studies have shown that image saturation occurring post canopy closure limits the utility of optical data for predicting stand parameters (Tomppo *et al*., 1999). In my target area, dominant species of younger vegetation may change rapidly from herbs to shrubs to pioneer trees in less than 7 years, whereas the rate of species turnover becomes slower in older secondary forest (Fujiki *et al*., 2017). The slow rate of change

in vegetation composition after 7 years may result in more homogeneous canopy and cause model saturation.

My results appear to demonstrate spatiotemporal patterns of the land dynamics that occur in a matrix landscape. The areas surrounding the protected areas are under the heavy influence of shifting cultivation and, as a result, consist of a variety of vegetation patches of different successional ages. Fujiki *et al*. (2017) classified the vegetation of the same area based on species composition using Two-Way Indicator Species Analysis (TWINSPAN). Their results correspond well with my own classification: the 1–3-year-old and 3–5-year-old vegetation corresponds with herbaceous communities; the 5–7-year-old vegetation corresponds with short scrub communities; the 7–30-year-old vegetation corresponds with scrub and short secondary forest communities; and the 30–50-year-old vegetation corresponds with old-growth secondary forest. The area under cultivation, as well as relatively young (< 7 years old) herbaceous or short scrub vegetation, comprises 30.7% of the entire area. On the other hand, the number of segments for a given age interval rapidly decreases after 6.5 years. This corresponds to the mean fallow period of the shifting cultivation by local people, which is 6.5 years in my study area. Thus, a relatively small proportion (30.7%) of my study area (but which contains many small land parcels) is intensively cultivated by local people using slash-and-burn methods. In contrast, a nearly equal area (33.3%, 7–50-yr-old vegetation) escapes from cultivation and develops into old-growth secondary forest; 32.5% of the area is well-protected. My analysis clearly reflects the behavior of local people and successional patterns of secondary vegetation.

Such stand age information has significant implications for policy and conservation applications, because it provides a critical dataset required for ecological modeling (Coursolle *et al*., 2012; He *et al*., 2012) and accurate carbon estimation (Zheng *et al*., 2007; Becknell and Powers, 2014). Stand age is one of the most

important proxies of ecological processes in dynamic vegetation (Hernández-Stefanoni *et al*., 2011). Understanding ecological processes in matrices consisting of protected areas interspersed with converted lands is essential to develop strategies to conserve biodiversity (Fischer *et al*., 2006) by enhancing connectivity between the protected areas. As for carbon estimation, it is well known that stand age is one of the best carbon stock proxies in secondary forests (Jepsen 2006, Kendawang *et al*. 2007, Kenzo *et al*., 2010). Stand age information based on my approach can drastically improve the estimation of carbon stock in a landscape context. It helps establish a credible carbon baseline against which emission reduction is calculated for implementing REDD+ (Reducing Emissions from Deforestation and Forest Degradation +) (UNFCCC, 2015). My approach provides valuable information to improve matrix management and evidence-based decision-making.

To acquire stand age information, my approach does not require extensive field inventories. They will be especially useful for mountainous regions, since the application of remote sensing to mountainous areas is restricted (Barbosa *et al*., 2014) and surveying vegetation in mountainous regions is laborious, expensive and time-consuming (Lu, 2006). A new methodology that avoids technical constraints and minimizes labor efforts is urgently needed for mountainous regions (Soenen *et al*., 2010). My approach can provide detailed stand age information even in mountainous areas covering a wide altitude range (in the present study, from 300 m to 1,700 m). The principle of combining time-series Landsat images and a high-resolution satellite image may also be applicable to other areas, since vegetation recovery after clearance is a widespread biological phenomenon. Considering that the newly launched Landsat 8 multispectral sensor is available from 2013 and is capable of detecting forest variables accurately (Dube and Mutanga, 2015a), my approach using time-series Landsat images will continue to be useful.

Although my approach could successfully reconstruct stand ages, particularly in a young successional sere, there are several remaining difficulties. First, to estimate stand ages, my approach requires a land-use history of complete vegetation clearance. Therefore, my methods cannot be applied to land mosaics that do not undergo complete denudation during land-use practices as well as to the areas where complete defoliation occurs during seasonal changes. Second, image saturation in older forests generally limits the utility of optical data for predicting stand structures. This problem appeared to occur in my study and I was unable to improve the accuracy of estimation for older forests. Further work is required to resolve this saturation problem. However, the primary objective of my study was to classify the small, complex vegetation patches of early successional stages into age units with relatively short time intervals; I achieved this objective by combining moderate-resolution time-series images with a high-resolution satellite image.

Human judgment in the manual procedure of segment sampling (i.e. 2.3.5: Segment sampling) may be another concern when one duplicates myapproach in other areas. The sampling procedure involving personal judgments is followed by the LDA to remove outlier segments, which can eliminate judgment errors. Therefore, my approach minimizes artifacts related to human judgments per se. However, its scalability must be further investigated in future research.

2.6. Conclusion

I estimated the stand ages of dynamic vegetation patches using models with object-based metrics and mapped the vegetation types based on stand age in a landscape matrix consisting of two protected areas and patches of slash-and-burn agriculture in north Borneo. I combined single-time, high-resolution WorldView-2 imagery with time-series Landsat images to derive models for estimating stand ages,

and subsequently applied the models to the entire landscape on the WorldView-2 imagery. The overall accuracy of identifying vegetation types was high (84.28%), which I attributed to the use of the object-based metrics derived from the high-resolution WorldView-2 imagery in the models. Time-series Landsat images were effective to derive the land history of the dynamic vegetation under slash-and-burn for which no other historical records were available. My approach combining a single-time WorldView-2 image with time-series Landsat images is effective (in places where no historical records are available), accurate, and cost-effective. The cost-effectiveness of the approach is related to the need for one high-resolution image only.

Tables

Table 2.1

Input layers for segmentation in object-based classification using WorldView-2

	Layer	Equation	Reference
Multi spectral band	Blue, Green, Red, NIR		
Vegetation Index	NDVI	(NIR-Red)/(NIR+Red)	Rouse *et al*. (1974)
	GNDVI	(NIR-Green)/(NIR+Green)	Gitelson *et al* (1996)
	SVI	NIR/Red	Birth and McVey (1968)
	TNDVI	$(NDVI+0.5)^{0.5}$	Deering *et al*.(1975)

NIR, near-infrared; NDVI, normalized difference vegetation index; GNDVI, green NDVI; SVI, simple vegetation index; TNDVI, transformed NDVI.

Table 2.2

The number of sample segments used to develop (Model) and validate the models (Validation). Sample segments were obtained from the inspection of high-resolution satellite data and from field reconnaissance. “Rubber” indicates rubber plantations, which is a distinct vegetation category. An independent model was established to predict this category.

	Age (cleared year)	Model	Validation	Sum
Satellite base	01 (2009)	238	118	357
	04 (2006)	113	57	170
	06 (2004)	159	79	238
	08 (2002)	158	79	237
	11 (1999)	106	53	159
	13 (1997)	93	46	139
	15 (1995)	72	36	108
	17 (1993)	73	37	110
	19 (1991)	180	90	270
	22 (1988)	68	34	102
Reconnaissance	30–40	4	2	6
	50	6	2	8
	100	15	8	23
	old	1,333	667	2,000
Rubber	Satellite-based	359	0	359
	Reconnaissance	0	44	44
Sum		2,503	1,296	4,325

Table 2.3

Variables selected by stepwise selection and coefficients of Model 1 and Model 2. Variables are arranged in order of decreasing correlation based on Pearson's correlation coefficient (r) for linear relationships between stand age and the object-based metrics derived from the WorlView-2 segments. R^2 and R^2adj are the coefficients of correlation of each model.

	R^2	R^2adj	Coefficient	SE	Pearson's r
Model 1 (for vegetation < 7 yr)					
Mean_Band2	0.841	0.838	-0.0086	6.97E-04	-0.78
Mean_GNDVI			13.6625	2.56E+00	0.716
GLCM_Dissimilarity (all dir.)			0.8749	6.94E-02	0.675
Max_GNDVI			-16.9153	2.60E+00	0.58
GLCM_Contrast (all dir.)			-0.0091	1.14E-03	0.57
GLCM_Correlation_Band2			-4.3475	6.41E-01	-0.511
GLCM_Entropy_NDVI			2.9493	6.34E-01	0.368
GLCM_Entropy_GNDVI			-2.0841	6.21E-01	0.356
GLCM_Standard deviation_SVI			-0.1453	2.23E-02	-0.245
GLCM_Mean_Band1			-0.1673	3.22E-02	-0.219
Standard deviation_Band4			0.0069	6.23E-04	0.179
GLCM_Homogeneity_Band3			-14.0958	3.63E+00	-0.135
GLCM_Standard deviation_Band2			-0.166	3.06E-02	0.055
Constant			33.3628	4.94E+00	
Model 2 (for vegetation > 7 yr)					
Mean_Band2	0.610	0.609	-0.0033	7.51E-05	-0.781
Constant			3.186	5.34E-02	

SE, standard error; GNDVI, green normalized difference vegetation index; NDVI, normalized difference vegetation index; SVI, simple vegetation index; GLCM, grey level co-occurrence matrix.

Table 2.4

Confusion matrix and accuracies of the stand age classification

		Actual unit								User's
		1–3 yr	3–5 yr	5–7 yr	7–30 yr	30–50 yr	Over 50 yr	rubber	Sum	accuracy (%)
	1–3 yr	105	7	0	0	0	2	0	114	92.11
	3–5 yr	9	30	11	3	0	5	2	60	50
	5–7 yr	1	13	42	27	0	5	4	92	45.65
Predicted	7–30 yr	1	5	21	282	0	15	1	325	86.77
Unit	30–50 yr	0	0	4	49	2	9	0	64	3.13
	Over 50 yr	2	1	0	6	0	641	2	652	98.31
	Rubber	0	1	0	6	0	0	35	42	83.33
	Sum	118	57	78	373	2	677	44	1349	
Producer's accuracy (%)		88.98	52.63	53.85	75.6	100	94.68	79.55		

The overall classification accuracy was 84.28%, and the overall kappa coefficient was 0.7677.

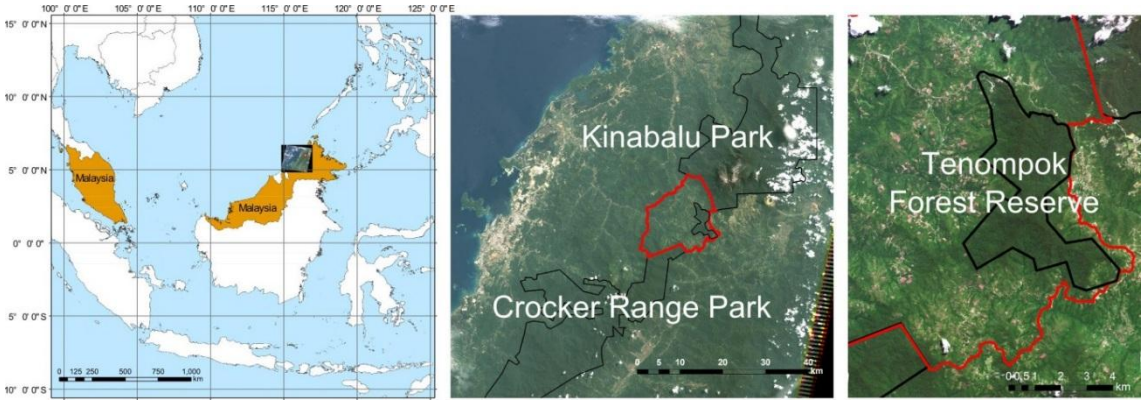

Figure 2.1. The location of the study site (left diagram), general area of the study site, bounded by the red line (central diagram,) and a close-up view of the study site with vegetation patches of slash-and-burn agriculture with the local forest reserve (Tenompok Forest Reserve) in the center (right diagram). The central diagram is derived from a Landsat-TM image. The right-hand diagram is derived from a WorldView-2 image.

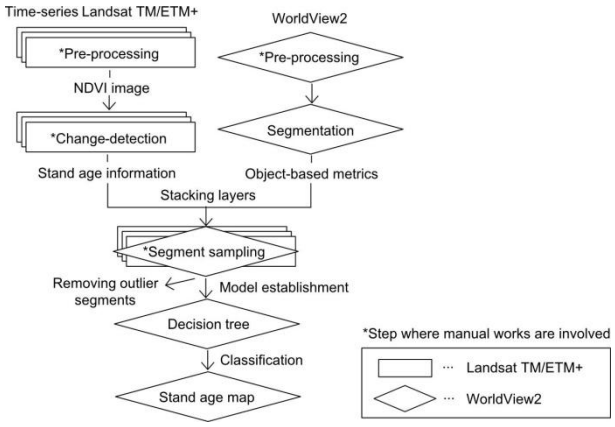

Figure 2.2. Overall workflow of the approach to classify vegetation based on stand ages. Rhomboid flames represent the WorldView-2 (2010) image; rectangular flames represent time-series Landsat images.

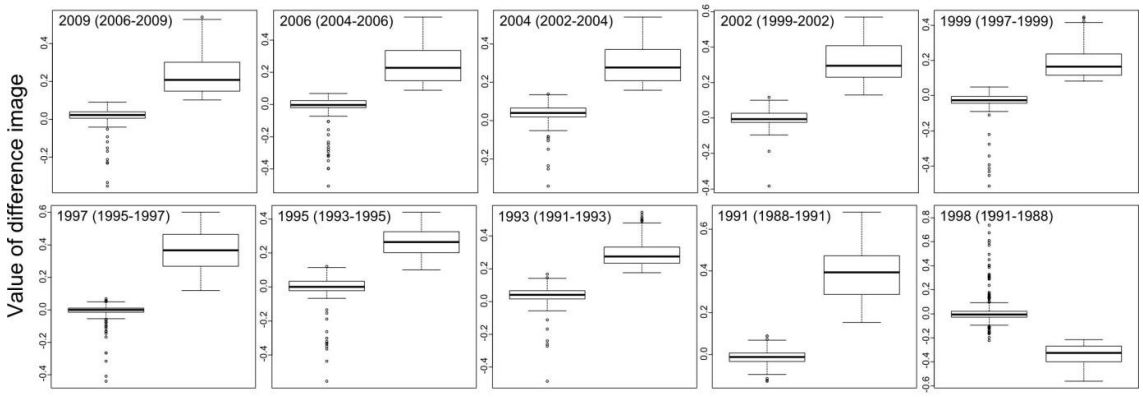

Figure 2.3. Comparison of normalized difference vegetation index (NDVI) changes during given years (numbers in parentheses) between non-cleared (left box) and cleared areas (right box). Differences between earlier-year NDVI minus later-year NDVI values based on approximately 300 pixels in each of cleared and non-cleared areas are shown as boxplots. Numbers in the upper left of each diagram indicate the year during which vegetation clearance occurred. Numbers in parentheses represent years of acquisition for NDVI images, from which difference images were calculated. A threshold of vegetation clearance was defined by the mean value of the first quartile of the right box and the third quartile of the left box in each diagram, except for the difference image in 1988. The threshold of vegetation clearance in 1988 was calculated by the mean value of the third quartile of the right box and the first quartile of the left box.

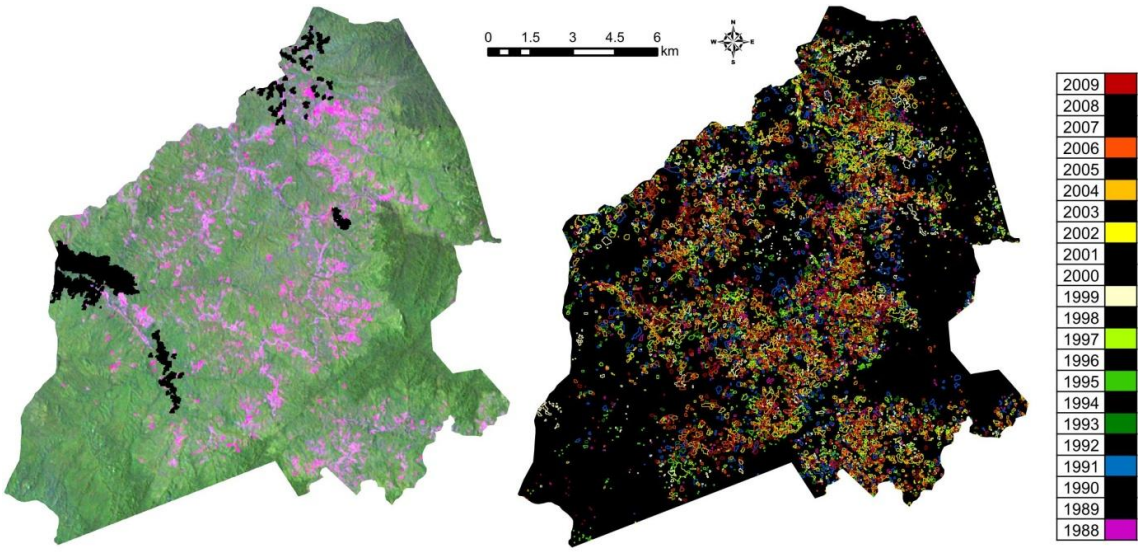

Figure 2.4. Landsat-TM 2009 image (RGB / Band7, Band4, Band3) (left) and the results of change-detection, which indicates the occurrence of vegetation clearance, presumably due to slash-and-burn practices (right). Different colors indicate years in which clearance took place.

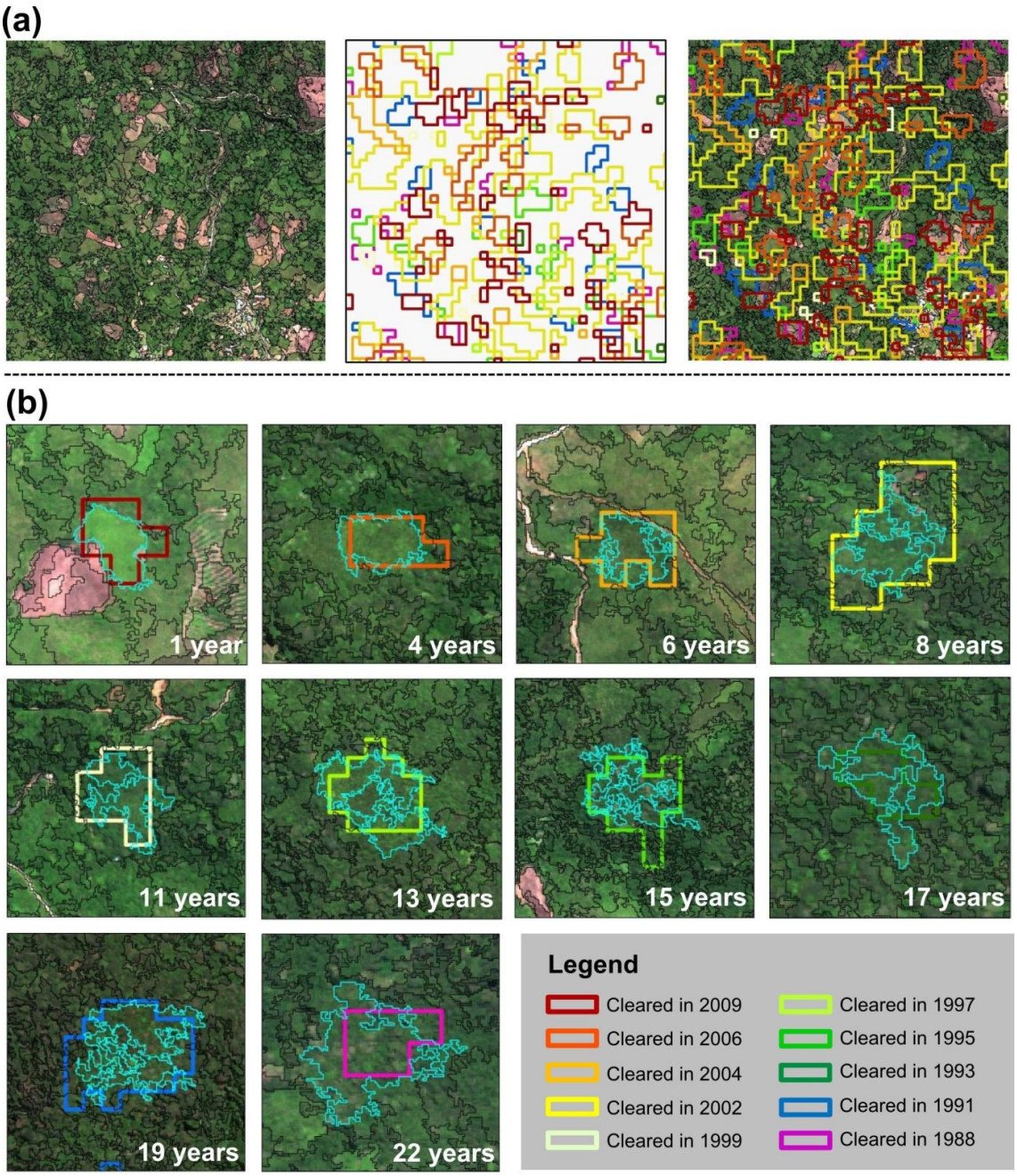

Figure 2.5. (a): The results of segmentation within a certain part of the study area (left diagram), in which each segment accommodates 106 object-based metrics; the results of change-detection analysis in the same area (central diagram); the image after stacking the left and central diagrams (right diagram). Different colors indicate years in which clearance took place. The legend is the same as for Figure 2.5(b). **(b):** Examples

of the overlay of cleared pixels derived from Landsat change-detection and a corresponding segment derived from object-based analysis of high-resolution WorldView-2. Light-blue segments indicate the extracted segments that corresponded with each cleared area detected by Landsat change-detection. Years indicate stand ages.

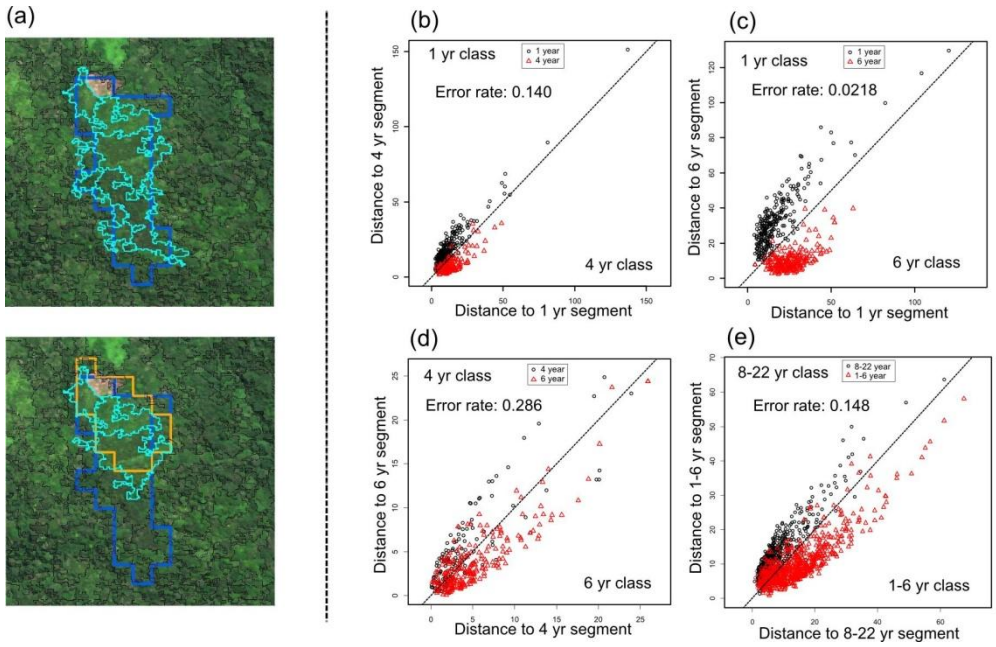

Figure 2.6. (a): Two examples of the overlay of a segment (derived from high-resolution WorldView-2 by object-based classification) and pixels (derived from the Landsat change-detection) cleared in 1991 (blue lines) and in 2004 (orange lines). Light-blue lines indicate extracted sample segments. The upper part of the segments cleared in 1991 (upper figure) was cleared again in 2004 (lower figure) **(b)–(e):** Results of linear discriminant analyses (LDA) dividing sample segments. In each diagram, a dotted line divides given samples into two units. "Distance" indicates the Mahalanobis squared distance of every sample to the center of gravity of two classes. Diagonal lines represent the boundary between two classes. Variables selected for LDA and confusion matrices of validation data are shown in Appendix 2.2–2.5.

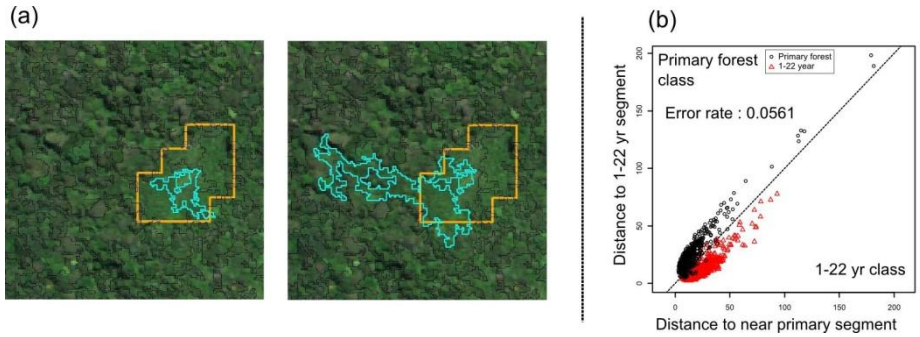

Figure 2.7. (a): Two examples of the overlay of a segment (derived from high-resolution WorldView-2 by object-based classification) and pixels of cleared area (derived from Landsat change-detection), demonstrating a complete match (left) and a partial match (right). Light-blue lines indicate segments, and orange lines indicate cleared pixels in 2004. **(b):** Results of LDA dividing sample segments into segments that are close to primary forest and segments that are classified as 1–22-year-old vegetation. Selected LDA variables and confusion matrices of validation data are shown in Appendix 2.6.

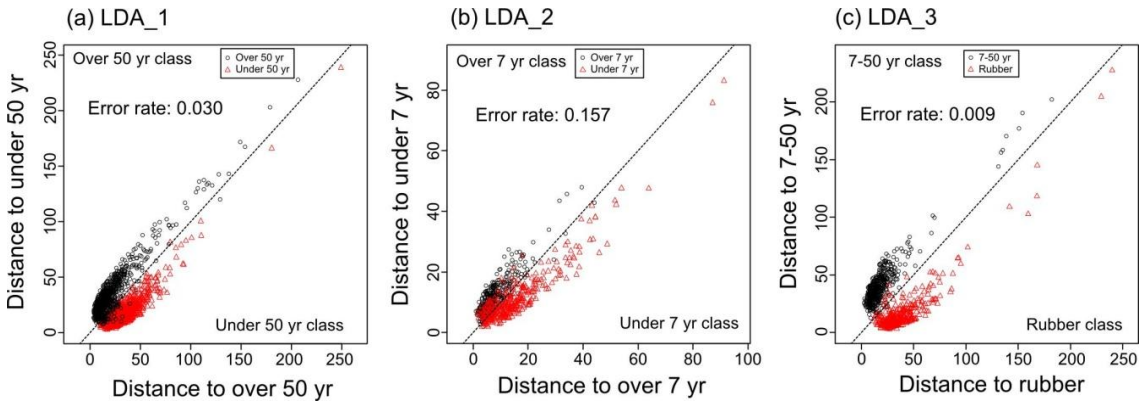

Figure 2.8. Results of LDA dividing of given samples into two units in the decision tree. "Distance" indicates the Mahalanobis squared distance of every sample to the center of gravity of two classes. The diagonal line represents the boundary between two classes. Selected variables are shown in Appendix 2.7–2.9.

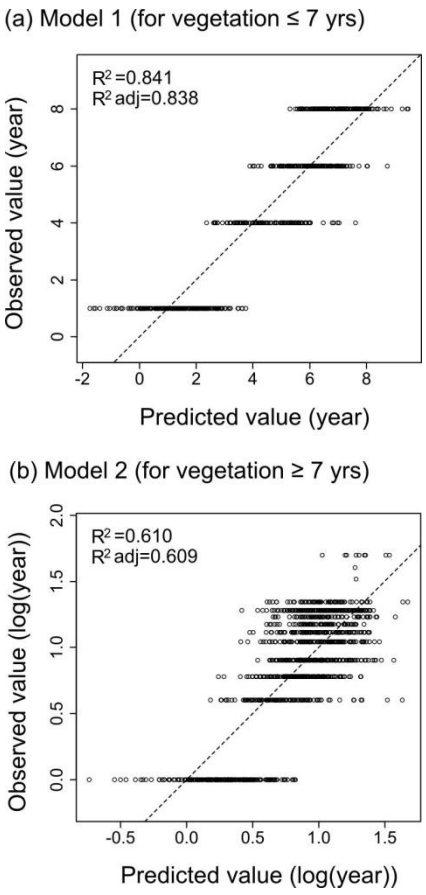

Figure 2.9. (a): Comparison of observed values against predicted values based on a multivariate regression model for vegetation less than 7 years old. **(b)**: Single regression model for vegetation more than 7 years old.

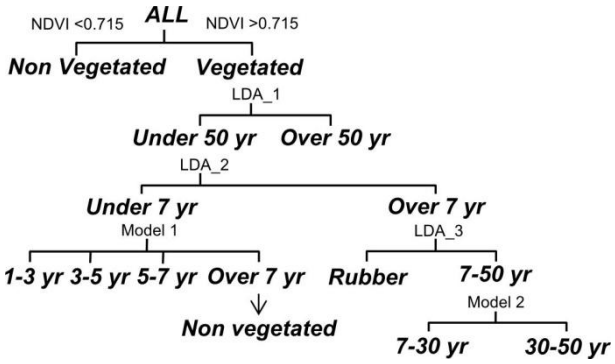

Figure 2.10. The decision tree for classification categories. Bold italic fonts represent vegetation units; roman-type gothic fonts represent criterions of discrimination; "LDA_1", "LDA_2" and "LDA_3" correspond to Figure 2.8a, b and c, respectively. "Model 1" and "Model 2" correspond to Figure 9a and b, respectively.

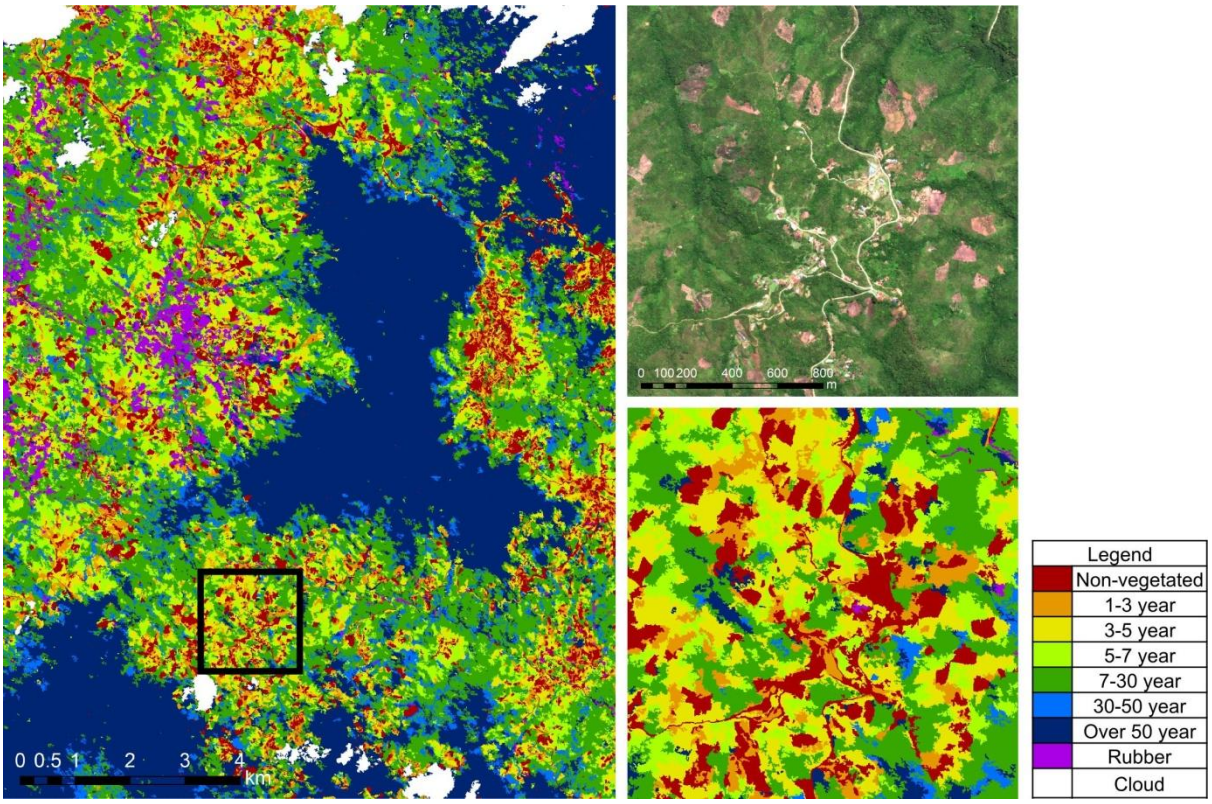

Figure 2.11. Results of the classification of the entire area (left diagram) and a close-up image (right diagram). Different colors indicate different vegetation units.

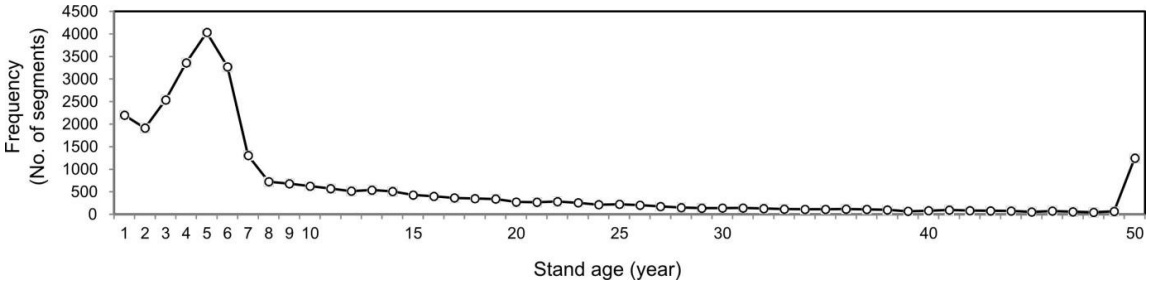

Figure 2.12. Histogram of the number of segments within stand age intervals based on Model 1 and Model 2 (Figure 2.9a, b). X axis indicates stand age and Y axis indicates the number of segments in the entire target area.

Chapter 3: Estimation and future prediction of spatio-temporal patterns of tree structure and community composition in tropical secondary forests after shifting cultivation

3.1. Abstract

Tropical countries are now facing the increasing global concern to conserve tropical forests, while they have to maintain cultivated lands (particularly shifting cultivation) for the subsistence of local people. To accomplish the effective conservation of tropical forest in harmony with subsistence shifting cultivation, I evaluated the relationships between ecosystem services (i.e. biodiversity and carbon stock) vs. the effects of shifting cultivation at a landscape level based on three land-use scenarios. The study area was the upland area between the Kinabalu Park and the Crocker Range Park in Sabah, northern Borneo, where local people conduct shifting cultivation for subsistence. In this area, vegetation patches of various stages of secondary succession admix with shifting cultivation lands. An earlier study in the same site depicted significant relationships between the stand ages of vegetation patches (which form a sere of secondary succession after the abandonment of cultivated land) and the above-ground biomass (i.e. carbon stock) and species composition of the stands. I incorporated these significant relationships to my age-estimation model described in Chapter 2. I first mapped the current (as of 2010) spatial patterns of the above-ground biomass and plant community composition for the whole landscape. Subsequently, I simulated the patterns of the above-ground biomass and plant community distributions using three land-use scenarios: 1) reduce the area of shifting cultivation by one half and protect the rest of the area, 2) shorten the minimum fallow period from 7 to 4 years while maintaining the same area of cultivation, and 3) elongate the minimum fallow period from 7 to 10 years while maintaining the same area of cultivation. Results

indicated that the land use based on the scenario 1) and 2) can increase the total carbon stock while maintaining cultivation. My methods were effective in mapping structure and composition of highly dynamic forests at a landscape level, and in predicting the future patterns of important ecosystem services based on land-use scenarios.

3.2. Introduction

Shifting cultivation is a widespread land use in the tropical region, and has formed the basis of livelihoods and customs for centuries (Metzger, 2003; Mertz *et al*., 2009; van Vliet *et al*., 2012; Dressler *et al*., 2015). This traditional land use still remains central to the livelihoods, culture and food security of millions of people in the tropical region (Dalle *et al*., 2011). At the same time, however, shifting cultivation is a direct cause of deforestation, and considered as a prominent source of carbon emissions (Geist and Lambin, 2002; Davidson et al., 2008) with an associated biodiversity loss (Novacek and Cleland, 2001; Brook *et al*., 2003; Pandit *et al*., 2007; Allnutt *et al*., 2008). Tropical countries are thus facing the increasing concern to conserve tropical forests, while they have to maintain cultivated lands (particularly shifting cultivation) for the subsistence of local people.

Where there is a long history of shifting cultivation, small patches of successional vegetation form spatiotemporally heterogeneous patterns (Gardner *et al*., 2010; Mertz *et al*., 2012). Such spatiotemporally dynamic landscapes with patches of successional vegetation mixed with conservation areas are called “matrix” (see also Chapter 2), and occur widely across many tropical countries (Fischer *et al*., 2006). Matrices are now regarded as an important provider of ecosystem services in contemporary landscapes dominated by humans (Padoch & Pinedo, 2010; Bonner *et al*., 2013).

In order to design appropriate conservation policies in a matrix, two different

approaches were proposed: a ‘land-sparing’ agriculture approach and a ‘land-sharing’ agriculture approach (Green *et al*., 2005; Padoch & Pinedo, 2010; Edwards *et al*., 2014). A land-sparing approach suggests reducing the area of farmland by emphasizing high-yielding, more intensive production, and trading reduced ecosystem services within the farmland for the retention of ecosystem services in protected areas. A land-sharing approach integrates food production with the protection of ecosystem services in the same land area (Green *et al*., 2005). If there is a sharp trade-off between the ecosystem services derived from strictly protected areas and the agricultural productions from farmlands in a given matrix or if both ecosystem services and agricultural productions can be enhanced in a matrix is an intriguing question. Both approaches can potentially cause a sharp trade-off or the reconciliation between ecosystem service and agriculture. However, such analyses are surprisingly lacking in the tropical region, partly due to the fact that a matrix is too dynamic to investigate (Scmidt-Vogt *et al*., 2009). Therefore, developing appropriate methodology to investigate the spatiotemporal relationships between ecosystem services and farmlands (particularly shifting cultivation) in a matrix is needed to design appropriate conservation policies (DeFries and Rosenzweig, 2010).

To evaluate the spatiotemporal relationships between ecosystem services and farmlands, integration of ecological understandings and remote sensing is crucial (Pettorelli *et al*., 2016). Temporally explicit patterns of ecosystem services derived from ecological plots using a space-for-time approach can be extrapolated to a landscape in remote sensing. Nishio (2014) and Fujiki *et al*., (2017) found that plant-species composition (richness) and above-ground biomass (a surrogate of carbon stock) demonstrated explicit temporal patterns after the abandonment of slash-and-burn cultivation in the same Bornean upland area where I conducted my study in Chapter 2. In this case, the time elapsed after slash and burn is the most

important determinant of species composition and biomass in the secondary-vegetation patches of this site. Provided that stand ages (i.e. time elapsed after slash and burn) of vegetation patches are identified by remote sensing, species composition and biomass can be mapped at a landscape level, and even their spatiotemporal patterns can be simulated as a function of time with appropriate land-use scenarios.

As I demonstrated in Chapter 2, indeed, it is possible to identify stand ages in a highly dynamic matrix. Therefore, the objective of this study in Chapter 3 is to evaluate the spatiotemporal relationships between ecosystem services and farmlands by extrapolating the explicit temporal patterns of species composition and biomass derived by Nishio (2014) and Fujiki et al. (2017) into the stand-age algorithm developed in Chapter 2. Firstly, I evaluated the spatial patterns of plant-species composition and biomass of vegetation patches as of 2010, the time when high-resolution satellite data were taken. Subsequently, I simulated the future patterns of above-ground biomass using three land-use scenarios and compared the results with the extant patterns as of 2010. One of the adopted land-use scenarios is based on the land-sparing approach, and two of them are based on the land-sharing approach. Lastly, I will discuss how to synergize the conservation of ecosystem services with shifting cultivation and suggest appropriate conservation policies by comparing the scenarios.

3.3. Materials and Methods

3.3.1. Study site and field survey

My study site is an upland area between the Kinabalu Park and the Crocker Range Park in Sabah, northern Borneo. I chose this area because it is located within one of the most species-rich forests in vascular species in the world (Beaman 2005) and at the same time very small patches of fragmented forest are scattered throughout the area. This area has long been inhabited by indigenous people who practice shifting

cultivation for subsistence. One family slashes and burns patches of young- to old-growth forests, cultivates hill paddy for the first year and abandons the land for fallow. In between the two parks, there is another local forest reserve with pristine vegetation, which is strictly protected from any subsistence uses by local regulations. Local people, therefore, conduct traditional shifting cultivation outside of the parks and the reserve. The center point of the study site is at 5°58′ N and 116°29′ E. The altitude of the area ranges from 300 m to 1,700 m. The total annual rainfall and mean annual temperature are approximately 2,000–2,500 mm and 15–24 °C, respectively. The geology of this area consists of tertiary sedimentary rock of the West Crocker Formation (ERE Consulting Group Sdn Bhd, 2011). The original vegetation of this area is the lower montane tropical rain forest dominated by the families Fagaceae, Myrtaceae and Lauraceae (Kitayama, 1992; Aiba & Kitayama, 1999).

Nishio (2014) and Fujiki *et al*. (2017) conducted field survey for 2 mo in the same site in August 2012 and August 2013. Details of the field survey were described in Nishio (2014) and Fujiki *et al*. (2017). In short, they randomly selected a total of 27 stands in this area to establish inventory plots. Twenty-five stands were selected to represent a few to 55 yr after shifting cultivation. Two stands were selected in an old-growth forest with more than 100 yr after slash and burn. Altitude of these stands varies between 900 m and 1400 m asl. A plot was placed in each stand. The size of a plot varied depending on stand age because dominant species changed greatly from herbs to trees; a 10 × 10-m plot for herbaceous communities, a 20 × 20-m plot for young-fallow stands with trees (age < 50 yr) and a 30 × 30-m plot for the old-fallow stands (age > 50 yr). They measured diameter at breast height (dbh) of each tree and inventoried all vascular species with estimates of cover abundances using the Braun-Blanquet scales in each plot. In young-fallow stands, trees with dbh ≥ 5 cm were measured in each of the 20 × 20-m main plot, while trees with 5 cm > dbh ≥ 1 cm

in a subplot (5 × 5 m) and small trees with dbh < 1 cm in four small plots (2 × 2 m). In old-fallow stands, trees with dbh ≥ 20 cm were measured in each of the 30 × 30-m main plot, while trees with 20 cm > dbh ≥ 5 cm in a subplot (20 × 20 m) and those with 5 cm > dbh ≥ 1 cm in a small plot (5 × 5 m). Subsequently, herbs and small trees (dbh < 1 cm) were harvested in each small plot, oven-dried at 70°C for 3 d, and weighed to determine biomass density per area. Description of stand age, altitude, above-ground biomass (AGB) and dominant species in each of the 27 vegetation stands are shown in Appendix 3.1 (cited from Nishio, 2014; Fujiki *et al*., 2017). I used the same stands for the following analyses to estimate AGB and plant-species composition.

I conducted additional field surveys in the same site in April and September 2014 to validate the accuracy of following AGB estimation. The details of the procedure are almost the same as field survey of Nishio (2014) and Fujiki *et al*. (2017). Twelve 400-m^2 circular plots were randomly established in the area to represent 4 to 26 yr after shifting cultivation (Appendix 3.2). Altitude of these plots varies between 1000 m and 1400 m asl. Dbh of all trees (dbh ≥5 cm) were measured in each of the main plot while trees with 5 cm > dbh ≥ 1 cm were measured in a subplot (25 m^2). Global positioning system (GPS) data were collected during the field surveys at the center of a plot with calibration for at least one hour in each plot. I used these additional plots only for validating the results of AGB estimation in the following remote sensing analysis.

3.3.3. Field data analysis

Nishio (2014) and Fujiki *et al*. (2017) estimated AGB and analyzed the species composition of plant communities with a multivariate DCA (detrended correspondence analysis) using the same 27 stands. To estimate the AGB of trees with dbh ≥ 1 cm, they used an empirical allometric relationship reported for tropical secondary forests after

shifting cultivation in Sarawak, Malaysia (Kenzo *et al*. 2009), with a similar climate and flora as my site:

$$AGB\ (kg\ m^{-2}) = 0.0829\ dbh^{2.43}$$

The AGB of trees with dbh ≥ 5 cm in the additional 12 plots were also calculated using the same allometric equation.

They conducted a multivariate DCA (detrended correspondence analysis) to elucidate the gradients in both species composition and their environmental controls using CANOCO Version 4.5 (ter Braak & Smilauer, 2002). DCA was run using the default options, detrending by segments and non-linear rescaling. They used relative abundance of each species based on coverage for all inventoried species per stand. They conducted these analyses using 25 stands (age ≤ 55 yr) excluding the two oldest stands (age > 100 yr), because exact ages of these stands could not be identified and their species composition was very different from the other stands. The results of DCA are shown by a biplot of stands and species in Appendix 3.3 (cited from Nishio, 2014; Fujiki *et al*., 2017). They also categorized the same 25 stands into five groups using TWINSPAN. The first group was categorized as herbaceous community with an average height of 3.3 m. The second group was a shrub community with an average height of 7.5 m. The third group was categorized as an upper montane short-forest community above 1100 m asl with an average height of 19.8 m. The fourth group was categorized as a lower montane short-forest community below 1100 m asl. The last group was categorized as a (old-fallow) forest community with the canopy height of 23.0 m. I used these categories to interpret the results of estimation of plant-community composition in the following remote sensing analysis.

3.3.4. Remote sensing analysis

3.3.4.1. Satellite images and image pre-processing

Orthorectified WorldView-2 multi spectral images (June 22, 2010), Landsat-5 TM (March 1, 1988; June 14, 1991; August 22, 1993; February 1, 1995; June 14, 1997; September 8, 1999; June 17, 2004; June 7, 2006; April 28, 2009) and Landsat-7 ETM+ (March 19, 2002) image were used in this study. Details of the pre-processing of the images were described in Chapter 2. Briefly, raw digital numbers of each image were converted into surface-reflectance values using the 6S (Second Simulation of a Satellite Signal in the Solar Spectrum) atmospheric correction model (Vermote *et al.*, 1997). Topographically induced local variations in angular viewing geometry were reduced using the method described by Ekstrand (1996). All clouds and cloud-shadows in each image were removed by unsupervised classification with ISODATA and visual inspection. ERDAS Imagine (ver.11.0; ERDAS Inc.) and ArcGIS 9.3 (ESRI, Redlands, CA, USA) were used during the entire pre-processing process.

3.3.4.2. Stand age estimation

Details of the process of stand age estimation were described in Chapter 2. In brief, I extracted temporal information (i.e., stand ages after shifting cultivation) from a change-detection analysis with Landsat time-series images and superimposed the stand ages on the segments classified by an object-based analysis using a WorldView-2. The basic units of object-based analysis are image segments, each of which is composed of spectrally coherent pixels clustered based on homogeneity criteria. Each segment identified by the object-based analysis reflects a land parcel of shifting cultivation where secondary succession has proceeded to a variety of stages. Stand ages from change-detection analysis were regarded as a response variable and object-based metrics of each segment as independent variables to develop regression models that

explain stand ages. Before establishing the regression models, I divided the WorldView-2 segments into some broad vegetation types (i.e., non-vegetated, 1–7 yr, 7–50 yr, over 50 yr and rubber plantations) with a decision tree method, using an NDVI threshold and linear discriminant analyses (LDA). Although each of the 1–7-yr and 7–50-yr vegetation type was subdivided into several age categories in Chapter 2, stand age was estimated as a continuous value ranging from 0 to 50 yr in this chapter using the same multiple regression models in Chapter 2. I used ERDAS Imagine (ver. 11.0; ERDAS Inc., Atlanta, GA, USA) for the change-detection analysis, and eCognition Developer (ver. 8.7; Definiens AG, Munich, Germany) for the object-based analyses.

3.3.4.3. Estimation of AGB and plant-community composition

I used the regression model between stand age and AGB developed by Nishio (2014) and Fujiki *et al*. (2017) (Appendix 3.4a) to estimate AGB at a landscape level, combined with my age-estimation algorithm described in Chapter 2. Nishio (2014) and Fujiki *et al*. (2017) found that species composition is primarily patterned by stand ages (as sorted along the axis-1 of the DCA) and secondly by stand altitudes (as sorted along the axis-2). I, therefore, derived correlation modes by regressing DCA axis-1 scores as a response variable with stand ages as an independent variable (Appendix 3.4b), and by regressing DCA axis-2 scores as a response variable with stand altitudes as an independent variable (Appendix 3.4c). The models used in this study are as follows:

AGB (Mg ha^{-1}) = 8.38 + 2.53 SA (R^2 = 0.88, P < 0.001)

DCA axis 1 = 1.568 + 1.255 ln (SA) (R^2 = 0.69, P < 0.001)

DCA axis 2 = 7.250 - 0.005 ALT (R^2 = 0.44, P < 0.001)

Where SA denotes stand age, and ALT denotes altitude.

The AGB model was extrapolated to the stand age map for the vegetation types between 1-50 yr old. For the fallow vegetation older than 50 yr, the mean AGB of the two old-fallow stands was uniformly assigned. The DCA axis-1 and axis-2 scores were respectively extrapolated to the stand age map and an elevation map. The elevation map was derived from the Shuttle Radar Topography Mission (SRTM). I removed the areas above 1400 m and below 900 m elevation from the analysis for plant-community composition, because the altitude of inventory plots ranged from 900 m to 1400 m. The estimated DCA axes scores were shown as a red/green composite image. Green colors were used to express the gradient of DCA axis-1 scores and red colors were used to express the gradient of DCA axis-2 scores. Base map was produced to reflect the condition as of June 22, 2010, the time when the WorldView-2 multi spectral image was taken. Therefore, extrapolated AGB and DCA axis scores reflect the ground patterns as of June 22, 2010.

3.3.4.4. Assessment of AGB estimation accuracy

The accuracy of AGB estimation map was assessed and expressed as a root mean square error (RMSE) determined by comparison between observed vs. estimated AGB values. To determine the RMSE, I used field observed AGB values of the 12 validation plots and corresponding AGB values estimated from WorldView-2 image. In contrast to the acquisition date of the WorldView-2 in 2010, the validation plots were established in 2014. Therefore, the AGB values of the validation plots were adjusted to the year 2010 for their intermediate growth, using the AGB accumulation model in section 3.3.4.3. An estimated AGB within the 11.3 m-radius (400 m^2) from the center of each validation plot was compared with the actually observed value. Then, the

relationship between estimated and observed values of AGB was derived as a linear regression.

3.3.5. Land-use scenarios and simulations

The total newly cultivated area as of 2010 was 635 ha and the number of newly cultivated parcels was 2660. The current minimum and maximum fallow period was approximately 7 yr and 20 yr, respectively (estimated from the histogram of the current vegetation pattern in Chapter 2). Maximum fallow period was defined as a maximum stand age of vegetation which local people selected to slash and burn.

In order to elucidate the effects of different practices of shifting cultivation on the future vegetation, I simulated the vegetation dynamics based on three scenarios, and then evaluated the associated AGB changes. I adopted the following scenarios: 1) 'reduced-cultivation' scenario; 2) 'shorter-fallow' scenario; and, 3) 'longer-fallow' scenario. In the scenario 1, I assumed that annual cultivation area would be reduced by one half and the minimum fallow period of shifting cultivation would be kept constant (i.e. 7 yr). In the scenario 2, annual cultivation area would be kept constant, but instead the minimum fallow period of shifting cultivation would be shortened from 7 yr to 4 yr. In the scenario 3, the minimum fallow period of shifting cultivation would be elongated from 7 yr to 10 yr while annual cultivation area would be kept constant.

The scenario 1 was based on the land-sparing approach, whereas the scenario 2 and 3 were based on the land-sharing approach. The longer fallow in scenario 3 was expected to promote forest succession and increase total AGB at a stand level without reduction of cultivation area. On the other hand, the shorter fallow period in scenario 2 was expected to promote forest succession at a landscape level with cultivated areas being confined to a more limited area, because shifting cultivation with a shorter fallow period tended to use the same area more intensively and thus the rest of the area

would escape from slash and burn.

Based on the three scenarios, I simulated the dynamics of vegetation patterns for ten years from 2010 to 2020. In the simulations, I assumed that one segment identified by the object-based analysis represented one parcel of vegetation patch (or one parcel of cultivated land), and controlled the number of annually cultivated segments each with a mean area of 3100 m^2. Actual segment area varies according to selected parcel. Therefore, total cultivated area actually varies among years. Each segment has a stand age as an integer, calculated from the two age-estimation regression models proposed in Chapter 2. I controlled two parameters in each simulation: a total number of annual cultivated segments (i.e. annual cultivation area), and min–max fallow period (i.e. min–max stand age of the segments which local people select to slash and burn). The min–max fallow period was set as 7–20 yr in the scenario 1 and as 4–20 yr in the scenario 2, and as 10–40 yr in the scenario 3. As will be shown, the land available for shifting cultivation actually was not enough in the scenario 3 because all of the 10–20-yr segments were converted into the vegetation younger than 10 yrs with 4 iterations of the simulation. Therefore, the maximum fallow period of 40 yr was exceptionally used in the scenario 3.

I estimated the stand age of all segments of the whole study area at one-year intervals from 2010 to 2020 in each simulation. In each year, 1330 segments for the scenario 1 (half of the annually cultivated segments in the current state) and 2660 segments for the scenario 2 and 3 were randomly selected from the segments with stand ages between a given min–max fallow period in each simulation. I converted the stand ages of the selected segments into 0 (i.e. occurrence of annual shifting cultivation), and added 1 to the stand age of the rest of segments (i.e. annual increment in stand age). This step was iterated for 10 times in each scenario. Subsequently, the AGB stock in 2020 was calculated from the segment ages derived from each

simulation. The histograms of segment age and AGB stock in 2020 were compared with those of the current state (as of 2010).

3.4. Results

3.4.1. AGB map and plant-community composition map

The results of the AGB estimation as of 2010 are shown in Figure 3.1. Each pixel in the map contains an AGB value, and the color gradation from red to green indicates a gradient of AGB value from low to high values. Vegetation with a medium AGB was densely distributed around the edge of the strictly protected areas (dark green color). On the other hand, lower-AGB vegetation was sparsely distributed over the whole area. Total AGB stock in the total area (15,000 ha) was 1,530,000 Mg (equivalent to 104 Mg ha^{-1}) and total AGB stock in the successional vegetation (1–50-yr-old vegetation including cultivated area; 9,300 ha) was 363,000 Mg (equivalent to 39 Mg ha^{-1}). The relationships between the estimated and observed AGB of 12 validation plots are shown in Figure 3.2. The RMSE between the estimated and observed AGB was 24.4 Mg ha^{-1}. However, the deviation of the regression line from the 1:1 line suggested an increasing overestimation of AGB in older vegetation.

The results of the estimation of plant-community composition are shown in Figure 3.3. Each pixel in the map shows both DCA axis-1 and DCA axis-2 scores as red/green spectral composite. Green-color spectrum is used for DCA axis-1 scores and red-color spectrum is used for DCA axis-2 scores. The spectral matrix shows gradation of the change of the composition. The spectral matrix was divided into five species-composition groups according to the category of Fujiki *et al*. (2017). Most of the area was covered with reddish colors which indicate herbaceous community. A green color indicates upper montane short forest community or old fallow community and these communities comprise the second largest land-cover component. The area of

lower montane short-forest community (yellow color) was relatively small.

3.4.2. Numerical simulation for the future vegetation pattern

The results of the simulations based on the three scenarios are shown in Figure 3.4 in terms of the frequency of vegetation patches (segments) per stand age. The black line indicates the vegetation pattern of the base map as of 2010 (see Chapter 2). The blue line in Figure 3.4a is the vegetation pattern for the year 2020 based on the scenario 1, where the cultivation area was reduced by one half for 10 years. Shifting-cultivation practices based on the scenario 1 decreased the frequency of vegetation younger than 7 yr and instead increased the frequency of vegetation with ages around 15 yr. As a result, the total AGB in the successional vegetation (1–50-yr-old vegetation including cultivated area) was increased by 123,000 Mg (equivalent to 13.2 Mg ha^{-1}). Based on the scenario 2, in which the minimum fallow period was reduced from 7 yr to 4 yr, the frequency of both vegetation older than 7 yr and younger than 4 yr increased (Figure 3.4b). The total AGB in the successional vegetation was increased by 54,000 Mg (equivalent to 5.8 Mg ha^{-1}). On the other hand, the results of scenario 3 showed a different pattern. Based on the scenario 3, in which the minimum fallow period was elongated from 7 yr to 10 yr, the simulation could not be continued after four times of iteration with a maximum fallow period of 20 yr. This was because the number of 10–20-yr segments became short for selecting new cultivation areas because all of the 10–20-yr segments were converted into the vegetation younger than 10 yrs. Therefore, the simulation in the Figure 3.4c was alternatively conducted in the vegetation with ages up to 40 yrs. As a result, almost all of the vegetation younger than 40 yrs were disturbed and converted into the vegetation younger than 10 yrs. The total AGB in the successional vegetation was decreased by 72,000 Mg (equivalent to 7.7 Mg ha^{-1}) in this simulation.

3.5. Discussion

The stand age map combined with the field-based AGB accumulation model was effective to estimate AGB of a matrix of shifting cultivation with secondary vegetation patches at a landscape level (RMSE: 24.4 Mg ha^{-1}). However, as shown in Figure 3.2, the AGB values were overestimated in the vegetation with higher AGB. This was probably because the identification of patch (segment) boundaries was not successfully done especially in the vegetation with higher AGB. The segments identified by the object-based analysis were sometimes mixed with the surrounding old-growth vegetation and erroneously regarded as extremely old (Chapter 2). Such erroneously identified segments occurred in my validation samples, and caused the overestimation in the vegetation with higher AGB. However, my AGB map is clearly useful for detecting the location and frequency of vegetation patches for a given AGB category.

The map of plant-community composition also clearly described the continuous gradients of the community shift in this area by red/green spectral composite of both DCA axis-1 and DCA axis-2 scores. Most of the study area is covered with herb community, upper montane short forest community and old fallow community whereas the area of lower montane short-forest community is smaller. Fischer *et al*. (2006) suggested that conserving native vegetation alone will not protect ecosystem services, and that landscapes in matrices should include patches of native vegetation, corridors and stepping stones between them, and buffers around the native vegetation. My map can identify the areas of potentially high conservation values, or those with less ecosystem services where mitigation measures are required. Such information is useful for the management of corridors and stepping stones between protected areas, and building buffers around them.

The stand age map can be used to predict future vegetation patterns with

land-use scenarios. With both the land-sparing (scenario 1) and land-sharing strategies (scenario 2), it is possible to promote forest succession and increase total AGB at a landscape level. The scenario 1 (reducing cultivation area) is the most effective scenario to promote forest biomass accumulation and probably associated biodiversity. The scenario 2 (fallow reduced from 7 yr to 3 yr, i.e. land-sharing) is also effective to promote forest biomass accumulation in a landscape. This is because shifting cultivation with a shorter fallow period uses the same area repeatedly, and therefore the rest of the area escapes from slash and burn. Based on the scenario 3 (fallow period elongated from 7 yr to 10 yr, i.e. land-sharing), local people cannot continue shifting cultivation in 4 years, and the total AGB stock in the successional vegetation is decreased.

Past ecological studies reported that shorter fallow periods of shifting cultivation lead to a decrease in species richness and diversity in situ (Uhl *et al*., 1981; Lawrence, 2004; Lawrence *et al*., 2010; Jakovac *et al*., 2015). However, my results suggest that shortening the fallow period of shifting cultivation results in promoting the forest succession and increase total AGB at a landscape level, provided that cultivation becomes intensified in a limited area. On the other hand, elongating the fallow period of shifting cultivation may promote broader deforestation at a landscape level. I suggest that forest dynamics in a whole landscape have to be taken into consideration for predicting the consequences of shifting cultivation.

Cultivation practices based on both the scenario 1 and scenario 2 may not be able to maintain cultivation yields. With the scenario 1, reduced cultivation area will directly decrease cultivation yields if the average yield per area is constant. With scenario 2, shorter fallow can also result in the reduction of cultivation yield, because a more intense land use can decrease soil nutrient availability such as phosphorus (Lawrence *et al*. 2007; Runyan *et al*., 2012; Fujiki *et al*., 2017). Such nutrient

reductions and the associated decreases of yields indicate the difficulty in maintaining the livelihood production with scenario 2. All three scenarios in this study, thus, may not be able to reconcile the livelihood production with forest conservation effectively.

In order to reconcile the livelihood production with forest conservation, the decreased yields have to be compensated through appropriate mechanisms such as REDD+ (Reducing Emissions from Deforestation and Forest Degradation Plus). REDD+ is an incentive based policy mechanism often described as a payment-for-performance system, where people can receive financial support for carbon increment. My method can provide quantitative information of current carbon stock as well as expected carbon increments with improved land-use scenarios. My method can also provide quantitative assessment how/if carbon increments can reconcile with the biodiversity conservation because maps derived from my method can elucidate both carbon and plant communities.

Once field based models (i.e. relationships of stand age with total AGB and plant-community composition) are established in a given area, the same models can be repeatedly applied to different stand-age maps derived from different satellite imageries to estimate carbon and plant communities at different times (Chapter 2). Therefore, my methods described in the Chapter 3 are potentially useful for monitoring ecosystem services over time and can contribute to realizing REDD+.

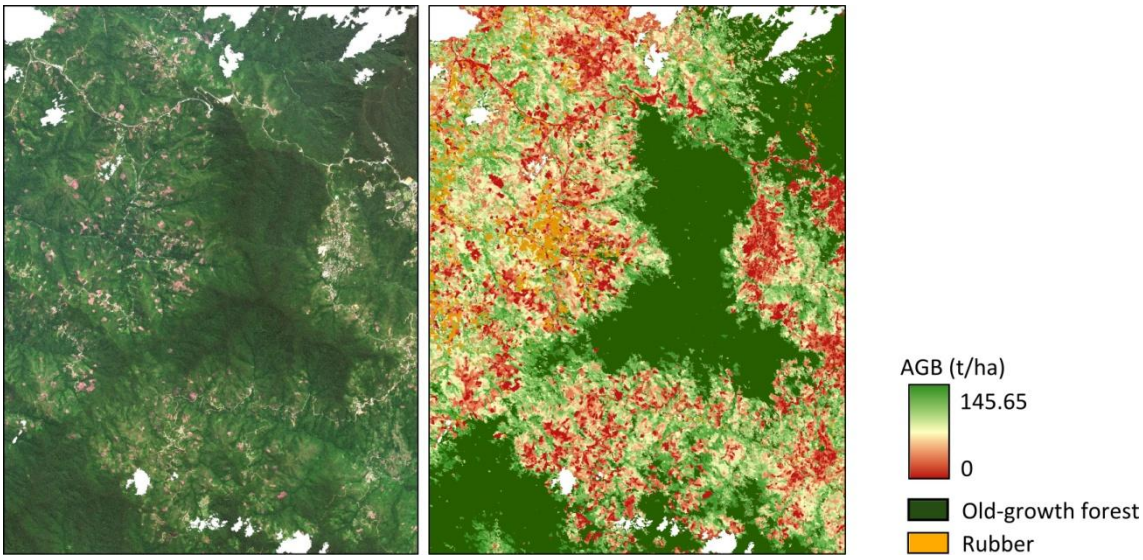

Figure 3.1. WorldView-2 image in 2010 (RGB / Band3, Band2, Band1) (left) and the results of the AGB map of the entire area (right). Each pixel in the map contains an AGB value, and the color gradation from red to green indicates a gradient of AGB value from low to high values.

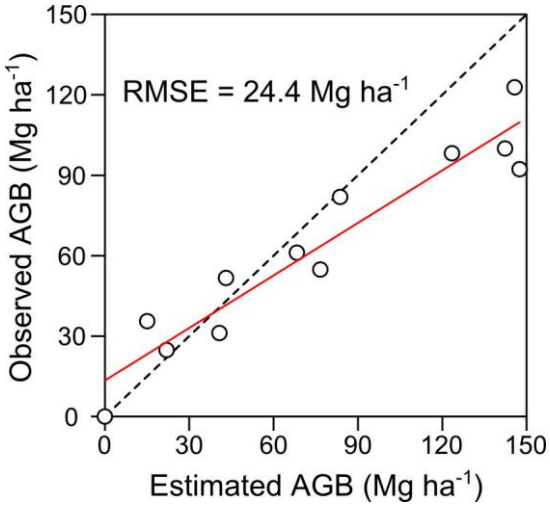

Figure 3.2.

Relationships between estimated vs. observed AGB of 12 validation plots. The red line indicates the regression line. Dashed line indicates a 1:1 line.

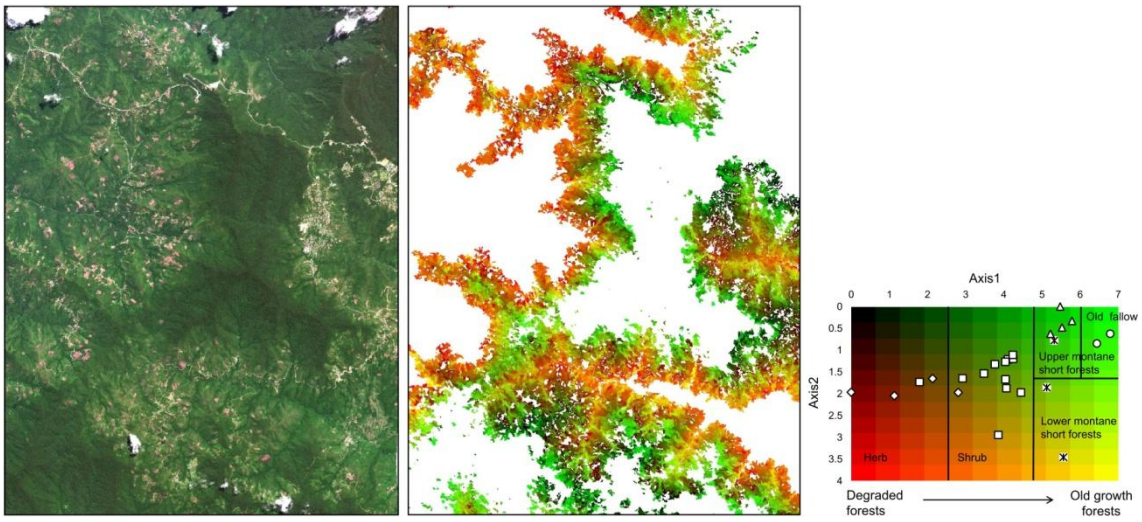

Figure 3.3. WorldView-2 image in 2010 (RGB / Band3, Band2, Band1) (left) and the derived plant-community composition map of the entire area (right). Each one pixel in the map indicates both DCA axis-1 and DCA axis-2 scores as red/green spectral composite. Green-color spectrum was used for the DCA axis-1 scores and red-color spectrum was used for the DCA axis-2 scores. The spectral matrix beside the map shows a gradation of the change of the composition. The matrix was divided into five vegetation types according to the category of Fujiki *et al*. (2017). Fujiki *et al*. (2017) categorized the same 25 stands into vegetation types using TWINSPAN.

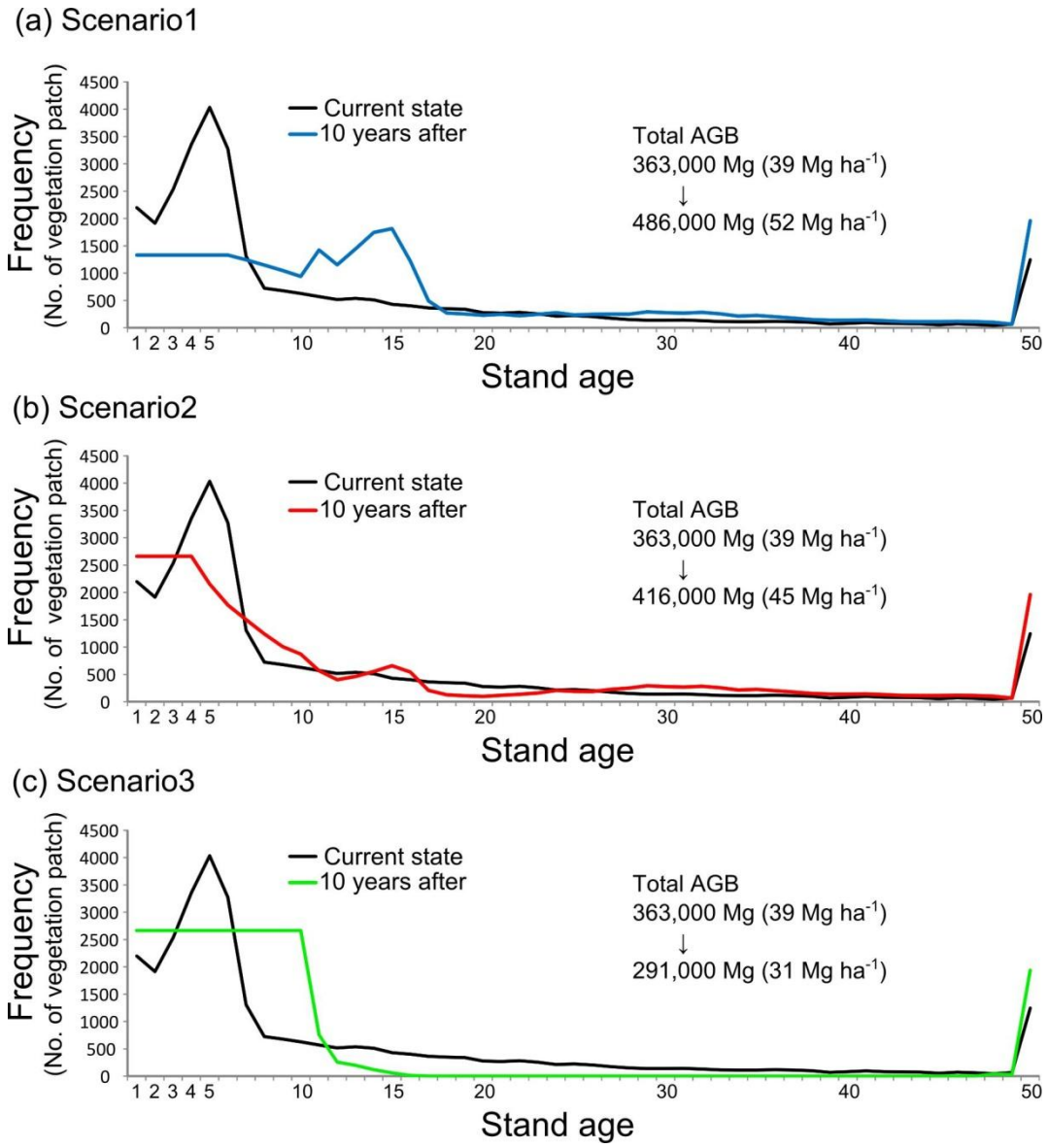

Figure 3.4. Histograms comparing the current state of vegetation with simulated future vegetation based on the three scenarios. The figures indicate frequency of vegetation patches per stand age. The black line indicates the current state of vegetation. Blue line is the vegetation pattern estimated based on the scenario 1 (a); red line indicates the vegetation pattern estimated based on the scenario 2 (b); green line indicates the vegetation pattern estimated based on the scenario 3 (c). See text for the detailed explanation of each scenario.

Chapter 4: Estimation of large-scale spatiotemporal changes in tree-community composition based on LANDSAT images in selectively-logged tropical rain forests

4.1. Abstract

Assessment of the progress of the Aichi Biodiversity Targets set by the Convention on Biological Diversity (CBD) and the safeguarding of ecosystems from the perverse negative impacts caused by Reducing Emissions from Deforestation and Forest Degradation Plus (REDD+) requires the development of spatiotemporally robust and sensitive indicators of biodiversity. Recently, it has been proposed that tree-community composition based on count-plot surveys could serve as a robust, sensitive, and cost-effective indicator for forest intactness, which is a surrogate of biodiversity in Bornean logged-over rain forests. In this study, I developed an algorithm to map tree-community composition across the entire landscape based on Landsat imagery. I targeted six forest management units (FMUs), each of which ranged from 50,000 to 100,000 ha in area, covering a broad geographic range spanning the most area of Borneo. Approximately fifty 20 m-radius circular plots were established in each FMU, and the differences in tree-community composition at a genus level among plots were examined for trees with diameter at breast height ≥10 cm using an ordination with non-metric multidimensional scaling (nMDS). Subsequently, I developed a linear regression model based on Landsat metrics (e.g., reflectance value, vegetation indices and textures) to explain the nMDS axis-1 scores of the plots, and extrapolated the model to the landscape to establish a tree-community composition map in each FMU. The adjusted R^2 values based on a cross-validation approach between the predicted and observed nMDS axis-1 scores indicated a close correlation, ranging from 0.51 to 0.74. Histograms of the frequency distributions and mean value of extrapolated nMDS

axis-1 scores were derived from each map and used to quantitatively diagnose the forest intactness of the FMUs. Combination of forest intactness map with the boot-strapping approach using confidence intervals of mean nMDS axis-1 scores was clearly useful for diagnosing spatial and temporal variations in forest intactness among/within FMUs under different management regimes. My study indicates that tree-community composition, which was reported as a robust indicator of forest intactness, can be mapped at a landscape level to quantitatively assess the spatio-temporal patterns of biodiversity in Bornean rain forests. My approach can be used for large-scale assessments of tree diversity and forest intactness to monitor both the progress of Aichi Biodiversity Targets and the effectiveness of REDD+ biodiversity safeguards in production forests in the tropics.

4.2. Introduction

Continued deforestation and forest degradation and the associated losses of biodiversity in tropical countries represent major global concerns (Hansen *et al*., 2013). To date, coordinated international efforts have resulted in two international conventions that attempt to reduce the rate of tropical deforestation and forest degradation and the associated biodiversity losses: the Convention on Biological Diversity (CBD) and the United Nations Framework Convention on Climate Change (UNFCCC) (see also Chapter 1). There is an urgent need to develop robust indicators to both accurately assess the progress of the Aichi Biodiversity Targets and avoid overall negative effects on biodiversity caused by the implementation of REDD+. However, there is so far no consensus about global, harmonized observation system for delivering regular, timely data on biodiversity change (Scholes *et al*., 2012; Pereira *et al*., 2013; Goetz *et al*., 2015).

For assessing the progress of the Aichi Biodiversity Targets and for verifying

biodiversity safeguards, an indicator must be robustness and sensitive for reflecting large-sacle spatiotemporal changes of (tropical) forests. In addition, they must be cost-effective, be easily identified, be proxies for ecosystem integrity, and have cross-taxon congruency to be reliable and practical (Su *et al*., 2004). Recently, Imai *et al*. (2014) proposed that the community composition of canopy trees can be used as a robust indicator for biodiversity in spatiotemporally dynamic Bornean production forests where timber is produced by selective logging. They used the axis-1 scores of the ordination of vegetation plots based on the relative species (or genus) abundances in logged-over forests to indicate forest intactness as a proxy for biodiversity. Derived axis-1 scores showed significant linear correlations with magnitude of logging intensity (i.e., the inverse of remaining aboveground biomass). This significant linear correlation was a result of the interaction of linearly increasing species number in the pioneer guild and linearly decreasing species number in the climax guild with increased logging intensity (Imai *et al*., 2014, Kitayama *et al*., 2013). Therefore, the indicator based on community composition (i.e., axis-1 scores of the ordination) actually indicated the compositional distance from an intact forest where there were zero or minimal effects from logging. The count-plot measurements on the ground were fast and inexpensive, and implemented by local foresters (Imai *et al*., 2014). Therefore, the methods of Imai *et al*. (2014) satisfied the above-listed requirements for indicators. However, a previously unresolved issue related to the indicators is spatial representativeness; indicators derived from plots on the ground need to be extrapolated to the landscape using remote sensing approaches.

To address the increasing need for a practical indicator that is spatially/temporally sensitive and robust, I developed a new algorithm using satellite remote sensing to map biodiversity in Bornean tropical rain forests based on the community composition indicator of Imai *et al*. (2014). I used generic abundances

instead of specific abundances because both specific and generic abundances demonstrated the same response to logging intensity (Imai *et al*., 2014). Specifically, I developed a new algorithm to map variation in tree-community composition using Landsat imagery as a proxy for forest biodiversity and/or forest intactness, and assessed whether my method could reliably diagnose the magnitude of spatiotemporal changes of tree-community composition among/within production forests under different management regimes. Such a method will contribute to the assessments of the progress of the Aichi Biodiversity Targets and effectiveness of REDD+ safeguards. It is needless to say that the method will also contribute to improving forest management on the ground in each forest management unit (FMU).

4.3. Materials and Methods

4.3.1. Study Site

I studied the community composition of canopy trees and mapped the patterns of tree-community composition in six Bornean FMUs that were conducting legal selective logging for commercial purposes. An FMU is a management entity with a valid logging license from the local government either from Malaysian states in Malaysian Borneo or from the Indonesian Government in Indonesian Borneo. In each FMU, the marketable trees (large dipterocarp species) within a certain size class are harvested for timber. FMUs in Borneo typically range from 50,000 to 100,000 ha in size and their land belongs to the respective governments. These areas are covered by lowland mixed dipterocarp forests with varying degrees of degradation reflecting their different logging histories.

The studied FMUs were Segaliud Lokan (5°20’–27’N, 117°23’–39’E, 576 km2), Deramakot (5°14’–28’N, 117°20’–38’E, 551 km2), Tangkulap (5°18’–31’N, 117°11’–22’E, 276 km2), and Sapulut (4°40’–55’N, 116°30’–117°00’E, 956 km2) in

Sabah, Malaysia; and, Roda Mas (0° 46'–1°05'N, 114°25'–115°06'E, 703 km2) and Ratah (0°7'S–0°13'N, 114°58'–115°30'E, 982 km2) in East Kalimantan, Indonesia (Figure 4.1). The areas of Segaliud Lokan, Deramakot, and Tangkulap were initially logged in 1958, 1956, and 1970, respectively, using conventional logging methods (i.e., high-impact logging with no environmental considerations; Sabah Forestry Department, 2005). The three FMUs were adjacent to one another. In Deramakot, conventional logging continued until 1989, when all logging activities were halted for regrowth. Then, stainable forest management with reduced-impact logging was introduced to Deramakot in 1995. Reduced-impact logging is an improved method of selective logging, including pre-harvest inventory, mapping of all canopy trees, directional felling, liana cutting, and planning of skid trails, log decks, and roads (Elias *et al*., 2001; Sabah Forestry Department, 2009). In combination with reduced-impact logging, a longer cutting cycle (i.e., 40 years) was strictly adhered to in accordance with the long-term management plan (Lagan *et al*., 2007). These combined approaches helped to preserve forest integrity (Pinard and Putz, 1996; Putz *et al*., 2008; Langner *et al*., 2012; Kitayama, 2013). Deramakot was the first tropical forest certified by the Forest Stewardship Council (FSC) in 1997, and was considered an exemplary model of sustainable forest management by the Sabah Government. Reflecting this logging history, I observed that the forests inside the Deramakot FMU were less disturbed based on aboveground biomass and varied biological communities (Kitayama, 2013). In contrast, Segaliud Lokan was repeatedly logged using conventional logging until 2002, after which reduced-impact logging has been implemented. Tangkulap was repeatedly logged using conventional logging until 2002, after which all logging activities have remained suspended. Sapulut was first logged in 1956 and repeatedly logged until 2000 using conventional logging after which reduced-impact logging has been carried out, but industrial tree plantations have been established and Sapulut now

consists of rubber and *Acacia* plantations over approximately 35% of its area. Reduced-impact logging was implemented in Roda Mas from at least 2008. It is highly likely that logging had been conducted earlier in the Roda Mas area, but there is no information about its logging history before 2008. I estimate that the logging intensity was relatively mild in the Roda Mas area because areas of intact forests still remain throughout the area. Ratah implemented conventional logging from 1972 to 2010, after which sustainable forest management with reduced-impact logging has been implemented. Deramakot, Tangkulap, Roda Mas, and Ratah are all certified by the FSC. Sapulut and Segaliud Lokan are certified by Malaysian Timber Certification Council (MTCC). Table 4.1 summarizes the target areas.

4.3.2. Field survey

I with my colleagues conducted count-plot surveys in the four FMUs: Segaliud Lokan, Sapulut, and Ratah in 2012 (Imai *et al.*, 2014); Deramakot, Tangkulap, Roda Mas in 2014; and, Ratah again in 2015. The number of the established plots in each FMU is shown in Table 4.1. Because Segaliud Lokan, Deramakot, and Tangkulap are adjacent to one another within the same forest type, I assume that all count-plot data obtained from the three FMUs can equally represent the variation of canopy species composition of the area.

The details of the procedure of the count-plot survey are described in Imai *et al.*, (2014). Briefly, to select representative vegetation plots from a heterogeneous forest with varying magnitudes of forest degradation, I classified each FMU into five strata based on Landsat imagery according to the extent of forest degradation, from intact forest (stratum 1) to open canopy area with several pioneer trees (stratum 5) (Imai *et al.*, 2014). Here, I defined the magnitude of forest degradation based on the remaining aboveground biomass according to the definition of the Intergovernmental

Panel on Climate Change (IPCC, 2003). Ten 20-m-radius circular plots (1257 m^2 in area) were randomly established at altitudes below 600 m asl in each stratum in each FMU (i.e., 50 plots in each FMU). To minimize spatial autocorrelation, plots were established at a distance of at least 100 m from one another. Global positioning system (GPS) data were collected during the field surveys at the center of a plot with calibration for at least one hour in each plot. I and colleagues measured diameter at breast height (dbh) of all trees (dbh ≥10 cm) and counted all measured species in each plot. Woody vines were excluded from the inventory. Trees with buttresses were measured well above (ca. 50 cm) protrusions. All trees were identified by local botanical experts. If trees could not be identified in the field, voucher specimens were collected and identified in local herbaria. Samples that could not be identified to the species level were distinguished as morphospecies. In addition, a total of 24 0.2-ha rectangle plots were established in Deramakot and Tangkulap in 2014 for increasing the analytical confidence through the same procedure as above. Consequently, I obtained inventory data from a total of 284 plots.

4.3.3. Field data analysis

A total of 14,783 stems from 85 families and 254 genera were recorded in the 284 plots (totaling 37.5 ha in area). The Chao distances (Chao *et al*., 2005) based on the number of trees of per genus as genus abundance were used to calculate the distance matrix for the inventoried plots in each FMU. Then, an ordination of plots was conducted to ordinate the inventoried plots for each FMU with non-metric multidimensional scaling (nMDS) using the metaMDS procedure in the vegan package in the R software program (Oksanen *et al*., 2013). Subsequently, the nMDS axis-1 scores were used as an index of tree-community composition. Imai *et al*. (2014) demonstrated that the nMDS axis-1 scores of plots correlated with the aboveground biomass values of the

plots, which was a proxy for forest degradation, in each FMU (R^2=0.52–0.71). Although plots were a considerable distance from one another, I was unable to completely rule out the possibility of spatial autocorrelations among plots. Therefore, I tested for autocorrelations among plots in each FMU and found insignificant effects of autocorrelations in all FMUs (see Appendix 4.1 and Appendix 4.2). Hence, the nMDS axis-1 scores of plots indicated intactness in terms of tree-community composition, which is the compositional distance from intact forests where there were no effects of logging. Intactness can also be functionally translated to ecosystem integrity because regeneration ability is assured in more intact forests.

To compare the differences between FMUs with the same index, the nMDS axis-1 scores were normalized by transforming the scores into new scores with a mean of 0 and a standard deviation of 1. In order to assure that a given normalized score can indicate the same forest condition in terms of forest intactness across FMUs, I regressed normalized nMDS axis-1 scores with relative abundance of pioneer species (genera) per plot in each FMU. Subsequently, significant differences in the slope and intercept of the regression lines among FMUs were tested with a multi regression analysis. Complete overlap of the regression lines suggests that a given normalized score can indicate the same forest condition across FMUs. Indeed, there were no significant differences in the intercept and slope among the regression lines in Segaliud Lokan and Sapulut (see Appendix 4.3). The intercept of Ratah and the intercept and slope of Roda Mas were exceptionally significantly different from the other FMUs, but the range of the deviation was still within that of the other FMUs. The results indicated that the normalized scores could indicate the same forest condition in terms of forest intactness across FMUs. Normalized scores will be used as “nMDS axis 1” in the following analyses.

4.3.4. Satellite Analysis

4.3.4.1. Satellite images and image pre-processing

The estimates of the nMDS axis-1 scores for the entire study area in each FMU were based on Landsat TM/OLI imagery. Descriptions of the data set (sensor, path/row and date) of the imageries used are given in the Appendix 4.4. No significant geolocation errors were observed in the images because the GPS ground positions collected on logging roads corresponded closely with the images.

As pre-processing, the raw digital numbers of each image were converted into top-of-atmosphere radiance. Subsequently, to compensate for atmospheric scattering and absorption effects, an atmospheric correction algorithm based on the Second Simulation of a Satellite Signal in the Solar Spectrum radiative transfer code (ver. 1.1, Kotchenova *et al*., 2006; Vermote *et al*., 1997) was used to convert top-of-atmosphere radiance into surface reflectance. Finally, the effects of differential illumination due to topography were reduced using the method described by Ekstrand (1996). Shuttle Radar Topography Mission (SRTM) data were used to correct the illumination effects. Then, pixels covered with clouds/shadow were removed using an object-based approach. I created image segments composed of spectrally coherent pixels that were clustered based on homogeneity criteria, and established a threshold to detect cloud/shadow segments. Then, I removed them using the threshold and visual inspection.

Subsequently, the missing data due to cloud cover were filled in using the cloud-free areas of temporally adjoining data. Where satellite imagery is subjected to high incidence of clouds or haze, which is often the case in tropical rain forests, the mosaicing of cloud-free parts of temporally adjoining data may be the best option for deriving cloud-free coverage (Helmer *et al*., 2005). In my study, in the mosaicing procedure, calibrated cloud-free parts of adjoining secondary images were embedded

in the missing parts of the base image. To calibrate secondary images to the base image, I used a linear regression model (Schott *et al*., 1988; Vogelmann, 1988; Hall *et al*., 1991; Olsson, 1993; Oetter *et al*., 2001; Song *et al*., 2001; Du *et al*., 2002). The basis for the model was the set of co-located, mutually clear pixels from each base- and secondary-scene pair. Before establishing regression models, I excluded pixels with marked spectral changes, which possibly occurred with land-cover changes, using a change-detection analysis with a normalized difference vegetation index (NDVI). Subsequently, pixel-level regression models were established using a robust regression. A regression model for Landsat-TM/OLI images has the following general form:

$$y_{base\ i} = f\ (\ x_{sec\ 1},\ x_{sec\ 2},\ x_{sec\ 3},\ x_{sec\ 4},\ x_{sec\ 5},\ x_{sec\ 6},\ x_{sec\ 7})$$

where $y_{base\ i}$ is the reflectance value of the pixel in the base image for the i^{th} band to be predicted, and $x_{sec\ 1}$ is the reflectance value of band 1 of the co-located pixel in the secondary images, $x_{sec\ 2}$ is the reflectance value of band 2, and so on. Missing data in each pixel in the base images were replaced by the calibrated pixels of secondary images using the regression models. Landsat-OLI (Jun/06/2014), Landsat-OLI (Jun/19/2013), Landsat-OLI (May/31/2015), Landsat-TM (Feb/10/2010), and Landsat-OLI (Mar/28/2015) were used as base images for Segaliud Lokan-Deramakot-Tangkulap (2014), Sapulut, Roda Mas, Ratah (2010), and Ratah (2015), respectively. eCognition Developer 8.7 was used to create image segments, and ERDAS Imagine ver.11.0 and ArcGIS 9.3.1 were used for pre-processing.

4.3.4.2. Extrapolation of nMDS axis-1 scores based on Landsat data

To estimate the nMDS axis-1 scores of the entire study area of each FMU, I established multiple linear regression models between the nMDS axis-1 scores of the

inventoried plots and corresponding metrics of the Landsat imagery (i.e., average value of Landsat metrics within the 20 m-radius from the center of the plots) in each FMU. Then the nMDS axis-1 scores were extrapolated to the entire area of each FMU based on the models. In Segaliud Lokan, Deramakot and Tangkulap, two models were separately established with Landsat-TM (2009) and Landsat-OLI (2014) for detecting temporal changes. The inventory plots established in 2012 were used for Landsat-TM (2009), and the plots established both in 2012 and 2014 were used for Landsat-OLI (2014) after assuring that no plots were affected by logging in between, because time gap between 2012 and 2014 would not significantly affect the tree-species composition in 2014. Also in Ratah, two models were separately established for Landsat-TM (2010) and Landsat-OLI (2015). Basically, the inventory plots established in 2012 were used for Landsat-TM (2010) and the plots established in 2015 were used for Landsat-OLI (2015), but the inventory plots with nearly-intact tree community (i.e., Stratum 1 and 2) were used both for Landsat-TM (2010) and Landsat-OLI (2015) regardless of the date of plot establishment. This is because the rate of temporal species turnover of these plots would be slow and the species turnover could be ignored within such a short period (2010–2015). The inventory plots that were located underneath cloud cover on the imagery used were eliminated in this procedure. I developed the models separately for each FMU rather than developing a single model for all FMUs to take regional floristic variation into account.

The normalized scores of nMDS axis-1 were considered response variables, and the Landsat metrics were considered independent variables. I used the following Landsat metrics: reflectance value of each band ($Band1_{TM/OLI}$, $Band2_{TM/OLI}$, $Band3_{TM/OLI}$, $Band4_{TM/OLI}$, $Band5_{TM/OLI}$, $Band6_{OLI}$, $Band7_{TM/OLI}$), NDVI (Rouse *et al.*, 1974), normalized difference water index (NDWI) (Gao, 1996; McFeeters, 1996), normalized difference soil index (NDSI) (Takeuchi and Yasuoka, 2004), and enhanced

vegetation index (EVI) (Huete *et al*., 2002). The mean values of the Landsat metrics within a 20-m radius from the center of the plots were used as the metrics corresponding to each plot. The indices were calculated from the following equations:

$$NDVI\text{-}TM_{(OLI)} = (Band4_{(Band5)} - Band3_{(Band4)}) / (Band4_{(Band5)} + Band3_{(Band4)})$$

$$NDWI\text{-}TM_{(OLI)} = (Band3_{(Band4)} - Band5_{(Band6)}) / (Band3_{(Band4)} + Band5_{(Band6)})$$

$$NDSI\text{-}TM_{(OLI)} = (Band5_{(Band6)} - Band4_{(Band5)}) / (Band5_{(Band6)} + Band4_{(Band5)})$$

$$EVI\text{-}TM_{(OLI)} = 2.5 * (Band4_{(Band5)} - Band3_{(Band4)}) / (Band4_{(Band5)} + 6 * Band3_{(Band4)} - 7.5 * Band1_{(Band2)} + 1)$$

In addition to the above metrics, the coefficient of variation (CV), standard deviation (SD), and textures of the gray level co-occurrence matrix (GLCM) (Haralick, 1986) were used as proxies for spectral heterogeneity because degradation of forest canopies might affect the heterogeneity of the spectral pattern. The CV, SD, and textures of the GLCM were calculated using a 3×3-pixel window based on the reflectance values and each of the indices. The GLCM is a tabulation of how often different combinations of gray levels occur at a specified distance and orientation in an image object (Baatz *et al*., 2004). The homogeneity, contrast, angular second moment, entropy, dissimilarity, correlation, mean, and standard deviation were calculated as the indices of the textures. A total of 120 and 132 metrics were generated based on Landsat TM and OLI, respectively. The independent variables of the regression models were chosen using a stepwise selection from all of the metrics to avoid multi-collinearity among the independent variables. The values of the variance inflation factor (VIF) of selected independent variables were all less than 10 except for Roda Mas, which indicated that there was no multicollinearity (see Appendix 4.5). I removed the areas above 600 m elevation from the analysis, because the potential natural vegetation

above 600 m differed from that of lowland natural forest (Kitayama, 1992; Aiba and Kitayama, 1999). eCognition developer 8.7 was used to calculate texture, R ver 3.20. was used to establish the models, and ERDAS Imagine ver.11.0 and ArcGIS 9.3.1 were used in the other procedures.

4.3.5. Validation of nMDS axis-1 model

I used a cross-validation approach (Roff, 2006; Langner *et al*., 2012) to assess the accuracy of the models. All plots used in each model were divided evenly into five classes according to the rank order of nMDS scores. Then four-fifths of the plots in each class were randomly selected and combined to construct an nMDS axis-1 model. Based on the model, I estimated the nMDS axis-1 scores of the other remaining one-fifth of the plots. Then I tested the correlation between the estimated nMDS axis-1 scores and the field-measured nMDS axis-1 scores. This step was reiterated 1,000 times in each FMU to derive the 95% confidence interval of the correlation coefficient. The statistical tests were conducted using R ver. 3.20.

4.3.6. Comparison of spatial variation in canopy conditions among FMUs

I calculated the histogram of relative frequency and mean value of the nMDS axis-1 scores for each FMU and compared them based on their management types to assess whether my method could reliably diagnose the variation of forest intactness among FMUs under different management regimes. In this analysis, I used the estimated nMDS axis-1 scores based on Landsat-OLI (2014), Landsat-OLI (2013), Landsat-OLI (2015) and Landsat-OLI (2015) in SegaliudLokan-Deramakot-Tangkulap, Sapulut, Roda Mas and Ratah, respectively.

The histograms were represented as probability density functions which indicate relative frequency of nMDS axis-1 scores in each FMU. The histogram of the

nMDS axis-1 scores of each FMU was used as an index of the spatial variability of the magnitude of forest intactness, and the mean value was used as the average condition in each FMU. To compare the histograms of the nMDS axis-1 scores among FMUs, a regression model based on all plots in each FMU was extrapolated to the entire area of the FMU, from which the histogram was derived.

To compare the differences in the mean nMDS axis-1 scores among the six FMUs, I calculated 95% confidence intervals of the mean values in each FMU. If the confidence intervals were not overlapped between a given pair of FMUs, then the difference in the mean nMDS axis-1 scores between the two FMUs was considered to be statistically significant. To calculate the confidence intervals of mean nMDS axis-1 scores, I repeated the model establishment using the same method as cross-validation approach (see also section 4.3.5) in each FMU. I extrapolated the models to the entire area with 1000 iterations. Then, I obtain the 1000 mean values of nMDS axis-1 scores of the targeted area. The 95% confidence interval was calculated as the 25^{th} (upper limit) and 975^{th} (lower limit) highest values in the 1000 samples. Then the relationships of the derived confidence intervals of mean nMDS axis-1 scores with the type of forest management were examined.

4.3.7. Detection of temporal changes of canopy-condition within FMUs

To assess whether my method could detect the temporal changes of forest intactness, I analyzed the changes in mean nMDS axis-1 scores between 2010 and 2015 in Ratah, and between 2009 and 2014 in Segaliud Lokan, Deramakot and Tangkulap. In this procedure, the estimated nMDS axis-1 scores based on Landsat-TM (2009) and Landsat-OLI (2014) were used for Segaliud Lokan, Deramakot and Tangkulap, and Landsat-TM (2010) and Landsat-OLI (2015) were used for Ratah. I used the same procedure as the comparison of spatial variation among FMUs (see section 4.3.6) to

detect temporal changes within each FMU. If the 95% confidence intervals of mean nMDS axis-1 scores were not overlapped, then the changes in forest intactness were considered to be statistically significant.

4.4. Results

4.4.1. Forest-intactness maps

The nMDS axis-1 scores based on the stepwise selection were mainly explained by the short-wave infrared (SWIR) reflectance, textures, and SD (Table 4.2). The correlation coefficient scores between the predicted and observed nMDS axis-1 scores ranged from 0.57 to 0.75 (Table 4.2, Figure 4.2). The derived forest-intactness maps of six FMUs are shown in Figure 4.3. The maps show the estimated nMDS axis-1 scores based on Landsat-OLI (2014) in Segaliud Lokan, Deramakot and Tangkulap, and Landsat-OLI (2013), Landsat-OLI (2015) and Landsat-OLI (2015) in Sapulut, Roda Mas and Ratah, respectively. Each pixel in the maps contains an nMDS axis-1 score, and the color gradation from blue to red indicates a gradient of nMDS axis-1 scores from high to low values as a proxy for the canopy tree composition at a genus level. The maps showed conspicuous blue areas corresponding to the tree-community composition of an intact forest as well as conspicuous red areas corresponding to the tree-community composition of the least intact forest. Intact forests and least-intact forests were indicated as the two extremes of a continuum of forest degradation in my method.

Several FMUs had areas of intact forests (e.g., along the left part of Deramakot, the left side in Ratah and upper-right side in Roda Mas). Some FMUs had conspicuous red-yellow areas, which corresponded to highly degraded areas. There was a conspicuous red-yellow area in the eastern part of Ratah, which corresponded to the land after forest fire in 1998. The red-yellow area at the western part of Roda Mas

was allocated to local people who practice slash and burn agriculture. Mosaics of red areas occurred in Sapulut, which corresponded to industrial tree plantations. The forest intactness inside the Deramakot was mostly high, reflecting the history of reduced-impact logging and a longer cutting cycle (i.e., 40 years). In contrast, the forest intactness in Segaliud Lokan, where reduced-impact logging had been implemented after 2002 was extremely low, probably because Segaliud Lokan was repeatedly logged using conventional logging until 2002 and the negative effects on canopy condition still remained in this FMU. Tangkulap where all logging activities had remained suspended after 2002 still had many yellow-red areas inside, indicating that the negative effects of the high-impact conventional logging that was conducted before 2002 still persisted even after 12 years.

4.4.2. Validation of community-composition (nMDS axis-1) models

The cross validation indicated that the accuracy of the model estimates varied among FMUs but was generally high. The means (95% confidence interval, CI) of the iteratively calculated correlation coefficients between the estimated nMDS axis-1 scores and actual observed scores (adjusted R^2 values) were 0.62 (CI 0.19–0.90), 0.64 (CI 0.42–0.83), 0.57 (CI 0.31–0.83), 0.74 (CI 0.49–0.92), 0.60 (CI 0.30–0.79), and 0.51 (CI 0.18–0.73) for Segaliud Lokan-Deramakot-Tangkulap (2009), Segaliud Lokan-Deramakot-Tangkulap (2014), Sapulut (2013), Roda Mas (2015), Ratah (2010), and Ratah (2015) respectively (Figure 4.3).

4.4.3. Spatio-temporal changes in nMDS axis-1 scores among/within FMUs

The histograms of the nMDS axis-1 scores in six FMUs as a snapshot for the same year (2013-2015) are shown in Figure 4.4. The histograms varied significantly among the FMUs in terms of mode and pattern; the ranges were the same because the

nMDS axis-1 scores were standardized across the FMUs. The mode of Roda Mas had the highest axis-1 score among the six FMUs, indicating that relatively intact forests occurred over a disproportionately greater area in Roda Mas. At the same time, the density of low nMDS axis-1 scores (nMDS axis-1 score $\leq$ -1) was also nominal in Roda Mas, indicating the occurrence of current logging activities and community encroachment. The mode in Deramakot, the model site of sustainable forest management in Sabah, had the second highest score among the FMUs. The mode of Segaliud Lokan had the lowest axis-1 score among the six FMUs, reflecting the longer history of conventional logging. The mode of Sapulut, where industrial tree plantations were included, had the second lowest score. Although all logging activities were suspended since 2002 in Tangkulap, the mode of Tangkulap was lower than the FMUs implementing logging with sustainable forest management (Deramakot, Roda Mas and Ratah), probably because the negative effects of past high-intensity logging persisted in this FMU. The nMDS axis-1 scores of the modes among six FMUs well reflected their logging intensity, history and/or management.

The mean values and 95% confidence intervals of the nMDS axis-1 scores of the six FMUs (derived from Figures 4.3 and 4.4) are shown in Figure 4.5a with increasing order of their mean nMDS axis-1 score. Deramakot, which was designated as a model of sustainable forest management by the Sabah Government, recorded the highest mean score, 0.333 (CI 0.271–0.405). The second-highest score was 0.276 (CI 0.209–0.348) in Roda Mas. The mean score was 0.209 (CI 0.116–0.278) in Ratah, 0.189 (CI -0.061–0.091) in Tangkulap, -0.083 (CI -0.183–0.010) in Sapulut and -0.289 (CI -0.367– -0.223) in Segaliud Lokan. The mean scores of the FMUs implementing sustainable forest management with reduced impact logging (i.e., Deramakot, Roda Mas and Ratah) except for Segaliud Lokan were significantly higher than the other FMUs.

The temporal changes of mean values and 95% confidence intervals of the nMDS axis-1 scores within each of four FMUs are shown in Figure 4.5b. The mean nMDS axis-1 scores of Segaliud Lokan significantly decreased between 2009 and 2014, while there was no significant change in the other FMUs. Although not significant, the mean nMDS axis-1 scores of Deramakot increased considerably. The mean nMDS axis-1 scores of Tangkulap and Ratah tended to decline, although all logging activities remained suspended in Tangkulap and sustainable forest management was implemented in Ratah.

4.5. Discussion

To address the increasing need for a practical method of assessing biodiversity that is spatially and temporally sensitive and robust, I developed an algorithm to map forest intactness based on tree-community composition. As a proxy for tree-community composition, I used the nMDS axis-1 score, a robust and sensitive indicator of forest intactness in Bornean natural production forests (Imai *et al.*, 2014). The maps based on the algorithm demonstrated a significant variation in composition of tree genera both among and within FMUs.

To date, several remote sensing methods have been developed to map tree-community composition using imaging spectroscopy (Schmidtlein & Sassin, 2004; Schmidtlein *et al.*, 2007; Feilhauer & Schmidtlein, 2009; Feilhauer *et al.*, 2011; Gu *et al.*, 2015). While imaging spectroscopy (also known as hyperspectral imagery) can characterize variation in tree compositional assemblages, multispectral imageries (e.g., Landsat) have been considered to lack the spectral resolution to effectively demonstrate compositional variation (Asner & Martin, 2008; Rocchini, 2007). However, my study shows that multispectral remote-sensing data of Landsat images are potentially useful for characterizing the variation in composition of tree genera

caused by logging and forest degradation. The concept of mapping compositional gradients using remote sensing is based on the assumption that the compositional gradients of vegetation are related to variation in canopy traits such as reflectance spectra, foliar chemistry, morphological traits, canopy form, and canopy structure (Feilhauer *et al*., 2011). Clearly, Landsat imagery may not effectively resolve subtle intra-guild trait variation (e.g., trait variation within climax guild) because of the low spatial/spectral resolution; however, Landsat imagery has been proven to be capable of detecting inter-guild trait differences (i.e., trait differences between pioneer and climax guilds) (Wittmann *et al*., 2002; Tangki & Chappell, 2008) as shown by my algorithm. The reason why the proxy for community composition (nMDS axis-1 score) used in my study is able to reflect canopy intactness is that the nMDS axis-1 scores can reflect the interaction of linearly increasing pioneer guild and linearly decreasing climax guild with increasing logging intensity (Imai *et al.*, 2014). Thus, the selected independent variables in my models and Landsat imageries reflect the interactions of these guilds. The variables selected by stepwise selection were principally related to SWIR reflectance and spectral heterogeneity information (i.e., texture and SD). SWIR reflectance is significantly related to stand age, height, volume, and biomass in tropical secondary forest (Steininger, 2000; Langner *et al*., 2012). In contrast, spectral heterogeneity information can be considered a proxy for species diversity (Rocchini *et al*., 2010). These patterns were also apparent in my study. SWIR reflectance was a proxy for tree growth (i.e., biomass) after logging, while texture and SD were related to the heterogeneity of the two major regeneration guilds. I suggest that SWIR reflectance and spectral heterogeneity information can reflect the interactions of the two guilds, and my algorithm is thus suitable for the characterization of the variation in composition of tree genera caused by logging disturbances.

It should also be noted that the selected independent variables and

coefficients varied among models. My study area covered the broad area of Borneo, spanning a large geographic area, and included significant floristic differences among the tropical rain forests (Slik *et al*., 2003). Therefore, the selected independent variables would be expected to vary among FMUs, reflecting variation in canopy structure and foliar traits.

My maps are clearly useful for differentiating between intact and highly disturbed forests within each FMU. It can identify the location and extent of intact forests as areas of potentially high conservation value, or those of least-intact forests where mitigation measures are required. Combining the maps with histogram and mean value of nMDS axis-1 score, I could quantitatively diagnose the magnitude of forest intactness. The histograms show the frequency distribution of nMDS axis-1 scores with varying degree of canopy degradations. Histograms and mean value of nMDS axis 1 scores derived from my maps could legitimately indicate the magnitude of forest intactness. My maps can also indicate ecosystem integrity and health of logged-over tropical rain forests because the areas of low nMDS scores suggest the dominance of pioneer guilds, which in turn suggests possible lack of regeneration, impoverishment of biodiversity of other taxa, possible lack of resilience and high susceptibility to fire (Asner *et al*., 2005; Langner *et al*., 2007).

The mean adjusted R^2 values (0.51–0.74) based on the cross-validation approach showed close correlation in all FMUs. The mean adjusted R^2 values were high despite the use of moderate-resolution Landsat data and the semi-qualitative nature of my metrics (i.e., tree-community composition), which were based on the mixing ratio of the canopy genera. However, the range of adjusted R^2 values (0.2–0.9) at the 95% confidence interval across all FMUs was fairly wide; this probably indicates that the number of plots used for cross validation may be small. Because of the wide variation in the R^2 values at the 95% confidence interval, it was difficult to

discriminate all FMUs from one another, despite the fact that the mean nMDS axis-1 scores per se differed among FMUs. However, I was able to statically differentiate the FMUs implementing sustainable forest management (i.e., Deramakot, Roda Mas and Ratah) from the other FMUs. The other FMUs with lower forest intactness were separated into further two units. Segaliud Lokan showed the lowest mean nMDS axis-1 score and was differentiated from the other FMUs. Because Segaliud Lokan had a longer history of high-impact conventional logging (from 1958 to 2002), the results clearly reflect the effect of the forest management history. Furthermore, the mean nMDS axis-1 scores of Segaliud Lokan significantly decreased between 2009 and 2014, while there was no significant change in the other FMUs. This indicates that the conversion of forests in Segaliud Lokan via either logging and/or plantation is greater in magnitude than the other FMUs. Combination of forest intactness map with the boot-strapping approach using confidence intervals is clearly useful for diagnosing spatial and temporal variations in forest intactness among/within FMUs under different management regimes.

The applicability of my method was verified over a broad geographic range (0°7’S–5°20’N, 114°25’–115°30’E) spanning the most area of Borneo. The principle of using tree-community composition may also be applicable to other forests outside Borneo because the occurrence of the two major regeneration guilds (i.e., the pioneer and climax guilds) is a common biological phenomenon; however, this needs to be tested in the future. One of the advantages of this method is the broad coverage and low cost based on using Landsat imagery. The spatial and temporal availability of Landsat imagery is superior to other remote sensing data, and therefore the Landsat-based tree-community composition map is suitable for regional and global biodiversity monitoring. These advantages are essential for a global biodiversity assessment of the Aichi Biodiversity Targets and REDD+ biodiversity safeguards. I

propose a practical method combining count-plot surveys on the ground with Landsat remote-sensing for large-scale forest biodiversity/ecosystem assessments of both the Aichi targets and REDD+ biodiversity safeguards in natural forests in the tropics.

Tables

Table 4.1. Profiles of the forest management units (FMUs) targeted in this study

Name	State/province, nation	Silviculture and timber harvest	Forest certification	Plot number
Segaliud Lokan	Sabah, Malaysia	1958–2002 CL, Since 2003 RIL	MTCC	50 (2012) 44 (2014)
Deramakot		1956–1985 CL, Since 1995 SFM with RIL	FSC	
Tangkulap		1970–2002 CL	FSC	
Sapulut		1956–2000 CL, Since 2001 RIL	MTCC	50 (2012)
Roda Mas	East Kalimantan, Indonesia	Since at least 2008 SFM with RIL	FSC	50 (2014)
Ratah		1972–2010 CL, Since 2010 SFM with RIL	FSC	50 (2012) 40 (2015)

Parentheses indicate years when plots were established. CL, conventional logging; RIL, reduced impact logging; SFM, sustainable forest management; FSC, Forest Stewardship Council; MTCC, Malaysian Timber Certification Council

Table 4.2. Description of established multivariate regression models based on all plots for each FMU.

	R^2	Coefficient	SE	T value	Pr (>|t|)
Segaliud Lokan-Deramakot-Tangkulap 2009 (N=50)					
$B5_{TM}$	0.61	-0.53599	3.88E-04	5.2435	<0.001
GLCM_mean_NDSI		0.37928	1.89E-02	3.79207	<0.001
Segaliud Lokan-Deramakot-Tangkulap 2014 (N=86)					
$B7_{OLI}$	0.64	-0.61447	8.92E-04	6.6404	<0.001
GLCM_mean_EVI		-0.16068	1.65E-02	2.4093	1.83E-02
GLCM_homogenity_$B3_{OLI}$		0.16754	7.36E+00	2.5411	1.30E-02
NDSI		-0.22618	2.99E+00	2.4598	1.60E-02
Sapulut (N=45)					
$B6_{OLI}$	0.60	-0.46159	2.40E-05	3.7795	< 0.001
GLCM_contrast_$B3_{OLI}$		0.37483	3.10E-05	3.8679	< 0.001
$B5_{OLI}$		-0.36385	1.20E-05	3.0253	4.30E-03
GLCM_mean_$B6_{OLI}$		-0.286	8.20E-03	2.8178	7.50E-03
Roda Mas (N=45)					
$B6_{OLI}$	0.75	-0.86698	7.50E-05	4.9699	< 0.001
SD_NDSI		-0.75056	1.20E-04	4.5416	< 0.001
SD_NDWI		-2.12925	2.20E-04	4.6781	< 0.001
SD_NDVI		2.00116	4.50E-04	3.373	1.70E-03
$B4_{OLI}$		0.56146	4.70E-04	2.3481	2.40E-02
Ratah 2010 (N=64)					
$B7_{TM}$	0.62	-1.42357	1.30E-03	7.02905	< 0.001
$B3_{TM}$		0.75859	2.80E-03	3.74366	< 0.001
GLCM_dissimilarity_$B4_{TM}$		0.25656	9.80E-03	3.2506	1.90E-03
Ratah 2015 (N=69)					
$B6_{OLI}$	0.57	0.78594	4.22E-05	9.5079	<0.001
GLCM_homogenity_$B6_{OLI}$		-0.22183	7.07E+00	2.6836	9.20E-03

N, number of plots used for each model; R^2, adjusted R-squared value; Coefficient,

standardized partial regression coefficient; SE, standard error; GLCM, grey level co-occurrence matrix; NDSI, normalized difference soil index; EVI, enhanced vegetation index; NDWI, normalized difference water index; NDVI, normalized difference vegetation index

Figures

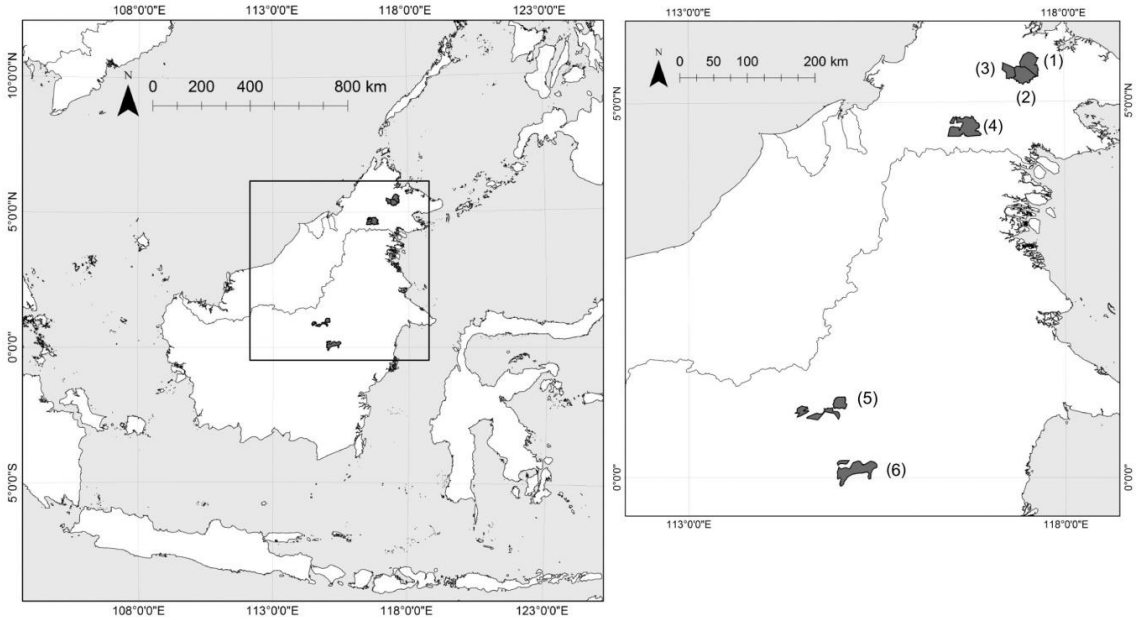

Figure 4.1. Locations of the six forest management units (FMUs) in this study: (1) Segaliud Lokan, (2) Deramakot, (3) Tangkulap, (4) Sapulut, (5) Roda Mas, and (6) Ratah.

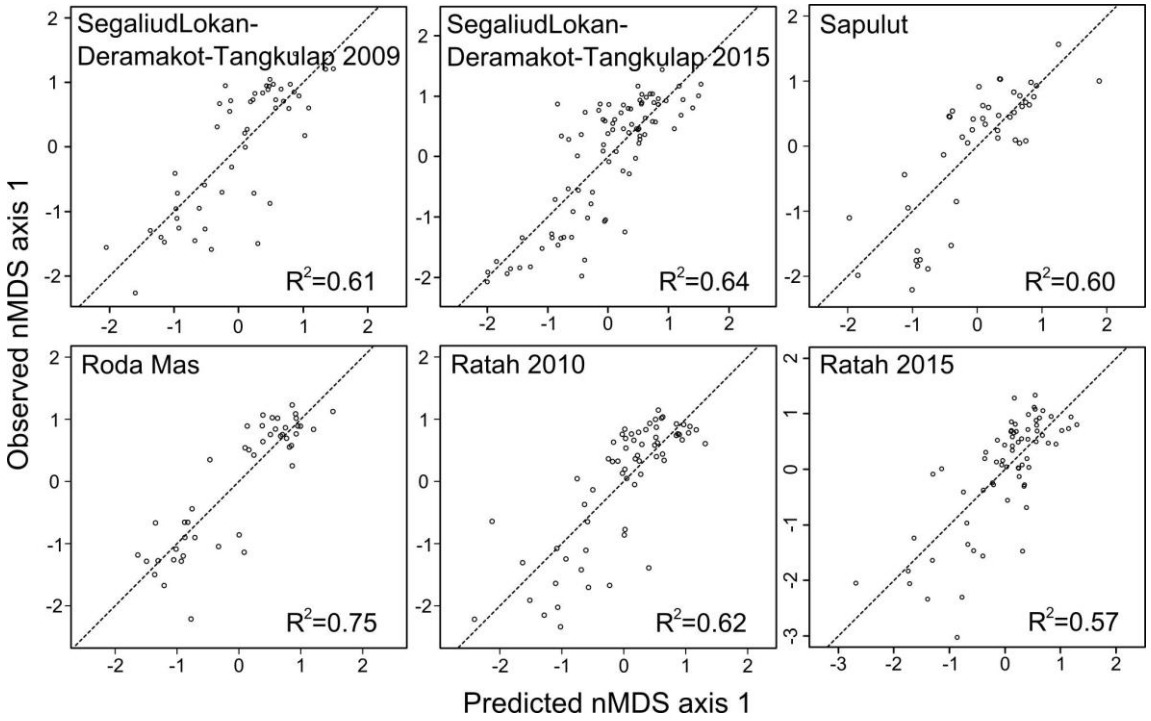

Figure 4.2. Model fits for all available inventory plots in each FMU. Scatter plots show relationships between predicted and observed scores.

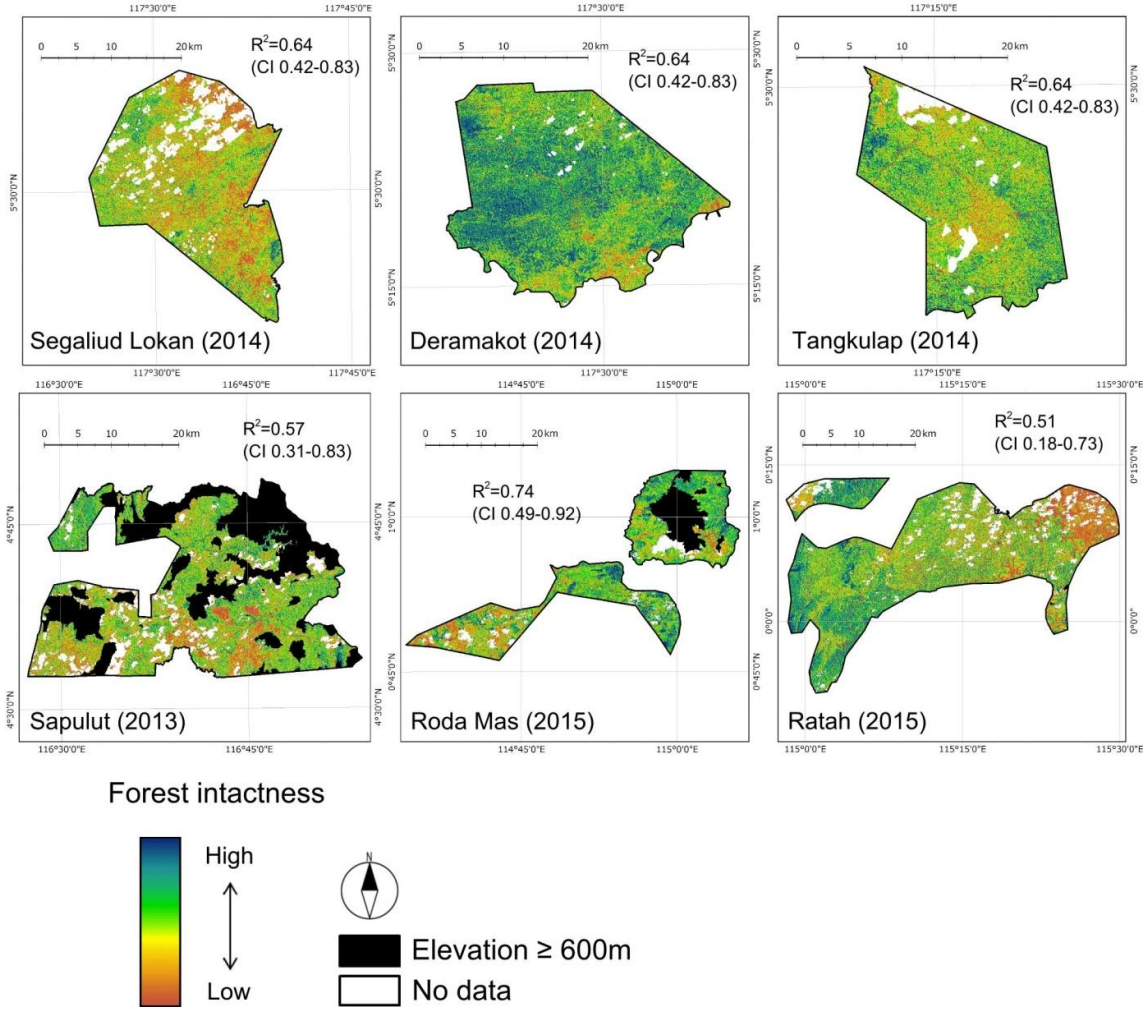

Figure 4.3. Tree-community composition maps of all FMUs. A color gradation from blue to red indicates a gradient of nMDS axis-1 scores from high to low values as a proxy for canopy generic composition.

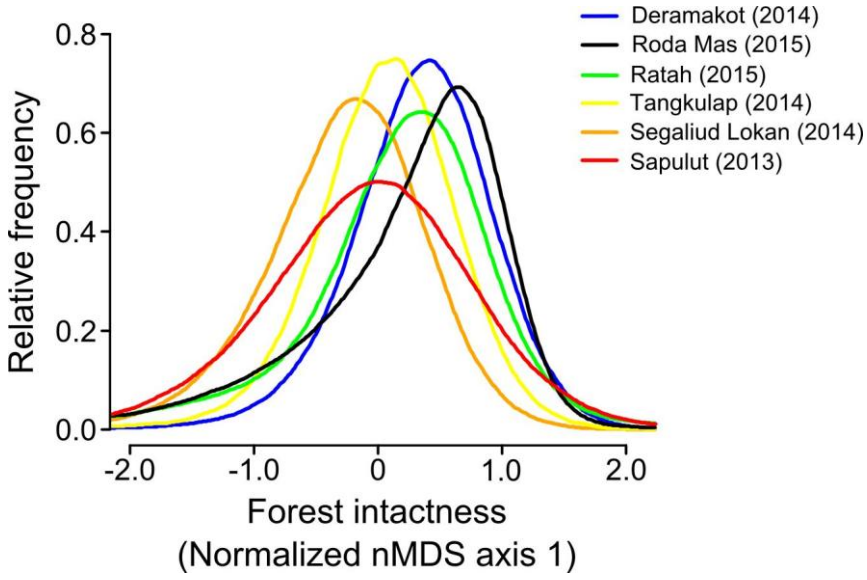

Figure 4.4. Histograms of nMDS axis-1 scores in all FMUs for the same period (2013-2015).

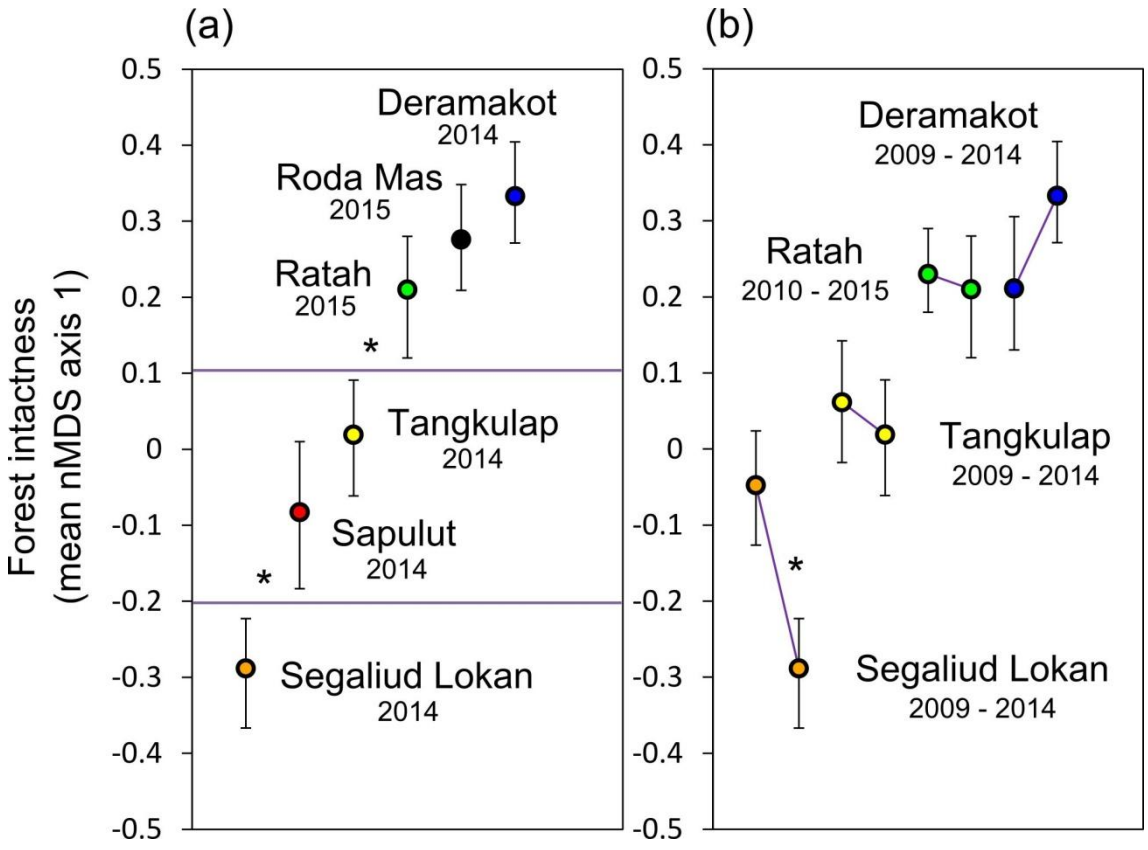

Figure 4.5. (a): Mean values and 95% confidence intervals of the nMDS axis-1 scores among six FMUs for the same period (2013-2015). The six FMUs are arranged in increasing order of their mean nMDS axis-1 score. **(b)**: Temporal changes of mean values and 95% confidence intervals of the nMDS axis-1 scores over 5 years in each of the four FMUs (Segaliud Lokan, Deramakot, Tangkulap and Ratah).

* Significant difference.

Chapter 5: General discussion

Facing the recent rapid loss of biodiversity in tropical forest ecosystems, there is an increasing need for developing a practical means for monitoring biodiversity, which is spatiotemporally sensitive and robust. A key obstacle is the lack of global, integrated observation systems for delivering regular, timely data on changes in biodiversity (Scholes *et al*., 2012; Pereira *et al*., 2013; Goetz *et al*., 2015). In the present thesis, I aimed to examine if tree (plant)-community composition can be extrapolated to a landscape and can reflect disturbance histories (spatial representativeness), and to develop practical methods for monitoring biodiversity based on plant-community composition in secondary vegetation after shifting cultivation (Chapter 2 & 3) and canopy-tree community composition in selectively logged lowland forests (Chapter 4). I targeted the two major types of tropical forests, secondary vegetation after shifting cultivation and selectively-logged lowland forests, because the two types of vegetation dominate the landscapes of Borneo and have a critical importance for ecosystem conservation (Langner *et al*., 2007; Stibig *et al*., 2007; Miettinen *et al*., 2014). Borneo is one of the biodiversity hot spots in the world (Myers *et al*., 2000) but at the same time cultivated land and logged-over secondary forests cover approximately 75 % of the total forest land (Langner *et al*., 2007). These forests are going to be cultivated and logged repeatedly in the near future. Evaluating the spatiotemporal effects of such repeated disturbances on biodiversity is critical for developing effective conservation policies on tropical biodiversity.

To examine the 1st and 2nd research question addressed in Chapter 1, I developed a new algorithm to estimate the ages of tropical secondary vegetation after shifting cultivation in Chapter 2. I demonstrated that a combination of a

high-resolution satellite image and time-series Landsat images provide reliable temporal information (stand age after shifting cultivation) of vegetation patches on a spatiotemporally dynamic landscape. Subsequently, in Chapter 3, I evaluated and predicted the spatiotemporal dynamics of vegetation by extrapolating the explicit temporal patterns of species composition and above-ground biomass derived by Nishio (2014) and Fujiki *et al*. (2017) into the stand-age algorithm.

The novelty of my algorithm is the data integration from two different resolution images. This mutually compensates for the weakness of high-resolution satellite images (i.e., unavailability of archived past images) and weakness of Landsat images (i.e., incapability of detailed mapping). Recent development of change detection techniques is remarkable (Kennedy *et al*., 2007; Masek *et al*., 2008; Helmer *et al*., 2009; Vogelmann *et al*. 2009; Huang *et al*., 2010; Hansen *et al*., 2013; Achard *et al*., 2014), but their main concern is how to improve accuracy of the detection. Most techniques are constrained by the resolution of images, such as time-series Landsat images. I could classify the stand age of vegetation at a shorter time span than previous studies, which was attributed to the combination of these two resolution imageries. My methods are effective in mapping structure and composition of highly dynamic forests at landscape level, and in predicting the future patterns of important ecosystem services based on land-use scenarios.

In Chapter 4, I investigated the 3rd and 4th research questions. I characterized canopy conditions of logged-over forests, which reflected the interaction of linearly increasing pioneer guilds and linearly decreasing climax guilds with increased logging intensity, on moderate-resolution satellite imageries. I developed method that can capture the effects of forest management practices using canopy-tree community composition in tropical production forests. Moderate-resolution satellite imagery (i.e. Landsat imagery) has been considered to lack the spectral resolution to effectively

demonstrate compositional variation (Asner & Martin, 2008; Rocchini, 2007). However, inclusion of texture parameters calculated using a 3×3 window pixel of Landsat in my method could improve this problem. Past studies reported that the texture metrics were useful to estimate above ground biomass (Kuplich *et al*., 2005; Sarker and Nichol, 2011; Xu *et al*., 2011; Eckert, 2012; Vashum and Jayakumar, 2012; Dube and Mutanga, 2015b), but there was no application in quantitative estimates of plant compositional variation. In the present thesis, texture metrics well reflected the inter-guild trait differences (i.e. trait differences between pioneer and climax guilds), and enhanced the estimation accuracy, probably because texture metrics were related to the mixing ratio of the two major regeneration guilds. As a result, the tree-community composition in selectively-logged production forests could be estimated with a high accuracy (R^2: 0.51–0.74). Subsequently, I calculated 95% confidence intervals of the mean values of the tree-compositional indicator to detect the spatial/temporal changes among/within the six forest management units (FMUs). My method could reliably distinguish the FMUs implementing sustainable forest management from the FMUs having a longer history of high-impact conventional logging, and detect significant changes in tree-community composition within each FMU. I suggest that the texture metrics of Landsat imagery are an important parameter to characterize tree-community composition in dynamic tropical forests, and the confidence intervals of the tree-compositional indicator is useful to test the spatiotemporal changes in tree-community composition among/within FMUs.

5.1. Spatial representativeness of tree compositional indicator

Both in secondary vegetation after shifting cultivation and selectively-logged lowland forests, I demonstrated that tree-community composition (partly included herbaceous and shrub communities in the secondary vegetation after shifting cultivation) can be

extrapolated to a landscape and can reflect disturbance histories. In secondary vegetation after shifting cultivation, I estimated plant-community composition indirectly. Stand ages of tropical secondary vegetation could be mapped with a high accuracy (84.28%) based on the developed algorithm. Because plant compositional indicator (DCA axis 1 in this case) is strongly correlated with stand age (R^2=0.69), plant-community composition can reliably be extrapolated to the landscape. On the other hand, I developed the models which directly estimate the tree-community composition from satellite images in selectively-logged lowland forests. The mean adjusted R^2 values based on the cross-validation approach showed a high accuracy (0.51–0.74) in my six models, despite the use of moderate-resolution Landsat data and the semi-qualitative nature of my metrics (i.e., tree-community composition). Compared with the accuracy of R^2 (0.66; 95% CI: 0.39–0.85; Langner *et al*., 2012) for the above-ground biomass (AGB) estimation in the same area using Landsat imagery (Deramakot and Tangkulap), the accuracy of my models is reasonable.

Imai *et al*. (2014) proposed that the tree-community composition as a reliable and practical biodiversity indicator for disturbance histories in spatiotemporally dynamic tropical forests. However, there has been an unresolved issue related to the tree compositional indicator, which is spatial representativeness. The studies using satellite remote sensing to quantitatively estimate plant-community composition based on ordination techniques were completely lacking in human-disturbed dynamic forests. My study indicated that tree (plant)-community composition could be mapped either directly or indirectly at a landscape level with high accuracy using satellite remote sensing. In this thesis, along with Imai *et al*. (2014), I propose a tree (plant)-community composition as a reliable and sensitive indicator of biodiversity, which can be extrapolated to landscape in spatiotemporally dynamic forests.

5.2. Practical methods for monitoring biodiversity

Appropriate biodiversity monitoring should fulfill certain conditions. It should have (1) high accuracy and sensitivity, (2) feasibility (cost-effectiveness), (3) scalability, and (4) relevance to the mechanisms of biodiversity conservation, such as REDD+ and the Aichi Biodiversity Targets (Pereira *et al*., 2013). The methods of biodiversity monitoring must satisfy these conditions.

5.2.1. Biodiversity monitoring in secondary vegetation after shifting cultivation

(1) *Accuracy, sensitivity*: Stand ages of tropical secondary vegetation after shifting cultivation could be mapped with a high accuracy (84.28%) based on the developed algorithm. Considering that the newly launched Landsat 8 multispectral sensor is available from 2013 and is capable of detecting vegetation variables accurately (Dube and Mutanga, 2015b), my algorithm can be used to detect deforestation caused by shifting cultivation at annual or several-years span. Therefore, my methods have both reliable accuracy and temporal sensitivity. (2) *Feasibility (cost effectiveness)*: High spatial resolution (pixel size < 10 m^2) of commercial satellites have provided new opportunities for habitat mapping at a fine spatial scale. However, the application of high-resolution satellite images to a multi-temporal analysis is difficult because associated monetary cost is high. In my algorithm, time-series Landsat images were used to derive the land history of slash-and-burn as an alternative to high-resolution satellite images. Therefore, my algorithm needs one high-resolution image only to conduct multi-temporal analyses. Furthermore, once field-based models are established, my method can repeatedly be used for carbon and biodiversity monitoring at a landscape level, because my algorithm does not require extensive field inventories to acquire stand age information. Such advantages minimize monetary costs associated with image acquisition and field surveys. (3) *Scalability*: The principle of combining

time-series Landsat images with a high-resolution satellite image may also be applicable to other areas, since vegetation recovery after clearance is a widespread biological phenomenon. However, the use of high-resolution imagery limits the scalability of this algorithm, because the application of a high-resolution imagery at a global or regional scale is too costly. The scalability of this algorithm is depending on the future advancement of satellite technology to reduce the costs. Human judgment in the manual procedure of segment sampling (i.e. Chapter 2: 2.3.3.5: Segment sampling) may be another concern when one duplicates our algorithm in other areas. My algorithm tried to minimize judgment errors by adding an LDA procedure, but omitting all human judgments is not possible. The scalability of my algorithm must be improved and investigated in the future. (4) *Relevance*: My algorithm can provide quantitative information of current status of CO_2 emission (baseline) and expected reduction based on some scenarios, both of which are prerequisite for REDD+. At the same time, it can provide biodiversity information based on tree-community composition to assess the effectiveness of REDD+ safeguards and progress of the Aichi Biodiversity Targets. Once field-based models are established, my method can repeatedly provide carbon and biodiversity information, which is useful for evaluating the progress of REDD+ and the Aichi Biodiversity Targets.

Although the scalability of my algorithm is inevitably limited due to the nature of high-resolution imagery, the algorithm is superior in sensitivity, feasibility and relevance to conservation mechanisms. I recommend that my algorithm be used as a means for repeatedly mapping carbon and biodiversity in a high-priority area for conservation such as a ‘matrix’, to develop adequate policies for reconciling the livelihood production and forest conservation.

5.2.2. Biodiversity monitoring in selectively-logged production forests

(1) *Accuracy, sensitivity*: The mean adjusted R^2 values (0.51–0.74) based on the cross-validation approach showed high accuracy in my models. Although it was difficult to differentiate all FMUs from one another, I was able to statically discriminate the FMUs according to forest management regimes. Combination of tree-community composition map with the boot-strapping approach using confidence intervals is a useful and reliable tool for diagnosing spatial and temporal variations in biodiversity among/within FMUs under different management regimes. (2) *Feasibility (cost effectiveness)*: My methods are clearly cost-effective in overall performance. There are three reasons. First, I use tree genera instead of tree species to calculate the ordination of community composition. Imai *et al*. (2014) concluded that the identification of canopy trees at a generic level could reduce the cost and time of identification by at least 60% compared with the conventional routine survey (i.e. identification at a species level). Second, before I and my colleagues established inventory plots, I classified each FMU into five strata according to the extent of forest degradation using satellite imagery. This procedure reduces the efforts of field survey compared with a completely randomized design. Third, I use Landsat imagery to map tree generic composition, and its cost is low due to the free availability of the imagery. (3) *Scalability*: The applicability of my method was verified over a broad geographic range (0°7’S–5°20’N, 114°25’–115°30’E) spanning the most area of Borneo. The principle of using tree-community composition may also be applicable to other forests outside Borneo because the occurrence of the two major regeneration guilds (i.e., the pioneer and climax guilds) is a common biological phenomenon; however, this needs to be tested in the future. (4) *Relevance*: One of the advantages of this method is the broad coverage and low cost based on using Landsat imagery. The spatial and temporal availability of Landsat imagery is superior to other remote sensing data, and therefore the Landsat-based tree-community composition map is suitable for regional and global

biodiversity monitoring. These advantages are essential for a global biodiversity assessment of the Aichi Biodiversity Targets and REDD+ biodiversity safeguards.

One of the advantages of this method is the broad coverage and low cost based on Landsat imagery. The spatial and temporal availability of Landsat imagery is superior to other remote sensing data, and therefore the Landsat-based tree-community composition map is suitable for regional and global biodiversity monitoring. These advantages are essential for a global biodiversity assessment of the Aichi Biodiversity Targets and REDD+ biodiversity safeguards. I propose a practical monitoring method combining count-plot surveys on the ground with Landsat remote-sensing for large-scale forest biodiversity/ecosystem assessments.

5.3. Conclusion

Demonstrating the new potentials of Landsat series is my original and novel contribution to the remote sensing science. The Landsat series have significant importance in terms of the utility of remote sensing for monitoring biodiversity because they have its continuity, affordability, and accessibility. However, with large pixel sizes of Landsat imagery (i.e., 30 m), pixel-level mixing of multiple species with different functional traits has been considered to prevent from comprehensive mapping of individual tree species or assemblages. In the present thesis, I tried to overcome such a limitation and demonstrated the potentials of Landsat imagery to elucidate tree (plant)-community composition.

This thesis demonstrated that tree (plant)-community composition could be mapped at a landscape level with a high accuracy based on the models developed between ordination scores of community composition and satellite reflectance in secondary vegetation after shifting cultivation and selectively-logged lowland forests in Borneo. The present thesis provides cost-effective means for repeatedly mapping

tree (plant)-community composition in two major types of tropical vegetation. Although it needs to be tested in other area with different vegetation types, the principle of using tree (plant)-community composition may be applicable to other forests outside Borneo because vegetation recovery after clearance and the occurrence of the two major regeneration guilds (i.e., the pioneer and climax guilds) after selective logging are a common biological phenomenon. In the present thesis, I propose two practical methods for large-scale forest biodiversity/ecosystem assessments, which can potentially be used for biodiversity assessment of the Aichi Biodiversity Targets and REDD+ biodiversity safeguards.

References

Achard, F., Beuchle, R., Mayaux, P., Stibig, H. J., Bodart, C., Brink, A., ... & Lupi, A. (2014). Determination of tropical deforestation rates and related carbon losses from 1990 to 2010. *Global change biology*, *20*(8), 2540-2554.

Achard, F., Eva, H. D., Stibig, H. J., Mayaux, P., Gallego, J., Richards, T., & Malingreau, J. P. (2002). Determination of deforestation rates of the world's humid tropical forests. *Science*, *297*(5583), 999-1002.

Aiba S, Kitayama K. (1999). Structure, composition and species diversity in an altitude-substrate matrix of rain forest tree communities on Mount Kinabalu, Borneo. *Plant Ecol* 140:139–157.

Allnutt, T. F., Ferrier, S., Manion, G., Powell, G. V., Ricketts, T. H., Fisher, B. L., ... & Lees, D. C. (2008). A method for quantifying biodiversity loss and its application to a 50 - year record of deforestation across Madagascar. *Conservation Letters*, *1*(4), 173-181.

Arvor, D., Durieux, L., Andrés, S., & Laporte, M. A. (2013). Advances in geographic object-based image analysis with ontologies: a review of main contributions and limitations from a remote sensing perspective. *ISPRS Journal of Photogrammetry and Remote Sensing*, 82, 125-137.

Asner, G. P. (2001). Cloud cover in Landsat observations of the Brazilian Amazon. *International Journal of Remote Sensing*, 22(18), 3855-3862.

Asner, G. P., & Vitousek, P. M. (2005). Remote analysis of biological invasion and biogeochemical change. *Proceedings of the National Academy of Sciences of the United States of America*, *102*(12), 4383-4386.

Asner, G. P., Knapp, D. E., Broadbent, E. N., Oliveira, P. J., Keller, M., & Silva, J. N. (2005). Selective logging in the Brazilian Amazon. *Science, 310(5747)*, 480-482.

Asner, G. P., & Martin, R. E., (2008). Airborne spectranomics: mapping canopy chemical and taxonomic diversity in tropical forests. *Frontiers in Ecology and the Environment*, *7*(5), 269-276.

Asner, G. P., Powell, G. V., Mascaro, J., Knapp, D. E., Clark, J. K., Jacobson, J., ... & Secada, L. (2010). High-resolution forest carbon stocks and emissions in the Amazon. *Proceedings of the National Academy of Sciences*, *107*(38), 16738-16742.

Asner, G. P., Martin, R. E., Tupayachi, R., Anderson, C. B., Sinca, F., Carranza-Jiménez, L., & Martinez, P. (2014). Amazonian functional diversity from forest canopy chemical assembly. *Proceedings of the National Academy of Sciences*, *111*(15), 5604-5609.

Asner, G. P., Martin, R. E., Anderson, C. B., & Knapp, D. E. (2015). Quantifying forest canopy traits: Imaging spectroscopy versus field survey. *Remote Sensing of Environment*, *158*, 15-27.

Baatz, M., Benz, U., Dehghani, S., Heynen, M., Höltje, A., Hofmann, P., *et al*., (2004). eCognition User Guide 4, 133−138. Munich, Germany: Definiens Imaging, Germany.

Baccini, A. G. S. J., Goetz, S. J., Walker, W. S., Laporte, N. T., Sun, M., Sulla-Menashe, D., ... & Samanta, S. (2012). Estimated carbon dioxide emissions from tropical deforestation improved by carbon-density maps. *Nature Climate Change*, *2*(3), 182-185.

Barbosa, J. M., Melendez-Pastor, I., Navarro-Pedreño, J., & Bitencourt, M. D. (2014). Remotely sensed biomass over steep slopes: An evaluation among successional stands of the Atlantic Forest, Brazil. *ISPRS Journal of Photogrammetry and Remote Sensing*, *88*, 91-100.

Baum, K. A., Haynes, K. J., Dillemuth, F. P., & Cronin, J. T. (2004). The matrix enhances the effectiveness of corridors and stepping stones. *Ecology, 85*(10), 2671-2676.

Bausch, W. C., Halvorson, A. D., & Cipra, J. (2008). Quickbird satellite and ground-based multispectral data correlations with agronomic parameters of irrigated maize grown in small plots. *Biosystems engineering*, *101*(3), 306-315.

Beaman, J. H. (2005). Mount Kinabalu: hotspot of plant diversity in Borneo. *Biologiske Skrifter*, *55*, 103-127.

Becknell, J. M., & Powers, J. S. (2014). Stand age and soils as drivers of plant functional traits and aboveground biomass in secondary tropical dry forest. *Canadian Journal of Forest Research, 44*(6), 604-613.

Bengtsson, J., Angelstam, P., Elmqvist, T., Emanuelsson, U., Folke, C., Ihse, M., ... & Nyström, M. (2003). Reserves, resilience and dynamic landscapes. *AMBIO: A Journal of the Human Environment, 32*(6), 389-396.

Benton, T. G., Vickery, J. A., & Wilson, J. D. (2003). Farmland biodiversity: is habitat heterogeneity the key?. *Trends in Ecology & Evolution, 18*(4), 182-188.

Birth, G. S., & McVey, G. R. (1968). Measuring the color of growing turf with a reflectance spectrophotometer. *Agronomy Journal, 60*(6), 640-643.

Blaschke, T., Hay, G. J., Kelly, M., Lang, S., Hofmann, P., Addink, E., ... & Tiede, D. (2014). Geographic object-based image analysis–towards a new paradigm. *ISPRS Journal of Photogrammetry and Remote Sensing, 87*, 180-191.

Bonner, M. T., Schmidt, S., & Shoo, L. P. (2013). A meta-analytical global comparison of aboveground biomass accumulation between tropical secondary forests and monoculture plantations. *Forest Ecology and Management, 291*, 73-86.

Broich, M., Hansen, M. C., Potapov, P., Adusei, B., Lindquist, E., & Stehman, S. V. (2011). Time-series analysis of multi-resolution optical imagery for quantifying forest cover loss in Sumatra and Kalimantan, Indonesia. *International Journal of Applied Earth Observation and Geoinformation, 13*(2), 277-291.

Brook, B. W., Sodhi, N. S., & Ng, P. K. (2003). Catastrophic extinctions follow deforestation in Singapore. *Nature*, *424*(6947), 420-426.

Burnett, C., & Blaschke, T. (2003). A multi-scale segmentation/object relationship modeling methodology for landscape analysis. *Ecological modelling, 168*(3), 233-249.

CBD (Convention on Biological Diversity) (2011). Aichi biodiversity targets. Convention on Biological Diversity.

CBD (Convention on Biological Diversity). (2014). CBD quick guides to the Aichi Biodiversity Targets. Available from https://www.cbd.int/nbsap/training/quick-guides/ (accessed September 2015).

CCBA. (2008). Climate, Community & Biodiversity Project Design Standards Second Edition. Arlington.

Chao, A., Chazdon, R. L., Colwell, R. K., & Shen, T. J. (2005). A new statistical approach for assessing similarity of species composition with incidence and abundance data. *Ecology Letters*, *8*(2), 148-159.

Chazdon, R. L. (2003). Tropical forest recovery: legacies of human impact and natural disturbances. *Perspectives in Plant Ecology, evolution and systematics*, *6*(1), 51-71.

Chen, J., Chen, J., Liao, A., Cao, X., Chen, L., Chen, X., ... & Zhang, W. (2015). Global land cover mapping at 30m resolution: A POK-based operational approach. *ISPRS Journal of Photogrammetry and Remote Sensing*, *103*, 7-27.

Clark, D. B., Read, J. M., Clark, M., Cruz, A. M., Dotti, M. F., & Clark, D. A. (2004). Application of 1-m and 4-m resolution satellite data to studies of tree demography, stand structure and land-use classification in tropical rain forest landscapes. *Ecological Applications*, *14*(1), 61-74.

Clark, M. L., Roberts, D. A., & Clark, D. B. (2005). Hyperspectral discrimination of tropical rain forest tree species at leaf to crown scales. *Remote sensing of environment*, *96*(3), 375-398.

Cochrane, M. A. (2003). Fire science for rainforests. *Nature*, *421*(6926), 913-919.

Coursolle, C., Margolis, H. A., Giasson, M. A., Bernier, P. Y., Amiro, B. D., Arain, M. A., ... & Chen, J. M. (2012). Influence of stand age on the magnitude and seasonality of carbon fluxes in Canadian forests. *Agricultural and Forest Meteorology*, *165*, 136-148.

Dahlin, K. M., Asner, G. P., & Field, C. B. (2013). Environmental and community controls on plant canopy chemistry in a Mediterranean-type ecosystem. *Proceedings of the National Academy of Sciences*, *110*(17), 6895-6900.

Dalle, S. P., Pulido, M. T., & Blois, S. D. (2011). Balancing shifting cultivation and forest conservation: lessons from a “sustainable landscape” in southeastern Mexico. *Ecological Applications*, *21*(5), 1557-1572.

Dash, J. P., Watt, M. S., Bhandari, S., & Watt, P. (2015). Characterising forest structure using combinations of airborne laser scanning data, RapidEye satellite imagery and environmental variables. *Forestry*, cpv048.

Davidson, E.A., de Abreusa, T.D., Carvalho, C.J.R., Figueiredo, R.D.O., Kato, M.D.A., Kato, O.R., Ishida, F.Y. (2008). An integrated greenhouse gas assessment of an alternative to slash-and-burn agriculture in eastern Amazonia. Glob. *Change Biol. 14*, 998–1007.

Davis, A. J. (2000). Does reduced-impact logging help preserve biodiversity in tropical rainforests? A case study from Borneo using dung beetles (Coleoptera: Scarabaeoidea) as indicators. *Environmental Entomology*, *29*(3), 467-475.

Deering, D. W., & Rouse, J. W. (1975). Measuring 'forage production' of grazing units from Landsat MSS data. In *International Symposium on Remote Sensing of Environment, 10 th, Ann Arbor, Mich* , 1169-1178.

DeFries, R., & Rosenzweig, C. (2010). Toward a whole-landscape approach for sustainable land use in the tropics. *Proceedings of the National Academy of Sciences*, *107*(46), 19627-19632.

Dent, D. H., & Wright, S. J. (2009). The future of tropical species in secondary forests: a quantitative review. *Biological conservation, 142*(12), 2833-2843.

Devereux, B. J., Amable, G. S., & Posada, C. C. (2004). An efficient image segmentation algorithm for landscape analysis. *International Journal of Applied Earth Observation and Geoinformation, 6*(1), 47-61.

Dressler, W., Wilson, D., Clendenning, J., Cramb, R., Mahanty, S., Lasco, R., ... & Gevana, D. (2015). Examining how long fallow swidden systems impact upon livelihood and ecosystem services outcomes compared with alternative land-uses in the uplands of Southeast Asia. *Journal of Development Effectiveness*, *7*(2), 210-229.

Du, Y., Teillet, P. M., & Cihlar, J. (2002). Radiometric normalization of multitemporal high-resolution satellite images with quality control for land cover change detection. *Remote sensing of Environment, 82*(1), 123-134.

Dube, T., & Mutanga, O. (2015a). Evaluating the utility of the medium-spatial resolution Landsat 8 multispectral sensor in quantifying aboveground biomass in uMgeni catchment, South Africa. *ISPRS Journal of Photogrammetry and Remote Sensing, 101*, 36-46.

Dube, T., & Mutanga, O. (2015b). Investigating the robustness of the new Landsat-8 Operational Land Imager derived texture metrics in estimating plantation forest aboveground biomass in resource constrained areas. *ISPRS Journal of Photogrammetry and Remote sensing, 108*, 12-32.

Duda, R. O., & Hart, P. E. (1973). Pattern classification and scene analysis (Vol. 3). New York: Wiley.

Duro, D. C., Coops, N. C., Wulder, M. A., & Han, T. (2007). Development of a large area biodiversity monitoring system driven by remote sensing. *Progress in Physical Geography*, *31*(3), 235-260.

Eckert, S. (2012). Improved forest biomass and carbon estimations using texture measures from WorldView-2 satellite data. *Remote sensing*, *4*(4), 810-829.

Edwards, D. P., Gilroy, J. J., Woodcock, P., Edwards, F. A., Larsen, T. H., Andrews, D. J., ... & Ota, T. (2014). Land‐sharing versus land‐sparing logging: reconciling timber extraction with biodiversity conservation. *Global change biology*, *20(1)*, 183-191.

Edwards, D. P., Larsen, T. H., Docherty, T. D., Ansell, F. A., Hsu, W. W., Derhé, M. A., ... & Wilcove, D. S. (2011). Degraded lands worth protecting: the biological importance of Southeast Asia's repeatedly logged forests. *Proceedings of the Royal Society of London B: Biological Sciences*, *278*(1702), 82-90.

Edwards, D. P., Woodcock, P., Edwards, F. A., Larsen, T. H., Hsu, W. W., Benedick, S., & Wilcove, D. S. (2012). Reduced‐impact logging and biodiversity conservation: a case study from Borneo. *Ecological Applications*, *22*(2), 561-571.

Ekstrand, S. (1996). Landsat TM-based forest damage assessment: correction for topographic effects. *Photogrammetric Engineering and Remote Sensing, 62*(2), 151-162.

Elias, Applegate, G., Kartawinata, K., Machfudh, Klassen, A. (2001). Reduced Impact Logging Guidelines for Indonesia. Center for International Forestry Research (CIFOR).

ERE Consulting Group Sdn Bhd. (2011). Study on the Establishment of Ecological Linkages connecting the Kinabalu Park and Crocker Range Park Final Report.

Feilhauer, H., & Schmidtlein, S. (2009). Mapping continuous fields of forest alpha and beta diversity. *Applied Vegetation Science, 12*(4), 429-439.

Feilhauer, H., Faude, U., & Schmidtlein, S. (2011). Combining Isomap ordination and imaging spectroscopy to map continuous floristic gradients in a heterogeneous landscape. *Remote Sensing of Environment, 115*(10), 2513-2524.

Finch, H. (2014). A Comparison of Methods for Group Prediction with High Dimensional Data. *Journal of Modern Applied Statistical Methods, 13*(2), 5.

Fischer, J., Fazey, I., Briese, R., & Lindenmayer, D. B. (2005). Making the matrix matter: challenges in Australian grazing landscapes. *Biodiversity & Conservation, 14*(3), 561-578.

Fischer, J., Lindenmayer, D. B., & Manning, A. D. (2006). Biodiversity, ecosystem function, and resilience: ten guiding principles for commodity production landscapes. *Frontiers in Ecology and the Environment, 4*(2), 80-86.

Food Agriculture Organization (FAO) (2006) Global Forest Assessment 2005. AO Forestry Paper 147. Food and Agriculture Organization (FAO) of the United Nations (UN), Rome.

Foody, G. M., Palubinskas, G., Lucas, R. M., Curran, P. J., & Honzak, M. (1996). Identifying terrestrial carbon sinks: classification of successional stages in regenerating tropical forest from Landsat TM data. *Remote Sensing of Environment, 55*(3), 205-216.

Foody, G. M., & Cutler, M. E. (2003). Tree biodiversity in protected and logged Bornean tropical rain forests and its measurement by satellite remote sensing. *Journal of Biogeography, 30*(7), 1053-1066.

Forman, R. T. (1995). Land mosaics: the ecology of landscapes and regions. Cambridge university press.

FSC (Forest Stewardship Council). (2012). Briefing Paper: Preliminary Outreach to FSC Membership in Preparation for the Development of FSC International Generic Indicators

Fujiki, S., Nishio, S., Okada, K. I., Nais, J., & Kitayama, K. (2017). Plant communities and ecosystem processes in a succession-altitude matrix after shifting cultivation in the

tropical montane forest zone of northern Borneo. *Journal of Tropical Ecology*, *33*(1), 33-49.

Fung, T., Ma, F. Y., & Siu, W. L. (1998). Hyperspectral data analysis for subtropical tree species recognition. Geoscience and Remote Sensing Symposium Proceedings, 1998. IGARSS'98. 1998 IEEE International (Vol. 3, pp. 1298-1300). IEEE.

Gao, B. C. (1996). NDWI—a normalized difference water index for remote sensing of vegetation liquid water from space. *Remote sensing of environment*, *58*(3), 257-266.

Gardner, T. A., Barlow, J., Chazdon, R., Ewers, R. M., Harvey, C. A., Peres, C. A., & Sodhi, N. S. (2009). Prospects for tropical forest biodiversity in a human‐modified world. *Ecology letters, 12(6),* 561-582.

Gardner, T. A., Barlow, J., Sodhi, N. S., & Peres, C. A. (2010). A multi-region assessment of tropical forest biodiversity in a human-modified world. *Biological Conservation, 143(10),* 2293-2300.

Gardner, T. A., Burgess, N. D., Aguilar-Amuchastegui, N., Barlow, J., Berenguer, E., Clements, T., ... & Vieira, I. C. (2012). A framework for integrating biodiversity concerns into national REDD+ programmes. *Biological Conservation, 154*, 61-71.

Gaveau, D. L., Kshatriya, M., Sheil, D., Sloan, S., Molidena, E., Wijaya, A., ... & Meijaard, E. (2013). Reconciling forest conservation and logging in Indonesian Borneo. *PloS One*, *8*(8), e69887.

Gaveau, D. L., Sloan, S., Molidena, E., Yaen, H., Sheil, D., Abram, N. K., ... & Meijaard, E. (2014). Four decades of forest persistence, clearance and logging on Borneo. *PloS one*, *9*(7), e101654.

GCS. (2011). Global Conservation Standard Version 1.2; Global Conservation Standard e.V.: Offenburg, Germany, 2011.

Geist, H. J., & Lambin, E. F. (2002). Proximate Causes and Underlying Driving Forces of Tropical Deforestation Tropical forests are disappearing as the result of many pressures, both local and regional, acting in various combinations in different geographical locations. *BioScience*, *52*(2), 143-150.

GEO BON. (2011). Adequacy of biodiversity observation systems to support the CBD 2020 targets. In A Report Prepared by the Group on Earth Observations Biodiversity Observation Network (GEO BON), for the Convention on Biological Diversity.

Gibson, L., Lee, T. M., Koh, L. P., Brook, B. W., Gardner, T. A., Barlow, J., ... & Sodhi, N. S. (2011). Primary forests are irreplaceable for sustaining tropical biodiversity. *Nature*, *478*(7369), 378-381.

Gillespie, T. W., Foody, G. M., Rocchini, D., Giorgi, A. P., & Saatchi, S. (2008). Measuring and modelling biodiversity from space. *Progress in Physical Geography*, *32*(2), 203-221.

Gitelson, A. A., Kaufman, Y. J., & Merzlyak, M. N. (1996). Use of a green channel in remote sensing of global vegetation from EOS-MODIS. *Remote Sensing of Environment, 58*(3), 289-298.

Goetz, S. J., Baccini, A., Laporte, N. T., Johns, T., Walker, W., Kellndorfer, J., ... & Sun, M. (2009). Mapping and monitoring carbon stocks with satellite observations: a comparison of methods. *Carbon balance and management*, *4*(1), 2.

Goetz, S. J., Hansen, M., Houghton, R. A., Walker, W., Laporte, N., & Busch, J. (2015). Measurement and monitoring needs, capabilities and potential for addressing reduced emissions from deforestation and forest degradation under REDD+. *Environmental Research Letters*, *10*(12), 123001.

Gong, P., Pu, R., & Yu, B. (1997). Conifer species recognition: an exploratory analysis of in situ hyperspectral data. *Remote Sensing of Environment, 62*(2), 189-200.

Goward, S. N., Markham, B., Dye, D. G., Dulaney, W., & Yang, J. (1991). Normalized difference vegetation index measurements from the Advanced Very High Resolution Radiometer. *Remote sensing of environment*, *35*(2), 257-277.

Green, R. E., Cornell, S. J., Scharlemann, J. P., & Balmford, A. (2005). Farming and the fate of wild nature. *Science*, *307*(5709), 550-555.

Groeneveld, J., Alves, L. F., Bernacci, L. C., Catharino, E. L. M., Knogge, C., Metzger, J. P., ... & Huth, A. (2009). The impact of fragmentation and density regulation on

forest succession in the Atlantic rain forest. *Ecological Modelling, 220*(19), 2450-2459.

Gu, H., Singh, A., & Townsend, P. A. (2015). Detection of gradients of forest composition in an urban area using imaging spectroscopy. *Remote Sensing of Environment, 167*, 168-180.

Hall, F. G., Strebel, D. E., Nickeson, J. E., & Goetz, S. J. (1991). Radiometric rectification: toward a common radiometric response among multidate, multisensor images. *Remote Sensing of Environment, 35*(1), 11-27.

Hamer, K. C., Hill, J. K., Benedick, S., Mustaffa, N., Sherratt, T. N., & Maryati, M. (2003). Ecology of butterflies in natural and selectively logged forests of northern Borneo: the importance of habitat heterogeneity. *Journal of Applied Ecology, 40*(1), 150-162.

Hansen, M. C., Stehman, S. V., Potapov, P. V., Loveland, T. R., Townshend, J. R., DeFries, R. S., ... & Carroll, M. (2008). Humid tropical forest clearing from 2000 to 2005 quantified by using multitemporal and multiresolution remotely sensed data. *Proceedings of the National Academy of Sciences, 105*(27), 9439-9444.

Hansen, M. C., Stehman, S. V., Potapov, P. V., Arunarwati, B., Stolle, F., & Pittman, K. (2009). Quantifying changes in the rates of forest clearing in Indonesia from 1990 to 2005 using remotely sensed data sets. *Environmental Research Letters, 4*(3), 034001.

Hansen, M. C., & Loveland, T. R. (2012). A review of large area monitoring of land cover change using Landsat data. *Remote sensing of Environment*, *122*, 66-74.

Hansen, M. C., Potapov, P. V., Moore, R., Hancher, M., Turubanova, S. A., Tyukavina, A., ... & Townshend, J. R. G. (2013). High-resolution global maps of 21st-century forest cover change. *Science*, *342*(6160), 850-853.

Haralick, R. M. (1986). Statistical image texture analysis. Handbook of Pattern Recognition and Image Processing, 86, 247-279.

Harper, K. A., Macdonald, S. E., Burton, P. J., Chen, J., Brosofske, K. D., Saunders, S. C., ... & Esseen, P. A. (2005). Edge influence on forest structure and composition in fragmented landscapes. *Conservation Biology*, *19*(3), 768-782.

He, L., Chen, J. M., Zhang, S., Gomez, G., Pan, Y., McCullough, K., ... & Masek, J. G. (2011). Normalized algorithm for mapping and dating forest disturbances and regrowth for the United States. *International Journal of Applied Earth Observation and Geoinformation*, *13*(2), 236-245.

He, L., Chen, J. M., Pan, Y., Birdsey, R., & Kattge, J. (2012). Relationships between net primary productivity and forest stand age in US forests. *Global Biogeochemical Cycles*, *26*(3).

Helmer, E. H., & Ruefenacht, B., (2005). Cloud-free satellite image mosaics with regression trees and histogram matching. *Photogrammetric Engineering & Remote Sensing*, *71*(9), 1079-1089.

Helmer, E. H., Lefsky, M. A., & Roberts, D. A. (2009). Biomass accumulation rates of Amazonian secondary forest and biomass of old-growth forests from Landsat time series and the Geoscience Laser Altimeter System. *Journal of Applied Remote Sensing*, *3*(1), 033505-033505.

Hernández-Stefanoni, J. L., Dupuy, J. M., Tun-Dzul, F., & May-Pat, F. (2011). Influence of landscape structure and stand age on species density and biomass of a tropical dry forest across spatial scales. *Landscape Ecology*, *26*(3), 355-370.

Higgins, M. A., Asner, G. P., Perez, E., Elespuru, N., Tuomisto, H., Ruokolainen, K., & Alonso, A. (2012). Use of Landsat and SRTM data to detect broad-scale biodiversity patterns in Northwestern Amazonia. *Remote Sensing*, *4*(8), 2401-2418.

Higgins, M. A., Asner, G. P., Anderson, C. B., Martin, R. E., Knapp, D. E., Tupayachi, R., ... & Alonso, A. (2015). Regional-scale drivers of forest structure and function in Northwestern Amazonia. *PloS one*, *10*(3), e0119887.

Hoekman, D. H. (1997). Radar monitoring system for sustainable forest management in Indonesia. In *Geoscience and Remote Sensing, 1997. IGARSS'97. Remote Sensing-A Scientific Vision for Sustainable Development., 1997 IEEE International* (Vol. 4, pp. 1731-1733). IEEE.

Hoekstra, J. M., Boucher, T. M., Ricketts, T. H., & Roberts, C. (2005). Confronting a biome crisis: global disparities of habitat loss and protection. *Ecology Letters*, *8*(1), 23-29.

Horning, N., Robinson, J.A., Sterling, E.J., Turner, W. & Spector, S. (2010) Remote Sensing for Ecology and Conservation, 467 pp. Oxford University Press, New York, USA.

Hosonuma, N., Herold, M., De Sy, V., De Fries, R. S., Brockhaus, M., Verchot, L., ... & Romijn, E. (2012). An assessment of deforestation and forest degradation drivers in developing countries. *Environmental Research Letters*, *7*(4), 044009.

Huang, C., Goward, S. N., Masek, J. G., Thomas, N., Zhu, Z., & Vogelmann, J. E. (2010). An automated approach for reconstructing recent forest disturbance history using dense Landsat time series stacks. *Remote Sensing of Environment*, *114*(1), 183-198.

Huberty, C. J., & Olejnik, S. (2006). Applied MANOVA and discriminant analysis (Vol. 498). John Wiley & Sons.

Huete, A., Didan, K., Miura, T., Rodriguez, E. P., Gao, X., & Ferreira, L. G. (2002). Overview of the radiometric and biophysical performance of the MODIS vegetation indices. *Remote sensing of environment*, *83*(1), 195-213.

Hussain, M., Chen, D., Cheng, A., Wei, H., & Stanley, D. (2013). Change detection from remotely sensed images: From pixel-based to object-based approaches. *ISPRS Journal of Photogrammetry and Remote Sensing*, *80*, 91-106.

Hyyppä, J., Hyyppä, H., Inkinen, M., Engdahl, M., Linko, S., & Zhu, Y. H. (2000). Accuracy comparison of various remote sensing data sources in the retrieval of forest stand attributes. *Forest Ecology and Management*, *128*(1), 109-120.

Imai, N., Tanaka, A., Samejima, H., Sugau, J. B., Pereira, J. T., Titin, J., ... & Kitayama, K. (2014). Tree community composition as an indicator in biodiversity monitoring of REDD+. *Forest Ecology and Management*, *313*, 169-179.

International Tropical Timber Organization (ITTO). (2006). Status of tropical forest management 2005, Yokohama.

Ioki, K., Tsuyuki, S., Hirata, Y., Phua, M. H., Wong, W. V. C., Ling, Z. Y., ... & Takao, G. (2016). Evaluation of the similarity in tree community composition in a tropical rainforest using airborne LiDAR data. *Remote Sensing of Environment*, *173*, 304-313.

IPCC. (2003). Definitions and methodological options to inventory emissions from direct human-induced degradation of forests and devegetation of other vegetation types. In: Penman, J., Gytarsky, M., Krug, T., Kruger, D., Pipatti, R., Buendia, L., Miwa, K., Ngara, T., Tanabe, K. and Wagner, F. IPCC-IGES, Kanagawa (eds.).

Jakovac, C. C., Peña - Claros, M., Kuyper, T. W., & Bongers, F. (2015). Loss of secondary - forest resilience by land - use intensification in the Amazon. *Journal of Ecology*, *103*(1), 67-77.

Jepsen, M. R. (2006). Above-ground carbon stocks in tropical fallows, Sarawak, Malaysia. *Forest Ecology and Management, 225*(1), 287-295.

Jones, H. G., & Vaughan, R. A. (2010). *Remote sensing of vegetation: principles, techniques, and applications*. Oxford university press.

Ke, Y., Quackenbush, L. J., & Im, J. (2010). Synergistic use of QuickBird multispectral imagery and LIDAR data for object-based forest species classification. *Remote Sensing of Environment, 114*(6), 1141-1154.

Kendawang, J. J., Ninomiya, I., Tanaka, K., Ozawa, T., Hattori, D., Tanaka, S., & Sakurai, K. (2007). Effects of burning strength in shifting cultivation on the early stage of secondary succession in Sarawak, Malaysia. *Tropics, 16*(4), 309-321.

Kennedy. E., Cohen, W. B., & Schroeder, T. A. (2007). Trajectory-based change detection for automated characterization of forest disturbance dynamics. *Remote Sensing of Environment, 110*(3), 370-386.

Kenzo, T., Ichie, T., Hattori, D., Itioka, T., Handa, C., Ohkubo, T., ... & Okamoto, M. (2009). Development of allometric relationships for accurate estimation of above-and below-ground biomass in tropical secondary forests in Sarawak, Malaysia. *Journal of Tropical Ecology*, *25*(04), 371-386.

Kenzo, T., Ichie, T., Hattori, D., Kendawang, J. J., Sakurai, K., & Ninomiya, I. (2010). Changes in above-and belowground biomass in early successional tropical secondary

forests after shifting cultivation in Sarawak, Malaysia. *Forest ecology and management, 260*(5), 875-882.

Kimes, D. S., Nelson, R. F., Salas, W. A., & Skole, D. L. (1999). Mapping secondary tropical forest and forest age from SPOT HRV data. *International Journal of Remote Sensing, 20*(18), 3625-3640.

Kitayama, K. (1992). An altitudinal transect study of the vegetation on Mount Kinabalu, Borneo. *Vegetatio, 102*(2), 149-171.

Kitayama, K. (Ed.), (2013). Co-benefits of Sustainable Forestry: Ecological Studies of a Certified Bornean Rain Forest. Springer, Tokyo.

Kotchenova, S. Y., Vermote, E. F., Matarrese, R., & Klemm, F. J. (2006). Validation of a vector version of the 6S radiative transfer code for atmospheric correction of satellite data. Part I: Path radiance. Applied Optics, 45, 6762–6774.

Kuplich, T. M., Curran, P. J., & Atkinson, P. M. (2005). Relating SAR image texture to the biomass of regenerating tropical forests. *International Journal of Remote Sensing, 26*(21), 4829-4854.

Kuplich, T. M. (2006). Classifying regenerating forest stages in Amazonia using remotely sensed images and a neural network. *Forest Ecology and Management, 234*(1), 1-9.

Lagan, P., Mannan, S., & Matsubayashi, H. (2007). Sustainable use of tropical forests by reduced-impact logging in Deramakot Forest Reserve, Sabah, Malaysia. *Ecological Research*, *22*(3), 414-421.

Laliberte, A. S., Rango, A., Havstad, K. M., Paris, J. F., Beck, R. F., McNeely, R., & Gonzalez, A. L. (2004). Object-oriented image analysis for mapping shrub encroachment from 1937 to 2003 in southern New Mexico. *Remote Sensing of Environment*, *93*(1), 198-210.

Langanke, T., Burnett, C., & Lang, S. (2007). Assessing the mire conservation status of a raised bog site in Salzburg using object-based monitoring and structural analysis. *Landscape and Urban Planning*, *79*(2), 160-169.

Langner, A., Miettinen, J., & Siegert, F. (2007). Land cover change 2002–2005 in Borneo and the role of fire derived from MODIS imagery. *Global Change Biology*, *13(11)*, 2329-2340.

Langner, A., Samejima, H., Ong, R. C., Titin, J., & Kitayama, K. (2012). Integration of carbon conservation into sustainable forest management using high resolution satellite imagery: A case study in Sabah, Malaysian Borneo. *International Journal of Applied Earth Observation and Geoinformation*, *18*, 305-312.

Laurance, W. F., & Laurance, S. G. (1996). Responses of five arboreal marsupials to recent selective logging in tropical Australia. *Biotropica*, 310-322.

Lawrence, D. (2004). Erosion of tree diversity during 200 years of shifting cultivation in Bornean rain forest. *Ecological Applications, 14*(6), 1855-1869.

Lawrence, D., D'Odorico, P., Diekmann, L., DeLonge, M., Das, R., & Eaton, J. (2007). Ecological feedbacks following deforestation create the potential for a catastrophic ecosystem shift in tropical dry forest. *Proceedings of the National Academy of Sciences, 104*(52), 20696-20701.

Lawrence, D., Radel, C., Tully, K., Schmook, B., & Schneider, L. (2010). Untangling a decline in tropical forest resilience: constraints on the sustainability of shifting cultivation across the globe. *Biotropica, 42*(1), 21-30.

Lindenmayer, D. B., & Franklin, J. F. (2002). Conserving forest biodiversity: a comprehensive multiscaled approach. Island Press.

Liu, J., Linderman, M., Ouyang, Z., An, L., Yang, J., & Zhang, H. (2001). Ecological degradation in protected areas: the case of Wolong Nature Reserve for giant pandas. *Science, 292*(5514), 98-101.

Lu, D. (2006). The potential and challenge of remote sensing - based biomass estimation. *International journal of remote sensing, 27*(7), 1297-1328.

Margules, C. R., & Presseyr. L. (2000). Systematic conservation planning. *Nature, 405*(6783), 243-253.

Martin, L. J., Blossey, B., & Ellis, E. (2012). Mapping where ecologists work: biases in the global distribution of terrestrial ecological observations. *Frontiers in Ecology and the Environment, 10*(4), 195-201.

Masek, J. G., Huang, C., Wolfe, R., Cohen, W., Hall, F., Kutler, J., & Nelson, P. (2008). North American forest disturbance mapped from a decadal Landsat record. *Remote Sensing of Environment, 112*(6), 2914-2926.

Mayfield, M. M., & Daily, G. C. (2005). Countryside biogeography of neotropical herbaceous and shrubby plants. *Ecological Applications, 15*(2), 423-439.

McFeeters, S. K. (1996). The use of the Normalized Difference Water Index (NDWI) in the delineation of open water features. *International journal of remote sensing, 17*(7), 1425-1432.

Mertz, O., Müller, D., Sikor, T., Hett, C., Heinimann, A., Castella, J. C., ... & Danielsen, F. (2012). The forgotten D: challenges of addressing forest degradation in complex mosaic landscapes under REDD+. *Geografisk Tidsskrift-Danish Journal of Geography*, *112*(1), 63-76.

Mertz, O., Padoch, C., Fox, J., Cramb, R. A., Leisz, S. J., Lam, N. T., & Vien, T. D. (2009). Swidden change in Southeast Asia: understanding causes and consequences. *Human Ecology*, *37*(3), 259-264.

Metzger, J. P. (2003). Effects of slash-and-burn fallow periods on landscape structure. *Environmental Conservation*, *30*(04), 325-333.

Miettinen, J., Shi, C., & Liew, S. C. (2011). Deforestation rates in insular Southeast Asia between 2000 and 2010. *Global Change Biology, 17(7)*, 2261-2270.

Miettinen, J., Stibig, H. J., & Achard, F. (2014). Remote sensing of forest degradation in Southeast Asia—Aiming for a regional view through 5–30 m satellite data. *Global Ecology and Conservation, 2*, 24-36.

Miles, L., Newton, A. C., DeFries, R. S., Ravilious, C., May, I., Blyth, S., ... & Gordon, J. E. (2006). A global overview of the conservation status of tropical dry forests. *Journal of Biogeography, 33*(3), 491-505.

Miles, L., & Kapos, V. (2008). Reducing greenhouse gas emissions from deforestation and forest degradation: global land-use implications. *Science, 320*(5882), 1454-1455.

Moran, E. F., Brondizio, E., Mausel, P., & Wu, Y. (1994). Integrating Amazonian vegetation, land-use, and satellite data. *BioScience, 44*(5), 329-339.

Myers, N., Mittermeier, R. A., Mittermeier, C. G., Da Fonseca, G. A., & Kent, J. (2000). Biodiversity hotspots for conservation priorities. *Nature, 403(6772)*, 853-858.

Nagendra, H. (2001). Using remote sensing to assess biodiversity. *International journal of remote sensing, 22*(12), 2377-2400.

Nagendra, H., Lucas, R., Honrado, J. P., Jongman, R. H., Tarantino, C., Adamo, M., & Mairota, P. (2013). Remote sensing for conservation monitoring: Assessing protected

areas, habitat extent, habitat condition, species diversity, and threats. *Ecological Indicators*, *33*, 45-59.

Nelson, R. F., Kimes, D. S., Salas, W. A., & Routhier, M. (2000). Secondary Forest Age and Tropical Forest Biomass Estimation Using Thematic Mapper Imagery: Single-year tropical forest age classes, a surrogate for standing biomass, cannot be reliably identified using single-date tm imagery. *Bioscience, 50*(5), 419-431.

Nichol, J. E., & Sarker, M. L. R. (2011). Improved biomass estimation using the texture parameters of two high-resolution optical sensors. *IEEE Transactions on Geoscience and Remote Sensing*, *49*(3), 930-948.

Nishio, S. (2014). Plant communities and ecosystem processes in a succession-altitude matrix after shifting cultivation in the tropical montane forest zone of northern Borneo. M.S. thesis, Kyoto University, Kyoto, Japan.

Novacek, M. J., & Cleland, E. E. (2001). The current biodiversity extinction event: scenarios for mitigation and recovery. *Proceedings of the National Academy of Sciences, 98*(10), 5466-5470.

Oetter, D. R., Cohen, W. B., Berterretche, M., Maiersperger, T. K., & Kennedy, R. E. (2001). Land cover mapping in an agricultural setting using multiseasonal Thematic Mapper data. *Remote Sensing of Environment, 76*(2), 139-155.

Ohmann, J. L., & Gregory, M. J. (2002). Predictive mapping of forest composition and structure with direct gradient analysis and nearest-neighbor imputation in coastal Oregon, USA. *Canadian Journal of Forest Research, 32*(4), 725-741.

Oksanen, J., Blanchet, F. G., Kindt, R., Legendre, P., Minchin, P. R., O'Hara, R. B., ... & Oksanen, M. J. (2013). Package 'vegan'. Community ecology package, version, 2(9).

Olsson, H. (1993). Regression functions for multitemporal relative calibration of Thematic Mapper data over boreal forest. *Remote Sensing of Environment, 46*(1), 89-102.

Ozdemir, I., & Karnieli, A. (2011). Predicting forest structural parameters using the image texture derived from WorldView-2 multispectral imagery in a dryland forest, Israel. *International Journal of Applied Earth Observation and Geoinformation, 13*(5), 701-710.

Padoch, C., & Pinedo - Vasquez, M. (2010). Saving slash - and - burn to save biodiversity. *Biotropica, 42*(5), 550-552.

Pandey, U., Kushwaha, S. P. S., Kachhwaha, T. S., Kunwar, P., & Dadhwal, V. K. (2010). Potential of Envisat ASAR data for woody biomass assessment.*Tropical Ecology, 51*(1), 117.

Pandit, M. K., Sodhi, N. S., Koh, L. P., Bhaskar, A., & Brook, B. W. (2007). Unreported yet massive deforestation driving loss of endemic biodiversity in Indian Himalaya. *Biodiversity and Conservation*, *16*(1), 153-163.

Paoli, G. D., Wells, P. L., Meijaard, E., Struebig, M. J., Marshall, A. J., Obidzinski, K., ... & d'Arcy, L. (2010). Biodiversity Conservation in the REDD. *Carbon balance and management*, *5*(1), 7.

Pereira, H. M., Ferrier, S., Walters, M., Geller, G. N., Jongman, R. H. G., Scholes, R. J., ... & Wegmann, M. (2013). Essential biodiversity variables. *Science*, *339*(6117), 277-278.

Peres, C. A., Barlow, J., & Laurance, W. F. (2006). Detecting anthropogenic disturbance in tropical forests. *Trends in Ecology & Evolution, 21(5),* 227-229.

Pettorelli, N., Vik, J. O., Mysterud, A., Gaillard, J. M., Tucker, C. J., & Stenseth, N. C., (2005). Using the satellite-derived NDVI to assess ecological responses to environmental change. *Trends in Ecology & Evolution, 20*(9), 503-510.

Pettorelli, N., Wegmann, M., Skidmore, A., Mücher, S., Dawson, T. P., Fernandez, M., ... & Jongman, R. H. (2016). Framing the concept of satellite remote sensing essential biodiversity variables: challenges and future directions. *Remote Sensing in Ecology and Conservation*.

Pinard, M. A., & Putz, F. E. (1996). Retaining forest biomass by reducing logging damage. *Biotropica*, 278-295.

Pu, R. (2009). Broadleaf species recognition with in situ hyperspectral data. *International Journal of Remote Sensing*, *30*(11), 2759-2779.

Putz, F. E., Zuidema, P. A., Pinard, M. A., Boot, R. G., Sayer, J. A., Sheil, D., ... & Vanclay, J. K. (2008). Improved tropical forest management for carbon retention. *PLoS Biol*, *6*(7), e166.

Putz, F. E., Zuidema, P. A., Synnott, T., Peña - Claros, M., Pinard, M. A., Sheil, D., ... & Palmer, J. (2012). Sustaining conservation values in selectively logged tropical forests: the attained and the attainable. *Conservation Letters*, *5*(4), 296-303.

Ranta, P., Blom, T., Niemela, J., Joensuu, E., & Siitonen, M. (1998). The fragmented Atlantic rain forest of Brazil: size, shape and distribution of forest fragments. *Biodiversity & Conservation*, *7*(3), 385-403.

Raši, R., Bodart, C., Stibig, H. J., Eva, H., Beuchle, R., Carboni, S., ... & Achard, F. (2011). An automated approach for segmenting and classifying a large sample of multi-date Landsat imagery for pan-tropical forest monitoring. *Remote Sensing of Environment*, *115*(12), 3659-3669.

Ries, L., Fletcher Jr, R. J., Battin, J., & Sisk, T. D. (2004). Ecological responses to habitat edges: mechanisms, models, and variability explained. *Annual Review of Ecology, Evolution, and Systematics*, 491-522.

Rignot, E., Salas, W. A., & Skole, D. L. (1997). Mapping deforestation and secondary growth in Rondônia, Brazil, using imaging radar and Thematic Mapper data. *Remote Sensing of Environment*, 59(2), 167-179.

Riswan, S. & Hartanti, L. (1995). Human impacts on tropical forest dynamics. *Vegetatio* 121:41–52.

Rocchini, D. (2007). Effects of spatial and spectral resolution in estimating ecosystem α-diversity by satellite imagery. *Remote Sensing of Environment*, *111*(4), 423-434.

Rocchini, D., Balkenhol, N., Carter, G. A., Foody, G. M., Gillespie, T. W., He, K. S., ... & Neteler, M. (2010). Remotely sensed spectral heterogeneity as a proxy of species diversity: recent advances and open challenges. *Ecological Informatics*, *5*(5), 318-329.

Rodrigues, A. S., Andelman, S. J., Bakarr, M. I., Boitani, L., Brooks, T. M., Cowling, R. M., ... & Yan, X. (2004). Effectiveness of the global protected area network in representing species diversity. *Nature*, *428*(6983), 640-643.

Roff, D. A. (2006). Introduction to computer-intensive methods of data analysis in biology. Cambridge University Press.

Rosenfield, G. H., & Fitzpatricklins, K. (1986). A coefficient of agreement as a measure of thematic classification accuracy. *Photogrammetric Engineering and Remote Sensing*, *52*(2), 223-227.

Roughgarden, J., Running, S. W., & Matson, P. A. (1991). What does remote sensing do for ecology?. *Ecology*, *72*(6), 1918-1922.

Rouse, J. W., Haas, R. H., Schell, J. A., Deering, D. W., and Harlan, J. C. (1974), Monitoring the vernal advancement of retrogradation of natural vegetation, NASA/GSFC, Type III, Final Report, Greenbelt, MD, 371.

Runyan, C. W., D'Odorico, P., & Lawrence, D. (2012). Effect of repeated deforestation on vegetation dynamics for phosphorus - limited tropical forests. *Journal of Geophysical Research: Biogeosciences*, *117*(G1).

Sabah Forestry Department. (2005). Forest Management Plan 2: Deramakot Forest Reserve, Forest Management Unit No. 19. Sabah Forestry Department, Sandakan.

Sabah Forestry Department. (2009). RIL Operation Guide Book, 3rd ed.; Sabah Forestry Department: Sandakan, Malaysia.

Sánchez‐Azofeifa, G. A., Quesada, M., Rodríguez, J. P., Nassar, J. M., Stoner, K. E., Castillo, A., ... & Fajardo, L. (2005). Research priorities for neotropical dry forests. *Biotropica*, *37*(4), 477-485.

Sarker, L. R., & Nichol, J. E. (2011). Improved forest biomass estimates using ALOS AVNIR-2 texture indices. *Remote Sensing of Environment*, *115*(4), 968-977.

Schmidtlein, S., & Sassin, J. (2004). Mapping of continuous floristic gradients in grasslands using hyperspectral imagery. *Remote Sensing of Environment*, *92*(1), 126-138.

Schmidtlein, S., Zimmermann, P., Schüpferling, R., & Weiss, C. (2007). Mapping the floristic continuum: Ordination space position estimated from imaging spectroscopy. *Journal of Vegetation Science*, *18*(1), 131-140.

Schmidt-Vogt, D., Leisz, S. J., Mertz, O., Heinimann, A., Thiha, T., Messerli, P., ... & Dao, T. M. (2009). An assessment of trends in the extent of swidden in Southeast Asia. *Human Ecology*, *37*(3), 269-280.

Scholes, R. J., Walters, M., Turak, E., Saarenmaa, H., Heip, C. H., Tuama, É. Ó., ... & Harrison, I. J. (2012). Building a global observing system for biodiversity. *Current Opinion in Environmental Sustainability*, *4*(1), 139-146.

Schott, J. R., Salvaggio, C., & Volchok, W. J. (1988). Radiometric scene normalization using pseudoinvariant features. *Remote Sensing of Environment*, *26*(1), 1-16.

Sekercioglu, C. H. (2002). Effects of forestry practices on vegetation structure and bird community of Kibale National Park, Uganda. *Biological Conservation*, *107*(2), 229-240.

Shamsoddini, A., Trinder, J. C., & Turner, R. (2013). Pine plantation structure mapping using WorldView-2 multispectral image. *International journal of remote sensing*, *34*(11), 3986-4007.

Slik, J. W. F., Poulsen, A. D., Ashton, P. S., Cannon, C. H., Eichhorn, K. A. O., Kartawinata, K., ... & Payne, J. (2003). A floristic analysis of the lowland dipterocarp forests of Borneo. *Journal of Biogeography, 30*(10), 1517-1531.

Sodhi, N. S., Koh, L. P., Clements, R., Wanger, T. C., Hill, J. K., Hamer, K. C., ... & Lee, T. M. (2010). Conserving Southeast Asian forest biodiversity in human-modified landscapes. *Biological Conservation*, *143*(10), 2375-2384.

Soenen, S. A., Peddle, D. R., Hall, R. J., Coburn, C. A., & Hall, F. G. (2010). Estimating aboveground forest biomass from canopy reflectance model inversion in mountainous terrain. *Remote Sensing of Environment, 114*(7), 1325-1337.

Song, C., Woodcock, C. E., Seto, K. C., Lenney, M. P., & Macomber, S. A. (2001). Classification and change detection using Landsat TM data: when and how to correct atmospheric effects?. *Remote sensing of Environment, 75*(2), 230-244.

Spies, T. A. (1998). Forest structure: a key to the ecosystem. *Northwest Science, 72*, 34-36.

Steininger, M. K. (2000). Satellite estimation of tropical secondary forest above-ground biomass: data from Brazil and Bolivia. *International Journal of Remote Sensing, 21*(6-7), 1139-1157.

Stibig, H. J., Achard, F., Carboni, S., Raši, R., & Miettinen, J. (2014). Change in tropical forest cover of Southeast Asia from 1990 to 2010. *Biogeosciences, 11*(2), 247-258.

Stibig, H. J., Belward, A. S., Roy, P. S., Rosalina - Wasrin, U., Agrawal, S., Joshi, P. K., ... & Giri, C. (2007). A land - cover map for South and Southeast Asia derived from SPOT - VEGETATION data. *Journal of Biogeography, 34*(4), 625-637.

Su, J. C., Debinski, D. M., Jakubauskas, M. E., & Kindscher, K. (2004). Beyond species richness: Community similarity as a measure of cross -taxon congruence for coarse- filter conservation. *Conservation Biology, 18*(1), 167-173.

Tabachnick, B. G., & Fidell, L. S. (2001). Using multivariate statistic. New York: Harper & Row.

Takeuchi, W., Yasuoka, Y. (2004). Development of normalized vegetation, soil and water indices derived from satellite remote sensing data. *Journal of the Japan Society of Photogrammetry and Remote Sensing 43*(6), 7-19 (In Japanese)

Tangki, H., & Chappell, N. A. (2008). Biomass variation across selectively logged forest within a 225-km 2 region of Borneo and its prediction by Landsat TM. *Forest Ecology and Management, 256*(11), 1960-1970.

Ter Braak, C. J., & Smilauer, P. (2002). CANOCO reference manual and CanoDraw for Windows user's guide: software for canonical community ordination (version 4.5).

Thessler, S., Ruokolainen, K., Tuomisto, H., & Tomppo, E. (2005). Mapping gradual landscape -scale floristic changes in Amazonian primary rain forests by combining ordination and remote sensing. *Global Ecology and Biogeography*, *14*(4), 315-325.

Tomppo, E., Goulding, C., & Katila, M. (1999). Adapting Finnish multi-source forest inventory techniques to the New Zealand preharvest inventory. *Scandinavian journal of forest research*, *14*(2), 182-192.

Townshend, J. R. G., & Justice, C. O. (1995). Spatial variability of images and the monitoring of changes in the normalized difference vegetation index. *International Journal of Remote Sensing*, *16*(12), 2187-2195.

Townshend, J. R., Masek, J. G., Huang, C., Vermote, E. F., Gao, F., Channan, S., ... & Song, K. (2012). Global characterization and monitoring of forest cover using Landsat data: opportunities and challenges. *International Journal of Digital Earth*, *5*(5), 373-397.

Trejo, I., & Dirzo, R. (2000). Deforestation of seasonally dry tropical forest: a national and local analysis in Mexico. *Biological conservation*, *94*(2), 133-142.

Turner, W., Rondinini, C., Pettorelli, N., Mora, B., Leidner, A. K., Szantoi, Z., ... & Koh, L. P. (2015). Free and open-access satellite data are key to biodiversity conservation. *Biological Conservation*, *182*, 173-176.

Turner, W., Spector, S., Gardiner, N., Fladeland, M., Sterling, E., & Steininger, M. (2003). Remote sensing for biodiversity science and conservation. *Trends in ecology & evolution*, *18*(6), 306-314.

Uhl, C., Clark, K., Clark, H., & Murphy, P. (1981). Early plant succession after cutting and burning in the upper Rio Negro region of the Amazon basin. *The Journal of Ecology*, 631-649.

United Nations Environment Programme World Conservation Monitoring Centre (UNEP-WCMC). (2008). State of the world's protected areas: an annual review of global conservation progress. UNEP-WCMC, Cambridge.

United Nations Framework Convention on Climate Change (UNFCCC). (2015). Intended nationally determined contributions (INDCs) United Nations Framework Convention on Climate Change United Nations

Ustin, S. L., Roberts, D. A., Gamon, J. A., Asner, G. P., & Green, R. O. (2004). Using imaging spectroscopy to study ecosystem processes and properties. *BioScience*, *54*(6), 523-534.

Van Aardt, J. A. (2000). Spectral separability among six southern tree species (Doctoral dissertation, Virginia Polytechnic Institute and State University).

Van der Werf, G. R., Morton, D. C., DeFries, R. S., Olivier, J. G., Kasibhatla, P. S., Jackson, R. B., ... & Randerson, J. T. (2009). CO2 emissions from forest loss. *Nature geoscience*, *2*(11), 737-738.

Van Vliet, N., Mertz, O., Heinimann, A., Langanke, T., Pascual, U., Schmook, B., ... & Castella, J. C. (2012). Trends, drivers and impacts of changes in swidden cultivation in tropical forest-agriculture frontiers: a global assessment. *Global Environmental Change*, *22*(2), 418-429.

Vashum, K. T., & Jayakumar, S. (2012). Methods to estimate above-ground biomass and carbon stock in natural forests-A review. *Journal of Ecosystem & Ecography*, 2012.

Veraverbeke, S., Gitas, I., Katagis, T., Polychronaki, A., Somers, B., & Goossens, R. (2012). Assessing post-fire vegetation recovery using red–near infrared vegetation indices: Accounting for background and vegetation variability. *ISPRS Journal of Photogrammetry and Remote Sensing*, *68*, 28-39.

Vermote, E. F., Tanré, D., Deuze, J. L., Herman, M., & Morcette, J. J. (1997). Second simulation of the satellite signal in the solar spectrum, 6S: An overview. *Geoscience and Remote Sensing, IEEE Transactions on*, *35*(3), 675-686.

Vieira, I. C. G., de Almeida, A. S., Davidson, E. A., Stone, T. A., Reis de Carvalho, C. J., & Guerrero, J. B. (2003). Classifying successional forests using Landsat spectral properties and ecological characteristics in eastern Amazonia. *Remote Sensing of Environment*, *87*(4), 470-481.

Vierling, K. T., Vierling, L. A., Gould, W. A., Martinuzzi, S., & Clawges, R. M. (2008). Lidar: shedding new light on habitat characterization and modeling. *Frontiers in Ecology and the Environment*, *6*(2), 90-98.

Vogelmann, J. E. (1988). Detection of forest change in the Green Mountains of Vermont using multispectral scanner data. *International Journal of Remote Sensing*, *9*(7), 1187-1200.

Vogelmann, J. E., Tolk, B., & Zhu, Z. (2009). Monitoring forest changes in the southwestern United States using multitemporal Landsat data. *Remote Sensing of Environment*, *113*(8), 1739-1748.

Vollmar, M., Rasi, R., Beuchle, R., Simonetti, D., Stibig, H. J., & Achard, F. (2013). Combining Landsat TM/ETM+ and ALOS AVNIR-2 Satellite Data for Tropical Forest Cover Change Detection. *IEEE Journal of Selected Topics in Applied Earth Observations and Remote Sensing*, *6*(1), 102-109.

Wang, Q., Adiku, S., Tenhunen, J., & Granier, A. (2005). On the relationship of NDVI with leaf area index in a deciduous forest site. *Remote sensing of environment*, *94*(2), 244-255.

Wilcove, D. S., Giam, X., Edwards, D. P., Fisher, B., & Koh, L. P. (2013). Navjot's nightmare revisited: logging, agriculture, and biodiversity in Southeast Asia. *Trends in Ecology & Evolution*, *28*(9), 531-540.

Willis, K. J., & Whittaker, R. J. (2002). Species diversity--scale matters. *Science*, *295*(5558), 1245-1248.

Wittmann, F., Anhuf, D., & Funk, W. J. (2002). Tree species distribution and community structure of central Amazonian várzea forests by remote-sensing techniques. *Journal of Tropical Ecology, 18*(06), 805-820.

Wulder, M. A., Hall, R. J., Coops, N. C., & Franklin, S. E. (2004). High spatial resolution remotely sensed data for ecosystem characterization. *BioScience, 54*(6), 511-521.

Xu, X., Du, H., Zhou, G., Ge, H., Shi, Y., Zhou, Y., ... & Fan, W. (2011). Estimation of aboveground carbon stock of Moso bamboo (Phyllostachys heterocycla var. pubescens) forest with a Landsat Thematic Mapper image. *International journal of remote sensing*, *32*(5), 1431-1448.

Zheng, G., Chen, J. M., Tian, Q. J., Ju, W. M., & Xia, X. Q. (2007). Combining remote sensing imagery and forest age inventory for biomass mapping. *Journal of Environmental Management, 85*(3), 616-623.

Zhu, Z., Woodcock, C. E., & Olofsson, P. (2012). Continuous monitoring of forest disturbance using all available Landsat imagery. *Remote Sensing of Environment*, *122*, 75-91.

Appendix

Appendix 2.1

Dominant species of each stand age

Stand age	Dominant species (relative dominance > 10 %)
2-yr old (5)	*Melastoma* sp., Poaceae sp., *Pteridium aquilinum, Eupatorium odoratum, Macaranga costulata*
3-yr old (4)	*Clethra canescens, Macaranga costulata, Melastoma* sp., *Pteridium aquilinum , Imperata cylindrica*
4-yr old (1)	*Clethra canescens, Macaranga costulata*
5-yr old (1)	*Macaranga costulata, Alphitonia excels, Melastoma* sp.
6-yr old (3)	*Clethra canescens, Macaranga costulata, Pteridium aquilinum, Carex* sp. *Melastoma* sp.
9-yr old (1)	*Alphitonia excels, Decaspermum fruticosum, Miscanthus sinensis, Pittosporum ferrugineum*
10-yr old (1)	*Clethra canescens, Alphitonia excels, Wendlandia paniculata, Itea macrophylla*
12-yr old (1)	*Adinandra dumosa, Clethra canescens, Itea macrophylla, Weinmannia flaxinea*
15-yr old (2)	*Clethra canescens, Tectaria* sp., *Adinandra dumosa, Ilex cissoidea, Wendlandia paniculata*
20-yr old (1)	*Clethra canescens, Itea macrophylla, Albizia falcataria, Mallotus minimifructus*
30-33 yr old (3)	*Astronia macrophylla, Tectaria* sp., *Clethra canescens, Ilex cymosa, Itea macrophylla*
55-yr old (2)	*Astronia macrophylla, Adinandra dumosa, Weinmannia flaxinea, Clethra canescens, Tectaria sp.*

The numbers in parentheses represent the number of research plots for vegetation inventory.

The species are arranged in the order of the relative dominance.

Appendix 2.2. (a)

Confusion matrix and accuracies of LDA among 1- and 4-year-old segments.

		Actual age			User's accuracy (%)
		1 yr	4 yr	Sum	
Predicted age	1 yr	121	11	132	91.66
	4 yr	8	53	61	86.88
	Sum	129	64	193	
Producer's accuracy (%)		93.8	82.8		

The overall classification accuracy was 90.15%

Appendix 2.2. (b)

Selected variables in LDA among 1- and 4-year-old segments.

Variable	**Coefficient**	**Normalized coefficient**
Mean_Band2	0.0184611	1.72329
GLCM_ Dissimilarity_(all dir.)	-1.4236542	-3.78899
GLCM_Entropy_Band2	-7.6457109	-4.66194
GLCM_Mean_Band3	0.5400582	0.95876
GLCM_Correlation_Band1	12.3413666	1.21577
GLCM_Correlation_SVI	-21.223293	-1.43665
GLCM_Contrast_(all dir.)	0.0186103	2.85582
GLCM_Correlation_GNDVI	13.411146	1.03132
GLCM_Entropy_Band4	5.8447232	3.65895
GLCM_Standard deviation_Band2	0.3822683	0.64969
Max_Band3	0.0025402	0.66826
Constant	-78.696868	

Appendix 2.3. (a)

Confusion matrix and accuracies of LDA among 1- and 6-year-old segments.

		Actual age			User's accuracy (%)
		1 yr	6 yr	Sum	
Predicted age	1 yr	125	5	130	96.15
	6 yr	4	106	110	96.36
	Sum	129	111	240	
Producer's accuracy (%)		96.89	95.49		

The overall classification accuracy was 96.25%

Appendix 2.3. (b)

Selected variables in LDA among 1- and 6-year-old segments.

Variable	**Coefficient**	**Normalized coefficient**
Mean_Band2	0.0538169	5.66301
GLCM_Dissimilarity (all dir.)	-3.0804618	-9.1185
GLCM_Contrast (all dir.)	0.0255927	4.37065
GLCM_Standard deviation_Band4	0.6624875	1.51808
Standard deviation_Band3	-0.0182326	-1.75809
GLCM_Standard deviation_Band2	0.8218527	1.32963
Min_Band2	-0.0156943	-2.03096
GLCM_Entropy_Band2	-2.4672018	-1.55874
Min_NDVI	-22.370194	-2.60123
Mean_Band3	-0.0281024	-2.36055
GLCM_Homogeneity_Band2	82.4637474	0.85872
GLCM_Contrast_NDVI	0.0035277	1.74588
GLCM_Correlationre_Band1	15.4867701	1.59369
Standard deviation_Band1	-0.0599393	-1.10896
Constant	-25.169895	

Appendix 2.4. (a)

Confusion matrix and accuracies of LDA among 4- and 6-year-old segments.

		Actual age			User's accuracy (%)
		4 yr	6 yr	Sum	
Predicted age	4 yr	46	31	77	59.74
	6 yr	18	80	98	81.63
	Sum	64	111	175	
Producer's accuracy (%)		71.87	72.07		

The overall classification accuracy was 72%

Appendix 2.4. (b)

Selected variables in LDA among 4- and 6-year-old segments.

Variable	**Coefficient**	**Normalized coefficient**
GLCM_Dissimilarity_(all dir.)	-1.4332205	-3.17633
GLCM_Contrast_(all dir.)	0.019329	2.74021
Mean_Band2	0.0081629	0.59549
GLCM_Correlation_Band2	5.0743992	0.39726
Constant	5.0994566	

Appendix 2.5. (a)

Confusion matrix and accuracies of LDA among 1- and 6-year-old segments.

		Actual age unit			User's accuracy (%)
		1-6 yr	8-22 yr	Sum	
Predicted age unit	1-6 yr	244	51	295	82.71
	8-22 yr	60	429	489	87.73
	Sum	304	480	784	
Producer's accuracy (%)		80.26	89.37		

The overall classification accuracy was 85.84%

Appendix 2.5. (b)

Selected variables in LDA among 1- and 6-year-old segments.

Variable	**Coefficient**	**Normalized coefficient**
Standard deviation_Band4	0.015318	1.48202
GLCM_Dissimilarity_Band4	0.203535	0.99067
GLCM_Entropy_TNDVI	1.33989	0.81966
GLCM_Dissimilarity_Band2	0.094024	0.47645
GLCM_Mean_Band1	-0.3744	-0.61544
Brightness	-0.013618	-1.41318
Min_SVI	0.292326	0.59804
Mean_GNDVI	15.731629	0.56997
GLCM_Homogeneity_Band1	-11.953878	-0.24051
Constant	20.633906	

Appendix 2.6. (a)

Confusion matrix and accuracies of LDA among 1–22-year-old segments and near primary-forest segments.

		Actual age unit			User's accuracy (%)
		1-22 yr	primary	Sum	
Predicted age unit	1-22 yr	744	52	796	93.46
	primary	40	615	655	93.89
	Sum	784	667	1451	
Producer's accuracy (%)		94.89	92.2		

The overall classification accuracy was 93.65%

Appendix 2.6. (b)

Selected variables in LDA among 1–22-year-old segments and near primary-forest segments.

Variable	**Coefficient**	**Normalized coefficient**
Mean_Band2	-0.0212615	-3.1748
GLCM_Mean_Band2	-0.5415276	-2.50478
Max_Band2	-0.0063361	-1.19229
Min_Band1	-0.0202629	-1.50909
GLCM_Entropy_Band2	-5.9500948	-5.46516
GLCM_Entropy_Band1	3.4767925	2.83307
GLCM_Dissimilarity_Band4	-0.9639356	-6.28807
GLCM_Contrast_Band4	0.0050818	4.36256
GLCM_Correlation_GNDVI	-7.9761095	-0.90942
GLCM_Standard deviation_Band4	0.4826677	1.58062
Standard deviation_SVI	-0.2927971	-0.52697
GLCM_Homogeneity_Band1	21.4304842	0.44846
Standard deviation_Band2	0.0429103	0.93089
GLCM_Entropy_Band3	2.1082176	1.85997
Constant	99.8686276	

Appendix 2.7

Selected variables in LDA among vegetation more than 50 years old and vegetation less than 50 years old

Variable	Coefficient	Normalized coefficient
Min_Band1	-0.032776	-2.51504
GLCM_Band2	-10.42187	-9.67204
GLCM_Band2	-0.651945	-3.06779
Min_Band4	-0.001922	-1.88237
Mean_Band2	-0.010308	-1.54375
GLCM_Entropy_Band1	3.6656362	3.03912
GLCM_Contrast_GNDVI	0.0025483	1.35609
GLCM_Standard deviation_Band4	0.7004423	2.38892
GLCM_Dissimilarity_Band4	-0.936556	-6.31619
GLCM_Entropy_Band3	5.9449979	5.2862
Mean_GNDVI	87.59461	3.05282
Mean_SVI	-0.494304	-1.54908
GLCM_Contrast_Band4	0.0042563	3.85443
Max_Band2	-0.007116	-1.32808
Standard deviation_Band2	0.0476624	1.05745
Min_Band3	0.0139894	1.22545
GLCM_Homogeneity_Band4	-76.76386	-0.66856
GLCM_Homogeneity_Band3	67.051575	0.88344
Constant	38.106555	

Appendix 2.8

Selected variables in LDA among vegetation less than 7 years old and vegetation more than 7 years old

Variable	Coefficient	Normalized coefficient
Mean_Band2	0.049658	4.15576
Standard deviation_Band4	0.027035	2.25426
GLCM_Dissimilarity_Band4	0.348588	1.59035
GLCM_Entropy_NDVI	6.849859	3.94449
GLCM_Entropy_GNDVI	-5.399215	-3.18226
GLCM_Homogeneity_Band1	-25.98683	-0.47784
GLCM_Mean_Band1	-0.632761	-0.92793
Brightness	-0.053089	-5.06405
Mean_GNDVI	126.218054	3.79608
Standard deviation_GNDVI	-114.067076	-0.59539
Constant	-25.172	

Appendix 2.9

Selected variables in LDA among 7–50-year-old vegetation and rubber plantations.

Variable	Coefficient	Normalized coefficient
Mean_Band1/Band2	-142.24	-9.7468
Standard deviation_SVI	-5.084984	-2.799
GLCM_Dissimilarity_SVI	-3.205411	-15.0195
GLCM_Dissimilarity (all dir.)	1.019476	2.7282
Standard deviation_Band4	0.037757	2.8342
GLCM_Mean_Band4	0.750006	3.8565
Brightness	0.035856	3.3475
GLCM_Homogeneity_TNDVI	-237.0329	-2.3492
GLCM_Standard deviation_SVI	0.576421	2.2874
GLCM_Contrast_SVI	0.01305	5.6433
Standard deviation_Band2	-0.076963	-1.1713
GLCM_Dissimilarity_Band1	-0.370123	-1.4377
Mean_SVI	-3.108125	-7.0892
Mean_GNDVI	217.58122	5.462
GLCM_Correlation_SVI	-101.5984	-6.8619
GLCM_Correlation_NDVI	61.945206	3.9686
Min_SVI	0.839853	1.701
Min_Band1	0.029513	1.3609
Constant	-98.51288	

Appendix 2.10

Confusion matrix and accuracies of the single-year stand age classification

		Actual age					User's accuracy (%)
		1 yr	4 yr	6 yr	Other	Sum	
Predicted age	1 yr	59	0	0	0	59	100
	2 yr	34	1	0	0	35	0
	3 yr	18	9	0	2	29	0
	4 yr	2	21	7	3	33	63.64
	5 yr	1	15	19	12	47	0
	6 yr	1	4	23	23	51	45.1
	7 yr	0	0	5	8	13	0
	Other	3	7	24	1,041	1,075	96.84
	Sum	118	57	78	1,089	1,342	
Producer's accuracy (%)		50	36.84	29.49	95.59		

Appendix 2.11

Variables selected by step-wise selection and coefficients of the secondary-vegetation model and the rubber-plantation model. Variables are arranged in order of decreasing correlation based on Pearson's correlation coefficients (r) for linear relationships between stand age and the object-based metrics derived from the WorldView-2 segments. R^2 and R^2adj are coefficients of correlation for each model.

	R^2	R^2adj	Coefficient	SE	Pearson's r
Secondary vegetation (Log(year))					
Mean_Band2			-0.002	8.63E-05	-0.781
GLCM_Dissimilarity_Band2			0.0737	7.78E-03	0.541
Max_Band1			-0.0003	6.37E-05	-0.478
GLCM_Contrast_Band2			-0.0004	6.88E-05	0.474
Standard deviation_NDVI			-4.7681	7.61E-01	-0.452
GLCM_Dissimilarity_Band4			0.0123	1.98E-03	0.396
GLCM_Entropy_Band1			0.1422	1.79E-02	0.29
Standard deviation_SVI			-0.0767	1.40E-02	0.29
Standard deviation_Band4	0.811	0.809	0.0006	1.19E-04	0.26
GLCM_Homogeneity_Band3			-2.3654	5.53E-01	-0.197
GLCM_Ang 2nd moment_Band1			15.5538	4.86E+00	-0.181
GLCM_Dissimilarity_GNDVI			-0.0134	2.21E-03	0.153
GLCM_Mean_Band1			-0.0506	3.75E-03	-0.149
GLCM_Standard deviation_Band2			-0.0383	4.99E-03	0.13
Standard deviation_Band2			0.0055	6.28E-04	-0.004
Constant			7.3443	6.13E-01	
Rubber plantation (Log(year))					
Mean_Band2	0.578	0.569	-0.002	2.58E-04	-0.76
Constant			2.2361	1.84E-01	

SE, standard error; NDVI, normalized difference vegetation index; SVI, simple vegetation index; GNDVI, green NDVI; GLCM, grey level co-occurrence matrix.

Appendix 3.1. Description of stand age, altitude and AGB and dominant species in each of the 27 vegetation stands in the upland area between the Kinabalu Park and the Crocker Range Park in Sabah, northern Borneo (cited from Nishio, 2014; Fujiki *et al*., 2017). In a main plot, AGB is measured for trees ≥ 5 cm dbh (age < 50 years), and for trees ≥ 20 cm dbh (age > 50 years). In a subplot, AGB is measured for trees 5 cm > and ≥ 1 cm dbh (age < 50 years), and for trees 20 cm > and ≥ 5 cm dbh (age > 50 years). In a small plot, AGB is measured for grasses or trees < 1 cm dbh (age < 50 years), and for trees 5 cm > and ≥ 1 cm dbh (age > 50 years). The two oldest stands (which are presumably older than 100 years) were not included in the vegetation analyses with TWINSPAN and DCA due to their unknown ages.

Stand Age (y)	Altitude (m)	Main plot size (m^2) (subplot) [small plot]	Total AGB (kg m^{-2})	AGB in main plot (kg m^{-2})	AGB in subplot (kg m^{-2})	AGB in small plot (kg m^{-2})	Dominant species (relative dominance > 10 % on each stand)
2	1153	[4×4]	0.41	-	-	0.41	*Erigeron* sp., *Eupatorium odoratum*
2	1053	[4×4]	0.6	-	-	0.6	*Eupatorium odoratum*, *Ficus condensa* King, *Melastoma malabathricum*, *Pteridium aquilinum*
2	1234	[4×4]	0.39	-	-	0.39	*Erigeron* sp., *Melastoma malabathricum*, *Pluchea odorata*
2	1076	(5×5)[4×4]	0.82	-	0.17	0.66	*Melastoma malabathricum*, Poaceae sp.
3	1170	[4×4]	0.3	-	-	0.3	*Eupatorium odoratum*,

							Imperata cylindrica, Paspalum conjugatum
3	1125	(5×5)[4×4]	0.94	-	0.54	0.4	*Clethra canescens* (Merr.) Sleumer, *Macaranga costulata* Pax & K.Hoffm., *Tectaria* sp.
3	1244	(5×5)[4×4]	1.65	-	1.17	0.48	*Clethra canescens, Macaranga costulata*
3	1191	(5×5)[4×4]	0.82	-	0.33	0.49	*Clethra canescens, Melastoma malabathricum, Pteridium aquilinum*
3	1091	(5×5)[4×4]	2.5	-	1.71	0.79	*Alphitonia excelsa, Clethra canescens, Macaranga costulata*
4	1115	(5×5)[4×4]	1.51	-	1.12	0.39	*Clethra canescens, Macaranga costulata*
5	1282	20×20(5×5)[4×4]	2.41	0.48	1.81	0.13	*Macaranga costulata*
6	1051	20×20(5×5)[4×4]	2.16	0.33	1.34	0.49	*Alphitonia excelsa, Eupatorium odoratum, Ficus* sp., *Lygodium japonicum (Thunb.) Sw., Melastoma malabathricum, Miscanthus sinensis, Pteridium aquilinum, Scleria terrestris, Schima wallichii* (DC.) Korth.
6	1236	20×20(5×5)	3.06	1.28	1.49	0.29	*Carex* sp., *Clethra*

		[4×4]					*canescens, Macaranga costulata, Pteridium aquilinum*
6	1063	20×20(5×5) [4×4]	2.22	0.61	1.11	0.51	*Clethra canescens, Macaranga costulata*
9	1054	20×20(5×5) [4×4]	2.82	1.54	1.03	0.24	*Alphitonia excelsa, Decaspermum fruticosum Forst., Miscanthus sinensis, Pittosporum ferrugineum* Dryand. ex W.T.Aiton
10	1044	20×20(5×5) [4×4]	3.85	2.62	0.93	0.29	*Alphitonia excelsa, Clethra canescens*
12	1218	20×20(5×5) [4×4]	6.85	5.18	1.53	0.14	*Adinandra dumosa, Clethra canescens*
15	1357	20×20(5×5) [4×4]	6.77	6.45	0.23	0.09	*Adinandra dumosa, Ilex cissoidea* Loes., *Tectaria* sp.
15	984	20×20(5×5) [4×4]	5.48	4.27	1.11	0.1	*Clethra canescens*
20	1098	20×20(5×5) [4×4]	7.69	6.35	1.28	0.06	*Albizia falcataria* (L.) Fosberg, *Clethra canescens, Itea macrophylla* Wall.
30	1237	20×20(5×5) [4×4]	7.45	6.26	1.04	0.15	*Astronia macrophylla, Tectaria* sp.
30	1147	20×20(5×5) [4×4]	9.3	8.48	0.74	0.09	*Itea macrophylla, Macaranga costulata*
33	1030	20×20(5×5) [4×4]	5.21	4.07	1.1	0.05	*Ilex cymosa* Bl.

55	1383	30×30(20×20)[5×5]	16.64	15.96	0.64	0.04	*Adinandra dumosa*, *Astronia macrophylla*, *Wendlandia paniculata* (Roxb.) DC.
55	1218	30×30(20×20)[5×5]	13.24	11.49	1.23	0.53	*Adinandra dumosa*, *Astronia macrophylla*, *Clethra canescens*, *Tectaria* sp., *Weinmannia fraxinea* (D.Don) Miq.
>100	1221	30×30(20×20)[5×5]	23.96	22.63	0.49	0.84	*Castanopsis acuminatissima* (Blume) A.DC.
>100	1151	30×30(20×20)[5×5]	19.66	18.14	0.44	1.08	Aracaceae sp.

Appendix 3.2. Description of stand age, altitude and AGB in each of the 12 validation plots in the upland area between the Kinabalu Park and the Crocker Range Park in Sabah, northern Borneo. In a main plot, AGB is measured for trees ≥ 5 cm dbh. In a subplot, AGB is measured for trees 5 cm > and ≥ 1 cm dbh.

Stand Age (y)	Altitude (m)	Main plot size (m^2) (subplot)	Total AGB (kg m^{-2})	AGB in main plot (kg m^{-2})	AGB in subplot (kg m-2)
4	1089	(25)	0.89	-	0.89
5	1501	400 (25)	4.57	3.6	0.98
8	1113	400 (25)	3.49	2.77	0.73
10	1198	400 (25)	11.02	9.94	1.08
12	1168	400 (25)	6.5	6.25	0.24
12	1368	400 (25)	10.83	10.2	0.63
17	1216	400 (25)	6.18	5.84	0.32
18	1045	400 (25)	4.13	3.8	0.33
21	1416	400 (25)	10.24	9.34	0.9
23	1067	400 (25)	7.13	6.23	0.89
23	1274	400 (25)	13.29	12.86	0.43
26	1132	400 (25)	9.21	9.12	0.09

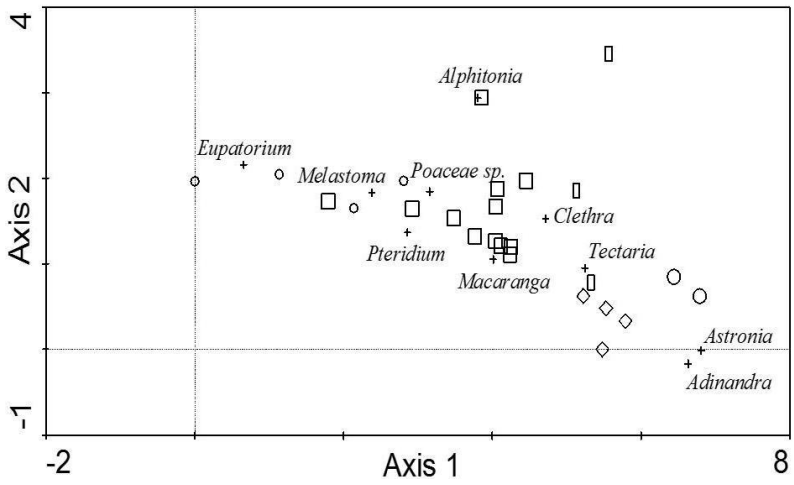

Appendix 3.3. The results of a DCA analysis on 25 vegetation stands in the upland area between the Kinabalu Park and the Crocker Range Park in Sabah, northern Borneo (cited from Nishio, 2014; Fujiki *et al*., 2017). Circles, diamonds, triangles and squares indicate stands, while crosses indicate dominant species. Different symbols of stands indicate the five plant communities (diamonds, herbaceous community; squares, shrub community; triangles, upper montane short forest community; inverted triangles, lower montane short-forest community; and circles, forest community) classified by TWINSPAN (Nishio, 2014; Fujiki *et al*., 2017). Eigenvalue is 0.786 for the axis 1, and 0.465 for the axis 2. Dominant species are represented by generic names.

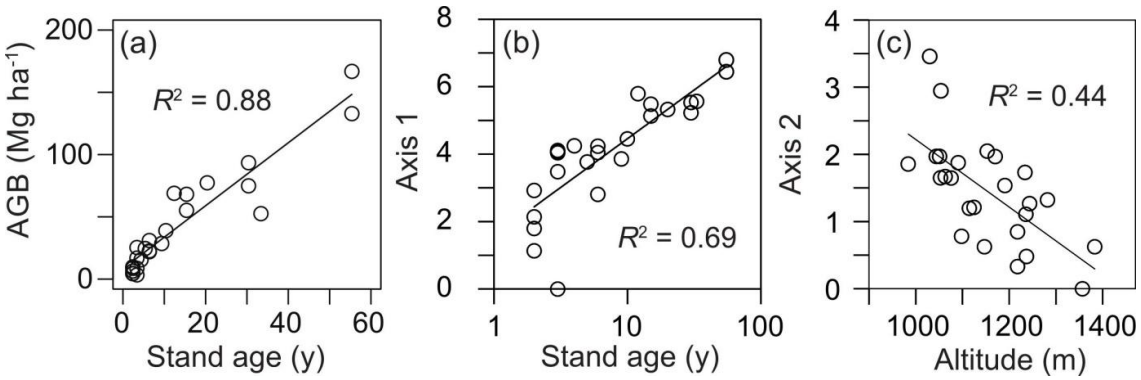

Appendix 3.4. The relationships between stand ages (years) and AGB (a), and stand ages (years) and axis-1 values (b), altitudes (m asl) and axis-2 values (c) for 25 vegetation stands in the upland area between the Kinabalu Park and the Crocker Range Park in Sabah, northern Borneo (modified from Nishio, 2014; Fujiki *et al*., 2017).

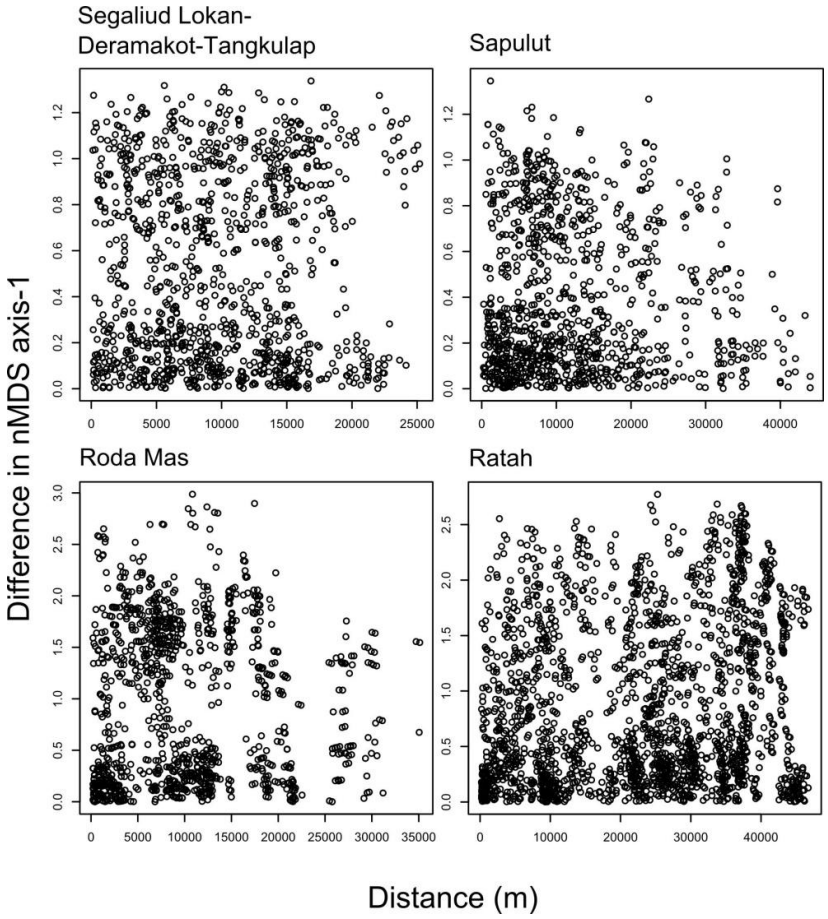

Appendix 4.1. The effects of distance on the difference in the nMDS axis-1 scores of paired vegetation plots. The distance was calculated using the center point of a given pair of vegetation plots. The difference was calculated as an absolute value of the difference in the nMDS axis-1 scores of the given pair of vegetation plots. See the main text for the details of the prediction model of nMDS axis-1 for each FMU. Positive relationships were observed for Ratah, potentially indicating the presence of spatial autocorrelations, but adjusted R2 scores were extremely low in all FMUs: SegaliudLokan-Deramakot-Tangkulap, R2 = -0.00, P > 0.05, n.s.; Sapulut, R2 = 0.00, P > 0.05, n.s.; Roda Mas, R2 = 0.00, P > 0.05, n.s.; Ratah, R2 = 0.03, P < 0.0001. n.s. denotes non-significance. Moreover, positive relationships may simply represent the consolidated occurrence of intact forests or disturbed forests.

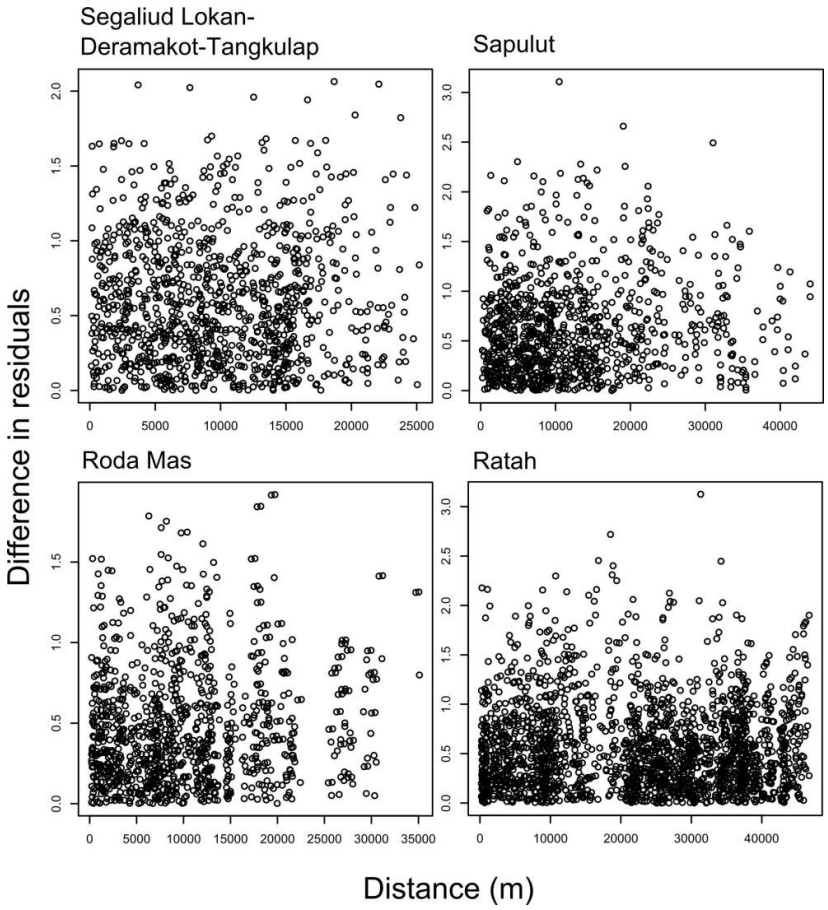

Appendix 4.2. The effects of distance on the difference in the residuals of nMDS axis-1 (i.e. observed nMDS axis-1 – predicted nMDS axis-1) of paired vegetation plots. The distance and the residuals were calculated using the center point of a given pair of vegetation plots. See the main text for the details of the prediction model of nMDS axis-1 for each FMU. Positive relationships were observed for two FMUs (Sapulut and Roda Mas), potentially indicating the presence of spatial autocorrelations, but adjusted R^2 scores were extremely low in all FMUs: SegaliudLokan-Deramakot-Tangkulap, R^2 = -0.00, P > 0.05, n.s.; Sapulut, R^2 = 0.01, P < 0.001; Roda Mas, R^2 = 0.01, P < 0.0001; Ratah, R^2 = 0.00, P > 0.05, n.s. denotes non-significance. Moreover, positive relationships may simply represent the consolidated occurrence of intact forests or disturbed forests.

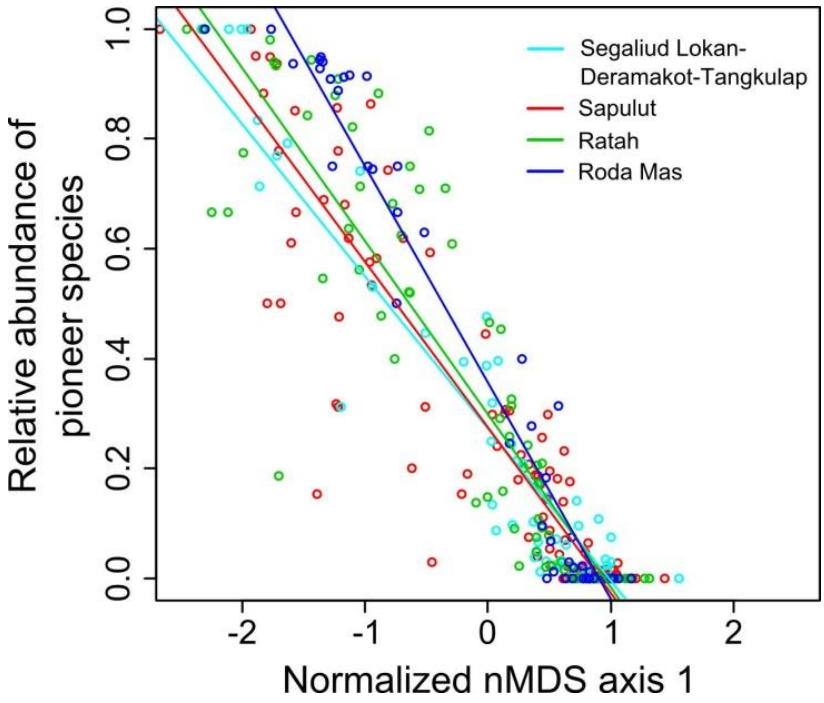

Appendix 4.3. The relationships between the normalized nMDS axis-1 scores and relative abundance of pioneer species (genera) in each FMU. The adjusted R^2 scores were significantly high in all FMUs: SegaliudLokan-Deramakot-Tangkulap, R^2 =0.72, $P < 0.001$; Sapulut, $R^2 = 0.90$, $P < 0.001$; Roda Mas, $R^2 = 0.95$, $P < 0.001$; Ratah, $R^2 = 0.82$, $P < 0.001$. T there were no significant differences in the intercept and slope among the regression lines in Segaliud Lokan and Sapulut. The intercept of Ratah ($P < 0.05$) and the intercept and slope of Roda Mas (intercept, $P < 0.05$; slope, $P < 0.001$) were exceptionally significantly different from the other FMUs, but the range of the deviation was still within that of the other FMUs.

Appendix 4.4.

Description of the Landsat imagery data set used in this study , including sensor, path / row and acquisition date

Name	Landsat sensor	Worldwide Reference System (WRS)	Acquisition date
Segaliud Lokan-Deramakot-Tangkulap 2009	TM	Path117/Row56	Aug/11/2009*
Segaliud Lokan-Deramakot-Tangkulap 2014	OLI	Path117/Row56	Jun/06/2014*, Dec/31/2014, Jul/15/2015
Sapulut	OLI	Path117/Row57	Jun/03/2013, Jun/19/2013*
Roda Mas	OLI	Path118/Row59	Oct/16/2013, Feb/05/2014, Sep/17/2014, Mar/28/2015, May/31/2015*
Ratah 2010	TM	Path117/Row60 Path118/Row60	Aug/11/2009 Feb/10/2010*
Ratah 2015	OLI	Path118/Row60	Apr/26/2014, Mar/28/2015*

*Used as a base image

Appendix 4.5.

Variance inflation factor (VIF) of the selected variable in the established multivariate regression models.

	VIF
SegaliudLokan-Deramakot-Tangkulap (2009)	
$B5_{TM}$	1.255569
GLCM_Mean_NDSI	1.255569
SegaliudLokan-Deramakot-Tangkulap (2014)	
$B7_{OLI}$	2.024439
GLCM_mean_EVI	1.051601
GLCM_homogenity_$B3_{OLI}$	1.02773
NDSI	1.99888
Sapulut (2013)	
$B6_{OLI}$	1.659212
GLCM_contrast_$B3_{OLI}$	1.044686
$B5_{OLI}$	1.609069
GLCM_mean_$B6_{OLI}$	1.146012
Roda Mas (2015)	
$B6_{OLI}$	5.371266
SD_NDSI	4.820667
SD_NDWI	36.564958
SD_NDVI	62.127144
$B4_{OLI}$	10.092117
Ratah (2010)	
$B7_{TM}$	6.705413
$B3_{TM}$	6.712582
GLCM_dissimilarity_$B4_{TM}$	1.018423
Ratah (2015)	
$B6_{OLI}$	1.069194
GLCM_homogenity_$B6_{OLI}$	1.069194